Force Analysis of Magnetic Abrasive Finishing of Non-ferromagnetic Material

A thesis submitted

In partial fulfillment of the requirements

for the degree of

Master of Technology

by

Kisun Kumar Saren

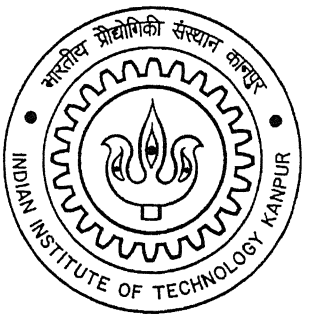

to the

Department of Mechanical Engineering
Indian Institute of Technology Kanpur
Kanpur (India)

August, 2004

Force Analysis of Magnetic Abrasive Finishing of Non-ferromagnetic Material

A thesis submitted

In partial fulfillment of the requirements

for the degree of

Master of Technology

by

Kisun Kumar Saren

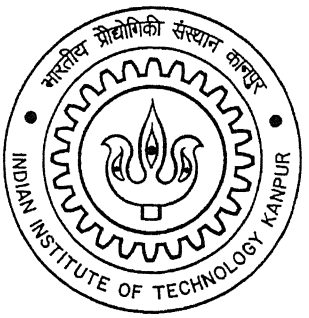

to the

Department of Mechanical Engineering
Indian Institute of Technology Kanpur
Kanpur (India)

August, 2004

CERTIFICATE

It is to certify that the work contained in this thesis, entitled "**Force analysis of Magnetic Abrasive Finishing of Non-ferromagnetic material**" by Mr. Kisun Kumar Saren, has been carried out under our supervision and that the same has not been submitted elsewhere for a degree.

(Dr. V. Raghuram)
Principal Research Engineer,
Dept. of Mechanical Engg.,
IIT Kanpur.

(Dr. V.K. Jain)
Professor,
Dept. of Mechanical Engg.,
IIT Kanpur.

Date : August 2, 2004

Acknowledgement

I express my unbound gratitude to my thesis supervisor Prof. V.K. Jain for suggesting and deciding the problem. I am deeply indebt to him for his meticulous guidance, devotion and inspiration throughout the tenure of this work.

I am indebted to Dr. V. Raghuram for his authentic and invaluable guidance, scrupulous attention, constant encouragement, inspiring advice throughout the course of my thesis work.

I am especially thankful to my senior Mr. D.K Singh for his consistent technical support and guidance. I am also thankful to Mr. Sunil Jha for his timely advices and guidance.

I am highly thankful to the Lab staff of the Manufacturing Science Lab, Mr. Phool Chand, Mr. Sanjeev Verma for providing valuable cooperation and technical support whenever required, during the design and manufacturing of the MAF setup. I am thankful to Mr. Virendra Singh and Mr. Rakesh Thapliyal for providing valuable help during the experimentation phase. I am thankful to my friends, Kullu, Anupam Sir, Commando, Deepak, Manas, Pritam, Suddi, Pad, Bijoy, Joshi, Pa, Bipin, Soumen da, Shukla, Prince, Ravisankar, Gatu, Mohanty, Shantanu for making my stay in IIT Kanpur a memorable one.

I am indebted to my parents for providing their support without which this journey would have been impossible.

I am thankful to everyone who helped me directly or indirectly to complete this work.

At last, but not the least at all, I am thankful to my friend Jagannath, who was always with me during the hard times of thesis load.

Kisun Kumar Saren

Abstract

Finishing a product is time consuming, difficult and costly process in a manufacturing process. Finishing cost can sometimes be as high as 15% of the total production cost. Finishing cost is always high when finishing very hard materials such as ceramics. So study of new cost effective finishing processes has always been an area of keen interest for production engineers. Magnetic Abrasive Finishing (MAF) is a new non-conventional finishing process that in spite of being in its research phase has shown vast potentials. In this process, a mixture of non-ferromagnetic abrasives and ferromagnetic iron particles is used to do finishing operation with the aid of magnetic force. The iron particles in the mixture are magnetically energized using a magnetic field. The iron particles form a lightly rigid matrix in which the abrasives are trapped. This is called Flexible Magnetic Abrasive Brush, which when given relative motion against a metal surface, polishes that surface.

Up till now, the major studies concerning MAF have been done regarding the behaviour of the process under the effect of various parameters like magnetic field applied, concentration of abrasives and iron particles in the iron – abrasive mixture, speed of relative motion and so on. All the works have been restricted to cylindrical and flat work-pieces only. But limited work has been done to analyze the forces that are generated during the process. Understanding the forces can help greatly in understanding the dynamics of the process and thereby easy to control and industrial implementation of the process. Both ferromagnetic and non-ferromagnetic materials have been finished with equal success using MAF.

The present work is aimed at studying the effect of the process parameters on the forces generated during MAF of non-ferromagnetic material in case of vertical MAF operation meant for flat work-pieces. For this, an experimental setup is designed and fabricated. Experiments are conducted on flat brass work-pieces using central composite rotatable design technique. The results of the experiments are statistically analyzed to form an empirical model for the tangential and normal forces generated during the process. The model is compared with that for a ferromagnetic alloy steel EN8.

Effect of applied magnetic field is seen to the most significant amongst all the parameters.

Contents

List of figures

List of tables

Nomenclature

b	Breadth of spindle housing holder section, mm
B	Slope of the linear regression curve for strain – vs – load for the dynamometer
BMAP	Bounded magnetic abrasive powder
C_F	Conversion factor of strain observed to thrust producing load
C_T	Conversion factor of strain observed to torque producing load
d_i	Inner diameter of the timing pulley, mm
d_o	Outer diameter of the timing pulley, mm
d_s	Diameter of spindle at the smallest section, mm
D_m	Diameter of electromagnet, mm
EN8	Euronorm steel #8
F	Force on electromagnet, N
Fa	Force of attraction between the EN8 work-piece and the electromagnet, N
F_a	Axial load on the spindle, N
Fc	Cutting force acting on a brass work-piece during MAF, N
Fc_f	Cutting force acting on an EN8 work-piece during MAF, N
F_e	Effective tension in the belt, N
Fmn	Normal thrust on a brass work-piece during MAF, N
Fmn_f	Normal thrust on an EN8 work-piece, N
F_N	Normal load on the dynamometer, N
Fnet	Net force measured by the dynamometer, N
Ft	Normal thrust imparted on a work-piece by the abrasives, N
F_T	Load producing torque on the dynamometer, N
F_x	Shearing force acting on a cross sectional area of spindle housing holder at a distance x from its tip, N
f_{bh}	Bearing stress on the spindle housing, N/m^2
f_{sh}	Shearing stress on the spindle housing, N/m^2
f_{sshh}	Maximum shear stress induced in the spindle housing holder, N/m^2

$(f_s)_{max}$ Maximum stress in the spindle due to combined torque, bending and axial load, MPa

f_{th} Tensile stress on the spindle housing, N/m^2

E Elastic limit of cast iron, N/m^2

FMAB Flexible magnetic abrasive brush

g Acceleration due to gravity, m/s^2

h Height to spindle housing holder section, mm

H_m Height of electromagnet, mm

I Moment of inertia, mm^4

L Distance between the axes of the electromagnet spindle and motor spindle, mm

LMAP Loosely bounded magnetic abrasive powder

M Bending moment, Nm

M_x Bending moment acting in the spindle housing holder at a distance x from its tip, Nm

MAF Magnetic Abrasive Finishing

MAP Magnetic Abrasive Powder

N Number of experimental observations

N_1 Maximum RPM to be required for finishing, min^{-1}

N_2 Overall design RPM, min^{-1}

P Probability of error

P_1 Design power, W

R_m Radius of electromagnet, mm

r Bearing resistance to spindle housing per unit length, N/mm

r_p Radius of the timing pulley, mm

s Strain observed in the dynamometer

s_w Weight per unit length of the spindle housing holder, N/mm

SD Standard deviation

T Rated torque of the motor, Nm

T_1 Torque required to rotate the electromagnet, Nm

T_2 Overall design torque, Nm

UMAP Unbounded magnetic abrasive powder

V_h Volume of spindle housing, mm^3

V_s Volume of spindle, m^3

VFD Variable frequency drive

W_p Weight of a timing pulley, N

W_1 Weight of spindle, N

W_2 Weight of ball bearings, N

W_3 Weight of electromagnet, N

W_4 Total weight of spindle, electromagnet and accessories, N

W_5 Spindle housing weight, N

W_6 Top cap weight, N

W_7 Bottom cap weight, N

W_8 Total weight of electromagnet, spindle and its accessories, spindle self weight, housing caps, N

x Length along the length of the spindle housing holder, mm

x_{ij} Level of an experimental parameter i^{th} and j^{th} observation

X Load applied on the dynamometer, g

X_1 Current supplied to the electromagnet, A

X_2 Working gap, mm

X_3 Speed of rotation of electromagnet, RPM

X_4 Mesh number of SiC abrasive

X_5 Percentage of oil

y Length perpendicular to the direction of x, mm

Y strain

Y_j Output observed for j^{th} combination of experimental parameters

z Section modulus, m^3

ρ_{CI} Density of cast iron, kg/m^3

ρ_s Density of stainless steel, kg/m^3

σ_{max} Maximum bending moment induced in the spindle housing holder, N/m^2

ω_2	Circumferential speed of electromagnet, rad/s
τ_p	Stress induced in the pulley due to motor torque, MPa
Φ	Response surface function
β	Coefficients in the Response

Chapter 1

INTRODUCTION

Usually in a machining process, simply finishing a product introduces an extra cost that sometimes is as high as 15% of the total cost of production. As the requirement for the surface quality increases, the finishing cost may still be more. This happens in case of high valued and extremely precise components such as aerospace components and so on. Previously, the requirement of surface quality used to be a need of only those industries making very sophisticated components for military or aerospace. But now it has become a requirement in civilian sectors also, as for instance, aerodynamic body of cars, engine cylinder walls and inner linings and so on. So there is now a need to economize finishing methods so as to bring more of sophistication into surface finishing, in civilian sectors, and at the same time make them flexible and efficient enough to work upon a wide range of components.

Conventional finishing processes such as grinding, lapping, honing, superfinishing though are good, have some problems such as limitation of producing flat and cylindrical surfaces only, high cost when finishing high strength materials accurately. The pressure they apply on the surface is high and sometimes may damage the surface on which they act. Magnetic Abrasive Finishing can solve some of the above stated problems.

1.1 Magnetic Abrasive Finishing (MAF)

MAF is a magnetic field assisted abrasive finishing process in which the cutting force is controlled by a magnetic field.

As stated earlier, control on the process is obtained by controlling the movement of the abrasives on the surface to be finished, with the aid of magnetic field. Abrasives are magnetically non-conducting. So they are mixed with magnetic particles to control them magnetically. Iron particles (Fig.1.1) are used for this purpose. A thorough mixture of abrasives and iron particles is prepared before applying them in the finishing process. This mixture is called Magnetic Abrasive Powder (MAP) and the particles are consequently, called as Magnetic Abrasive particles. The schematic view of a Magnetic Abrasive Particle is shown in Fig. 1.2. Hence the process is called Magnetic Abrasive Finishing (MAF). Sometimes the particles are bonded properly by sintering the magnetic and abrasive particle mixture. The powder is then called bounded magnetic abrasive powder (BMAP). Otherwise, lubricating oil is added to the mixture to obtain bonding strength

called as loosely bounded magnetic abrasive powder (LMAP). Or, it may be a simple mechanical mixture of the two, called as unbounded magnetic abrasive powder (UMAP).

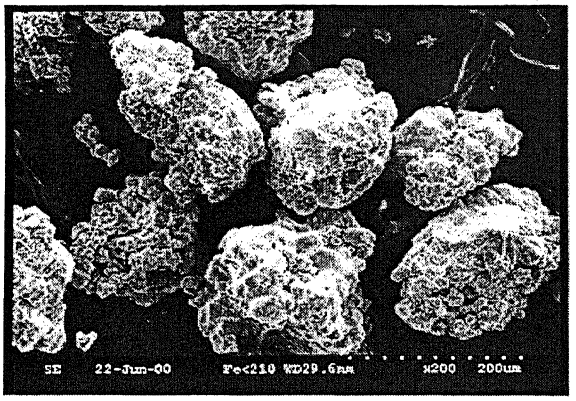

Figure 1.1 SEM micrographs of iron particles (180 μm in diameter) [13]

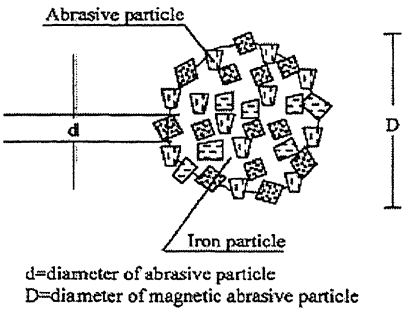

Figure 1.2 Schematic view of a magnetic abrasive particle [12]

A magnet with face, resembling the shape of the surface on which finishing operation is to be done, is brought on to the surface of the work-piece maintaining some gap which, depends on some governing factors. The gap is known as finishing gap or machining gap. The Magnetic Abrasive Powder is put in this gap distributing it uniformly. The magnet holds this powder by the magnetic force it generates. When magnetic field is applied by the magnet, the iron particles in the powder mixture get magnetized and get aligned along the lines of magnetic force generated from the magnet. The abrasive particles in the mixture get trapped in the iron particle matrix or otherwise stated, get sandwiched between the iron particles and thereby, are held by the magnetic force too. Overall, this alignment of the magnetic abrasive particles forms a brush like structure known as Flexible Magnetic Abrasive Brush (FMAB). The brush is termed "Flexible" due to its capacity to take the shape of any of surface profile irregularities, if present on the intended surface. Then relative motion between the magnet and work-piece is generated, consequently creating relative motion between the work-piece and this Magnetic Abrasive Brush. This relative motion helps to generate the necessary shearing stress in the abrasive – work-piece interface to remove material from the work-piece. The pressure imparted on the work-piece in this process is very less compared to rest of the conventional processes due to the absence of a very rigid structure to hold the abrasives. So material removed is in the form of chips which are very small (so called microchips) giving the effect of finishing.

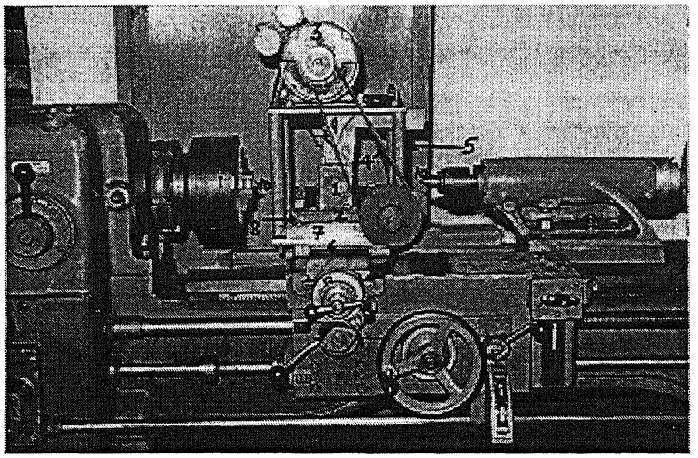

Figure 1.3 MAF setup mounted on lathe - 1:magnet, 2:carriage, 3:electric motor, 4:belt, 5:frame, 6:cross-slide, 7:rail, 8:wheel, 9:feeding system, 10:lathe centres [12]

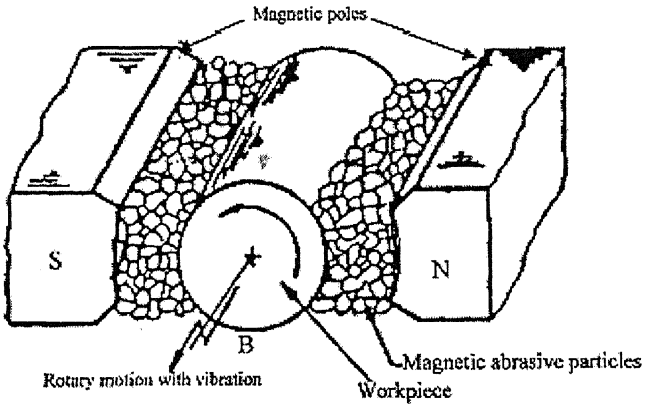

Figure 1.4 Schematic view of cylindrical MAF [12]

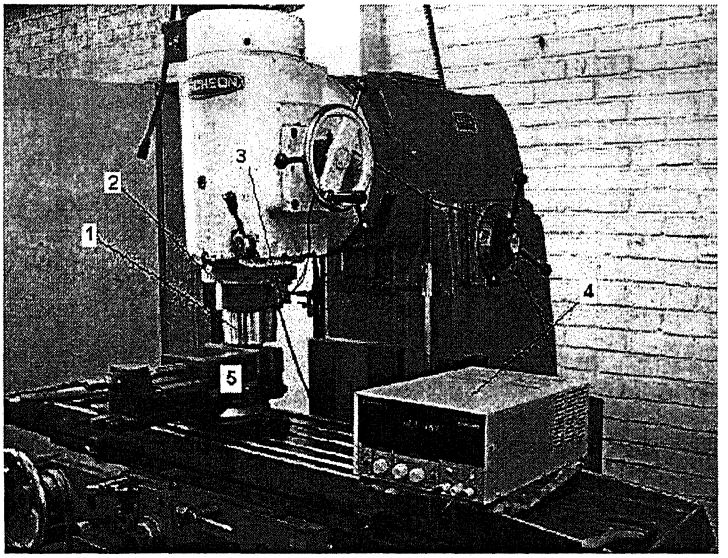

Figure 1.5 MAF setup mounted on vertical milling machine - 1:magnet, 2:casing, 3:sliding conductor contact, 4:dc supply, 5:machine vice [17]

All the work done in the field of MAF has been done on flat and cylindrical surfaces only. ere is a common approach followed by many previous researches to arrange the setup for AF. For cylindrical work-pieces, lathes have been modified to hold magnets and work-pieces shown in Fig. 1.3 and 1.4. For finishing flat work-pieces, finishing set-ups have been installed vertical milling machines or separate set-ups have been fabricated (Fig. 1.5). A finishing setup which the magnet is stationary and the work-piece rotates is called a work-piece rotation stem. And the reverse in which the magnet rotates and the work-piece is stationary is called ole rotation system. In pole rotation system, there are again two approaches. Firstly, either the agnet itself is rotated and the MAP is applied below the magnet face or, a detachable pole ometimes called as pole shoe) is attached on the magnet face which is rotated keeping the agnet stationary. The MAP is put on the detachable pole. Sometimes notches are made on this etachable pole, or it is made tapered to help concentrate magnetic force and thereby increase nishing efficiency.

.2 Forces in MAF process:

The forces generated in the process of MAF are responsible for the finishing operation.

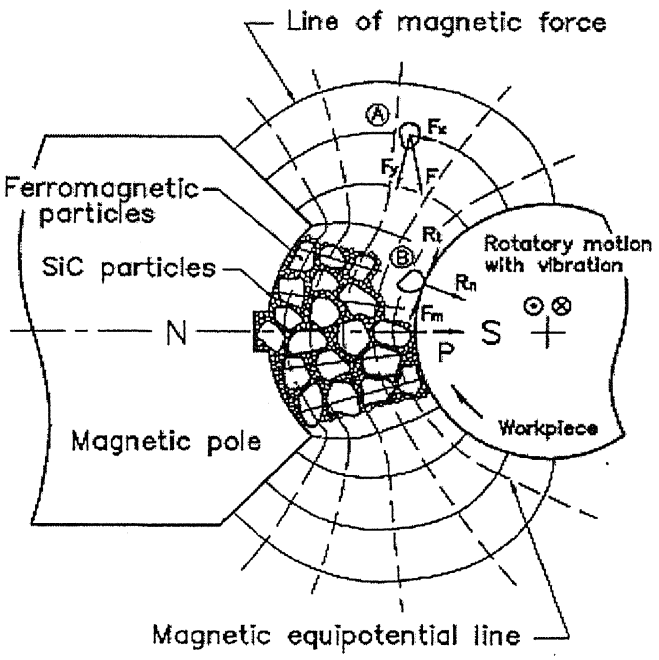

Figure 1.6 Schematic view of magnetic field distribution and magnetic force acting on a ferromagnetic particle in case of horizontal MAF [131]

The forces generated in the work-piece and FMAB interface region are basically the product of interaction between the magnetized iron particles, abrasives and the work-piece.

The magnetic force acting upon the particle at point 'A' in the magnetic field is 'F' can be resolved into two components as follows [19]:

$$F_x = V\chi\mu_0 H\frac{\partial H}{\partial x} \quad \text{.....(1.1)}$$

$$\text{and } F_y = V\chi\mu_0 H\frac{\partial H}{\partial y} \text{.....(1.2)}$$

where x is the direction of line of magnetic force, y is the direction of equipotential line, χ is the susceptibility of the particle, μ_0 is the permeability of vacuum, V is the volume of the particle, $\partial H/\partial x$ and $\partial H/\partial y$ are the gradients of the magnetic field strength in the x and y directions, respectively. These magnetic forces help to keep the MAP in the working zone where the magnetic field is strongest and prevent the particles from splashing off when the electromagnet rotates.

The diagram shown in Fig. 1.6 is a case of cylindrical MAF in which work-piece rotates. This congregation of MAP forms FMAB in the working gap, with particles lined up along the magnetic lines of force. The MAP exerts pressure on the work-piece. This pressure creates the necessary abrasion required for finishing. The pressure (P) is given by the formula [19]

$$P = \frac{\mu_0 H^2(1-1/\mu_m)}{2}$$

where, μ_m is the relative magnetic permeability of the iron particles. The iron particles near the

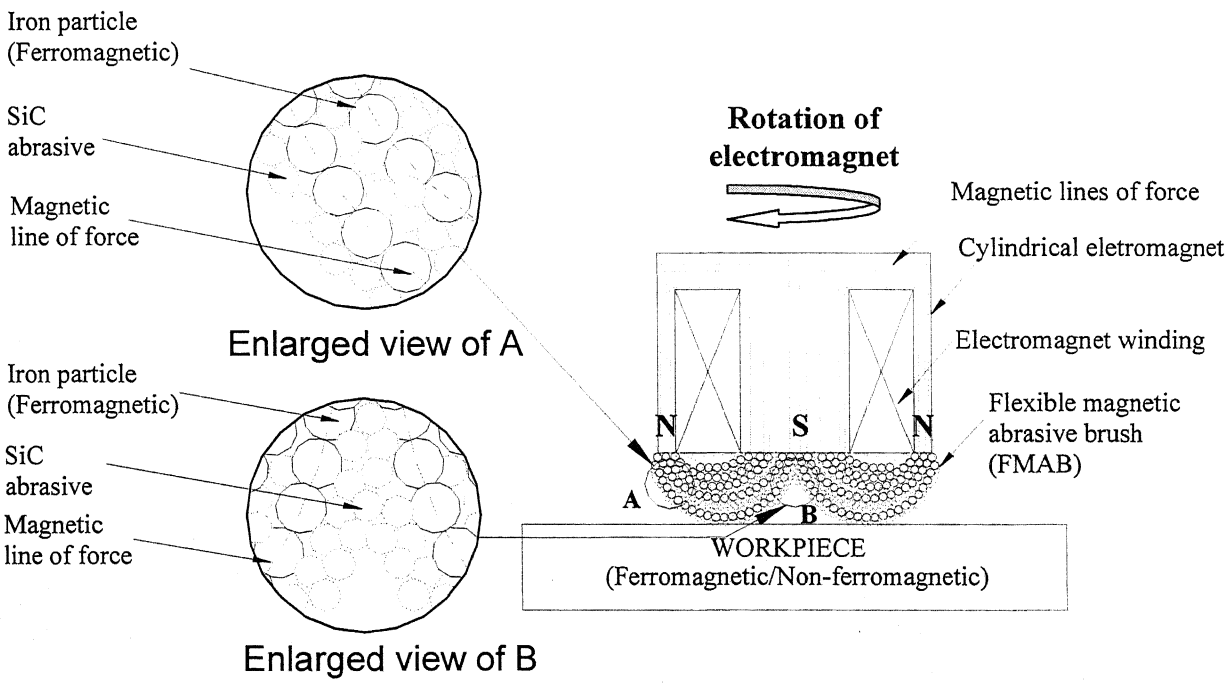

Figure 1.7 Scheme of polishing in vertical MAF

The magnetic force acting upon the particle at point 'A' in the magnetic field is 'F' can be resolved into two components as follows [19]:

$$F_x = V\chi\mu_0 H\frac{\partial H}{\partial x} \quad \text{.....(1.1)}$$

$$\text{and } F_y = V\chi\mu_0 H\frac{\partial H}{\partial y} \text{.....(1.2)}$$

where x is the direction of line of magnetic force, y is the direction of equipotential line, χ is the susceptibility of the particle, μ_0 is the permeability of vacuum, V is the volume of the particle, $\partial H/\partial x$ and $\partial H/\partial y$ are the gradients of the magnetic field strength in the x and y directions, respectively. These magnetic forces help to keep the MAP in the working zone where the magnetic field is strongest and prevent the particles from splashing off when the electromagnet rotates.

The diagram shown in Fig. 1.6 is a case of cylindrical MAF in which work-piece rotates. This congregation of MAP forms FMAB in the working gap, with particles lined up along the magnetic lines of force. The MAP exerts pressure on the work-piece. This pressure creates the necessary abrasion required for finishing. The pressure (P) is given by the formula [19]

$$P = \frac{\mu_0 H^2(1-1/\mu_m)}{2}$$

where, μ_m is the relative magnetic permeability of the iron particles. The iron particles near the

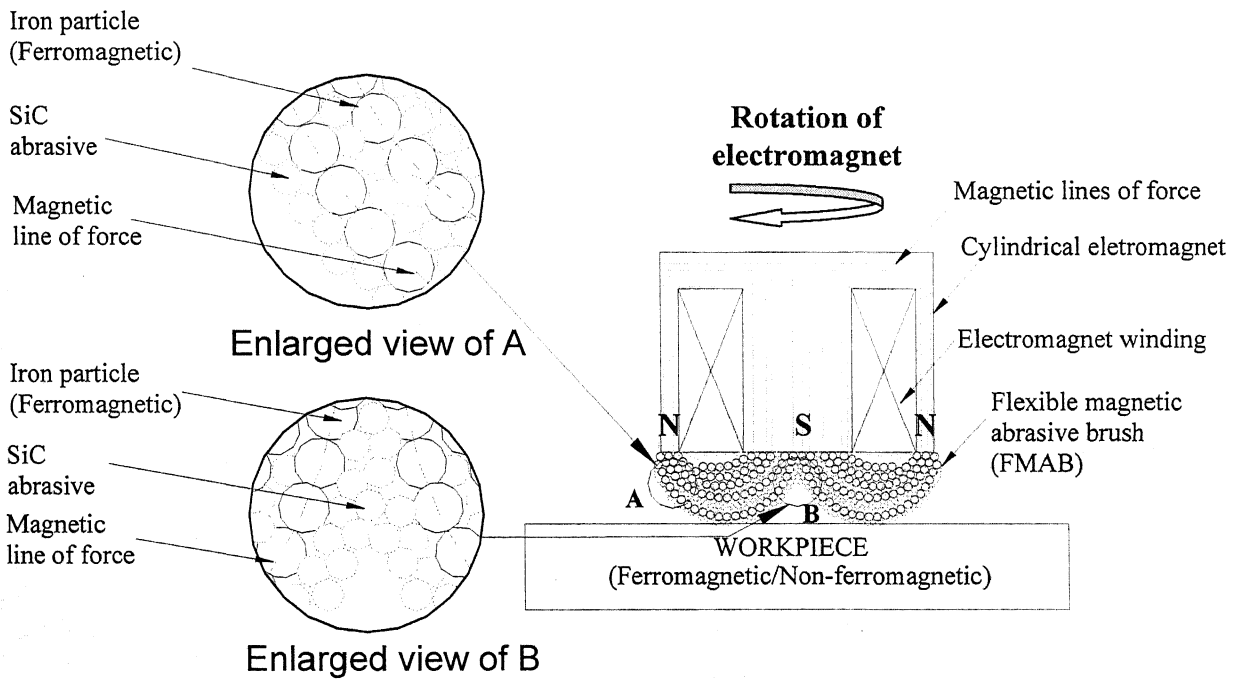

Figure 1.7 Scheme of polishing in vertical MAF

'ork-piece surface experience a cutting resistance Rt (Fig. 1.6) when the relative motion etween the electromagnet and the work-piece is started. The iron particles, in opposition to this utting resistance, experience a force Fm induced by the magnetic field. This force is the ıagnetic force of attraction between the iron particles. It helps in aligning the iron particles along ıe magnetic lines of force and prevents splashing of particles due to the relative motion between he electromagnet and the work-piece. These iron particles exert pressure force on the work-piece vhich is designated by Rn. Polishing is a combined effect of these three forces, Rt, Fm and Rn.

In the present thesis work, an electromagnet has been used for vertical MAF operation. The schematic diagram of the same is shown in Fig. 1.7.

The enlarged view of a portion of the magnetic abrasive brush is shown with the iron particles (ferromagnetic) aligned along the lines of magnetic force and the SiC abrasives sandwiched between a pair of iron particles chain. '**N**' and '**S**' represent the north and south poles of the electromagnet, respectively. The configuration of polarity in an electromagnet depends on he direction of flow of current through the winding. The forces generated in case of vertical MAF are similar to those that are created in cylindrical operation.

MAF provides the following advantages compared to other finishing processes:

1. MAF has the potential of giving ultra clean finishing of advanced engineering materials such as silicon nitride, silicon carbide and aluminum oxide which are used in high-technology industries and are difficult to finish by conventional grinding and polishing techniques with high accuracy.
2. MAF puts a very small amount of pressure on the work-piece surface. So it does not create any surface defects, such as thermal stresses and cracks, neither at micro nor macro level.
3. It generates residual compressive stress on the work-piece surface which improves its fatigue strength.
4. It is economic and faster as compared to conventional fine finishing processes.

1.3 Literature survey

As stated earlier, the idea of finishing using magnetic field was conceived and researched upon in erstwhile Soviet Union early in the 1900s. Later the centre of research in this field shifted to U.S.A. and Japan. Now, most of the research on MAF is being done in Japan.

The drafting of the literature survey done in the following paragraphs is aimed at validating the objective of the presented thesis that, a quantitative force analysis is required. The summarization of literature survey is done systematically starting with discussion of works

ling with MAF cylindrical work-pieces. Then the discussion is focused on works dealing with work-pieces.

In discussion for MAF of cylindrical work-pieces, the works concerning external MAF, MAF of solid cylindrical work-pieces is discussed.

In one of the early previous works of Shinmura et al [1], they studied the effects of ious working factors on the finishing characteristics using a test apparatus which they made trial. They used a ∅30 mm and length 45 mm non-ferromagnetic SS41 stainless steel as rk-piece. They used work-piece vibration of 15 Hz as a means to assist the MAF finishing of s work-piece. They used 29 m/min circumferential speed, 1.5 mm working clearance, 1.2 T gnetic flux density, 1.5 mm amplitude of work-piece vibration, 4 min finishing time, 6 g asive as parameters and found increase of finishing efficiency of MAF due to application of ration.

Shinmura et al [2] tried to explain the principle of MAF process. They inferred from the alysis of the process that the distribution of magnetic strength controlling the magnetic force the ferromagnetic particles in the MAP is affected by the material, shape and size of the work-ece, and shape and size of the magnetic pole. They measured the magnetic abrasive pressure duced by a particular value of flux density using a pressure sensor. They found that the essure increases with increase in flux density. They did their research on ferromagnetic steel.

Shinmura et al [3] studied the ability of the process to deburr and rounding off in 1985. ney used similar ∅30 mm and 45 mm length non-ferromagnetic steel work-pieces. They owed experimentally that MAF as a process has the ability of deburring and rounding off. They asoned that burrs are removed faster than normal surfaces because of the concentration of agnetic field at the sharp corners of the burrs thereby concentrating the magnetic abrasives ere.

Shinmura et al [5] again studied the effect of abrasive diameter and ferromagnetic particle iameter in the magnetic abrasive powder by taking non-ferromagnetic SS41 steel as work-piece. hey found out experimentally that the effect of abrasive grain diameter on stock removal was ot significant, but it was very prominently visible in case of surface roughness. The diameter of on particles affects the stock removal greatly. Greater is the diameter of iron particles, greater is ie stock removal. They also concluded by doing steel ball experiments that in a brush, the novement of particles is the smallest where the larger sized iron particles are concentrated, the rush being stiffer in those regions of the brush.

Jain et al [12] studied the performance of the MAF process under the effect of working and circumferential speed of the stainless steel work-piece. They evaluated the performance :erms of change and percentage improvement of surface roughness and material removal. :y studied the performance experimentally doing experiments on non-magnetic stainless steel rk-piece using loosely bounded MAP comprising of 600 mesh alumina abrasive and 300 mesh n particles. At small working gap, FMAB is strong and so abrasives make deep cut on the rk-piece giving heavy material removal. This phenomenon increases with increase in cumferential speed. The change in surface roughness also increases with increase in cumferential speed since the number of abrasive grains coming in contact with the work-piece :face increases with increase in circumferential speed. With increase in working gap, the rcentage improvement in surface roughness increases initially, reaches a maximum value and :n it starts decreasing.

Chang et al [13] studied the potential of unbounded MAP. They experimented on SKD11 ol steel using iron and steel grits as ferromagnetic particles and SiC as abrasive. SKD11 has a rdness of HRC55. They found that steel grit is better than iron because it is harder than iron id its shape is that of polyhedron which has sharp cutting edges. Iron particles are somewhat und. If the hardness of a work-piece is increased, steel grit MAP gives good finish compared to softer material because in hard material, the indentation of the grit is shallower. A SiC abrasive f any particular size will give better finish in case of a hard material as compared to a softer aterial under the same experimental conditions. MAF does not change the surface hardness of ie surface on which it acts.

In the next series of discussions, works concerning internal MAF is discussed. These esearches have been done using cylindrical work-pieces which are hollow from inside, as for nstance, pipes, glass jars.

Shinmura et al [6] studied the potential of MAF process to finish internal surfaces of stainless steel sanitary tubes. Though they couldn't give experimental verification of so, they stated that the process can be used to do the finishing of internal surfaces of stainless steel tubes. They used work-piece speed of 100 m/min, magnetic flux density of 0.9 T and 40 g of MAP consisting of alumina and iron particles mixed by chemical reaction. They also used 4 Hz frequency and 14 mm amplitude work-piece vibration as an aid to the process. They could improve surface roughness of 4 μm Rmax to 0.1 μm Rmax. Surface roughness improved with increase of finishing time. The roundness profile of the inner tube surface didn't change after finishing which concluded that MAF is a process that does uniform finishing.

Shinmura et al [9] studied the effect of particle and weight percentage of iron in an iron - sive mixture for the efficient finishing of a non-ferromagnetic glass gas bomb. They used particles of diameter ranging from 75 μm to 1680 μm in diameter and found that 330 μm ıeter iron particles are the most efficient in obtaining best finish in the lowest time in the iron ıent range of 60% to 80% by weight in the iron-abrasive mixture. The MAP using 75 μm neter iron particle is not able to remove material and so the surface roughness remained the ıe. But using 1680 μm diameter iron particles, large amount of material is removed and the ace roughness is also not good. Using iron particles alone for finishing also not effective in shing as it creates shortage of cutting edges. So a mixed type MAP where iron particles are ıed with abrasives is more efficient. They found out experimentally that the optimized portion of iron particles in the mixed type MAP is approximately 80% by weight.

Yamaguchi et al [10] studied the effectiveness of MAF as a finishing process for internal .shing of ferromagnetic and non-ferromagnetic tubes. MAF had been considered an inefficient cess for internal finishing of ferromagnetic tubes during to magnetic shielding of the finishing ion. This problem can be solved by reducing the thickness of the ferromagnetic tube. There is ıaximum limit for the thickness of the ferromagnetic tube. For non-ferromagnetic tubes, there no shielding effect due to the non-magnetizing effect of the work-piece and so the magnetic es of force pass through the material of the tube to reach the working gap region.

Yamaguchi [11] studied the in-process abrasive behavior in view of the magnetic field ıtribution and its effects on the finishing characteristics. They experimented by finishing ernal surface of non-ferromagnetic SUS304 stainless tubes using a pole rotation system with ixed type MAP consisting of iron particles (510 μm diameter) and WA magnetic abrasive (80 n diameter). They measured the pressure force on the work-piece using a pressure transducer hile changing the shape of the magnetic poles from flat to taper. They measured higher pressure case of flat pole. Abrasive behavior is determined by magnetic force and the friction force ıting on the abrasive against the inner surface of the tube. When the magnetic force is greater an the friction force, the abrasive follows the rotation of the magnetic field and this generates lative motion of the abrasive against the inner surface, removing material from the work-piece.

Finally, those research works dealing with flat work-pieces are discussed.

Shinmura et al [4] used MAF to finish 1.2 mm thick flat work-pieces of stainless steel SUS304) using ∅5 μm Al_2O_3 (alumina) abrasives and did the finishing operation for 5 min. hey studied the effect of peripheral speed of magnet, magnetic flux density in the finishing zone nd working clearance or gap on the surface finish and material removal. They found that all the

ve three factors contributed in improving the surface finish of the work-piece. Higher speed, ıer magnetic flux and lower gap help in improving the surface roughness.

Shinmura et al [7] carried on the work done on plane work-pieces. They applied MAF on ne non-ferromagnetic work-pieces of hardened steel, ceramics and stainless steel using mina as abrasive. They used a stationary type of electromagnet with adjustable rotating poles different shapes and sizes, but all with notches cut on them. The stationary type electromagnet s an improvement over the previous rotating type in terms of scaling down of magnet ;embly size. The notches were cut to provide stronger magnetic field at the pole edges. They ınd that surface roughness of work-pieces can be improved easily using a stationary type :ctromagnet. For non-ferromagnetic materials, they commented that non-ferromagnetic ıterials must be machined for longer time as the magnetic field gets weakened in their case. ırd materials like ceramics can be finished better by using composite magnetic abrasives ɔrmal MAF powder plus diamond grains).

Shinmura et al [8] for the first time tried to analyze the effect of various working rameters on the forces generated during MAF. They conducted experiments on plane ceramic ates using MAP consisting of iron particles and magnetic diamond abrasives. They found that r non-ferromagnetic materials where it is difficult to maintain high magnetic field in the ıishing zone, the problem of weak field can be compensated by using a ferromagnetic particle ' larger diameter. Thus the finishing efficiency can be improved. Rigidity of the magnetic brush also an important factor that directly affects the finishing efficiency. The rigidity of a brush can ɛ improved by using magnetic abrasives of larger diameter. They concluded that the diameter ıd the mixing proportion of ferromagnetic particles in a mixture of iron – abrasive mixture can ave remarkable effect on the finishing characteristics. Larger diameter ensures rigidity, but at ıe same time consumes more volume in the work space thereby reducing the number of ınishing abrasives.

Mori et al [14] tried to explain the mechanism behind MAF process using experimental ata obtained from MAF operation done on plane stainless steel disks. They stated that the 'MAB is formed due to the magnetizing energy supplied by the electromagnet to the erromagnetic particles. Upon magnetization, the iron particles form bundles. In order to form the 'MAB, the energy supplied by the electromagnet has to supply energy to magnetize the iron ɔarticles in the MAP, to counter the repulsion between the ferromagnetic particles and to counter he repulsion between the bundles.

Yamaguchi et al [15] applied the process of MAF for non-ferromagnetic alumina ceramics which have a wide range of applications but are difficult and so, costly to machine and

ı. They conducted experiments on alumina tubes with 99.5% alumina content using iron and ond abrasive MAP. They finished the internal surfaces of the tubes at 1800 min^{-1} work-piece ıon and 0.37 T magnetic flux density. They found that 330 μm diameter iron particles ıve optimum material from the work-piece to give best surface compared to iron particles of :r or smaller diameter. Reducing the diameter of abrasive particles increases the number of sive particles sandwiched between the iron particles. The magnetic force on an iron particle stributed among the adjacent abrasives. As the number of abrasives increases, the force per abrasive reduces i.e., lower is the force with which an abrasive particle indents on the work- e surface. So abrasive indentation is low and surface finish is smooth. There is no change in residual stress in the work-piece after MAF operation.

Dhirendra et al [16] studied the effect of electromagnet input voltage, working gap, RPM lectromagnet, and mesh number of SiC abrasive grains by mass on the surface finishing and erial characteristics in case of a ferromagnetic material. The experiments were designed using uchi's orthogonal array experimental design method. Forces, normal magnetic and tangential ing, were measured using a force transducer. They found that voltage and working gap are parameters that influence surface finish more than the RPM and the mesh number of abrasive.

Baron et al [17] applied MAF process to finish burrs created during drilling. They eloped a method to finish the internal surface of a drilled hole, both in case of ferromagnetic l non-ferromagnetic work-piece material. In work-pieces made of ferromagnetic material, burr ıoval is easier as the burrs act as concentrators of magnetic flux accumulating the magnetic ce lines in its domain. So the burr is removed faster in case of a ferromagnetic material.

4 Objectives of the present work

The columns of literature survey show that majority of the previous research was based the study of the effect of the various machining parameters on the surface roughness provement and material removal rate. Most of the work has been done in case of processes volving horizontal MAF operation. No in depth work has been done to quantize the forces nerated during the process of MAF. So the objectives of the present work are

1. To design and develop an experimental setup for vertical MAF operation.
2. To analyze the forces generated during MAF operation of non-ferromagnetic material. The non-ferromagnetic material taken for experimentation is brass.
3. To conduct the parametric analysis to study the effect of process parameters on the forces acting during MAF of non-magnetic material and to compare with the

forces generated on the magnetic materials during MAF under the same machining conditions.

Chapter 2

DESIGN OF EXPERIMENTAL SETUP

2.1 Introduction

In the present study of Magnetic Abrasive Finishing (MAF) process, an experimental setup has been designed and fabricated.

The setup has been designed keeping in view the fundamental principles of MAF operation. Since the purpose of the thesis has been to investigate the effects of the process parameters (discussed in section 2.15) on the forces acting on the work-piece in case of vertical operation, the main idea behind the design has been to

- have a vertical spindle with the electromagnet attached at its bottom,
- create the essential components to hold the spindle, and
- give drive to the spindle from a motor of desired ratings.

The setup consists of the following components:

1. Frame
2. Cylindrical electromagnet
3. Spindle, Spindle Housing, Housing caps
4. Housing Holder
5. Holder attachment to the face plate over the front sliders
6. Motor
7. Motor holding L-shaped holding device
8. Variable frequency drives (VFD) to control speed of the motors
9. Pulleys
10. Work-piece fixture
11. Dynamometer
12. D.C. Supply
13. PC with required DAC (data acquisition card) to acquire in-process data from the finishing process

2.2 Frame:

The frame was not designed for this setup. Instead a horizontal grinding machine frame was used as a frame for the setup. Some of the components of this machine used to hold the grinding wheel were modified to hold the spindle vertically and it's housing.

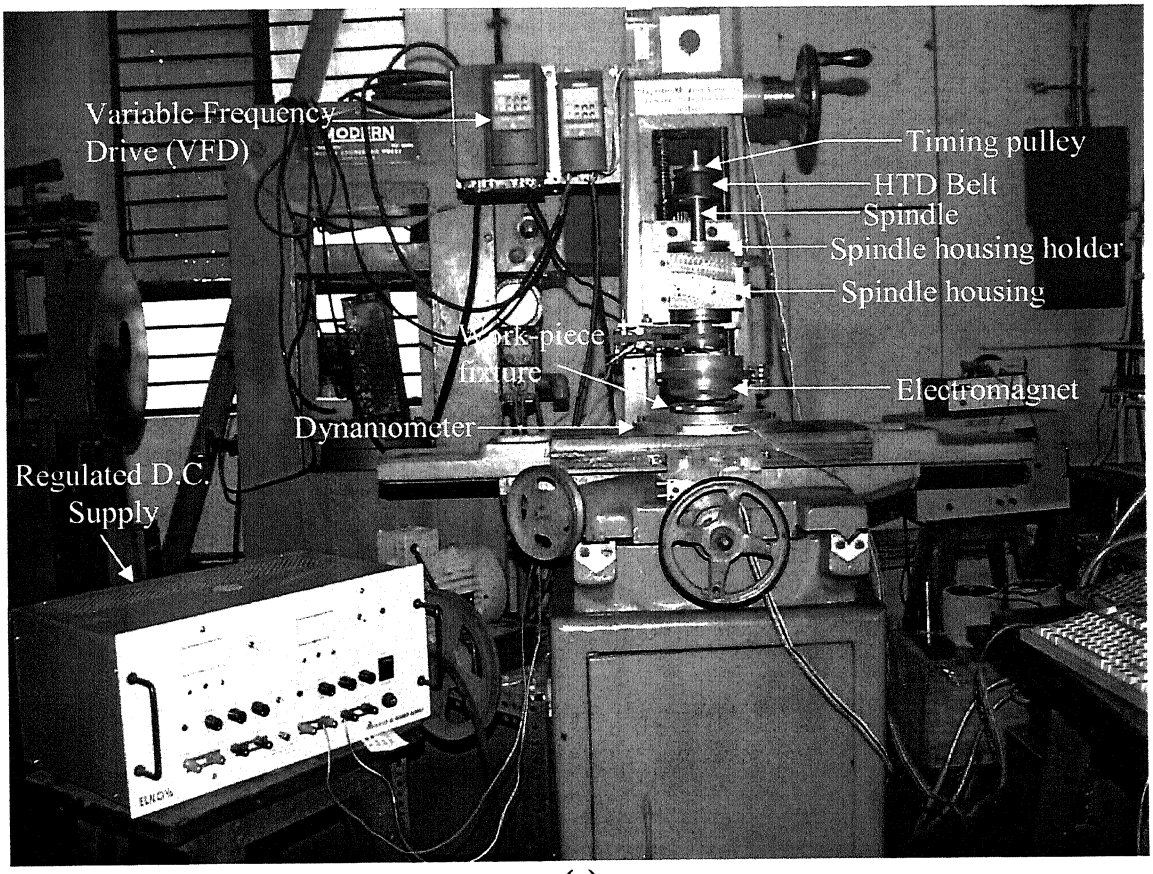

(a)

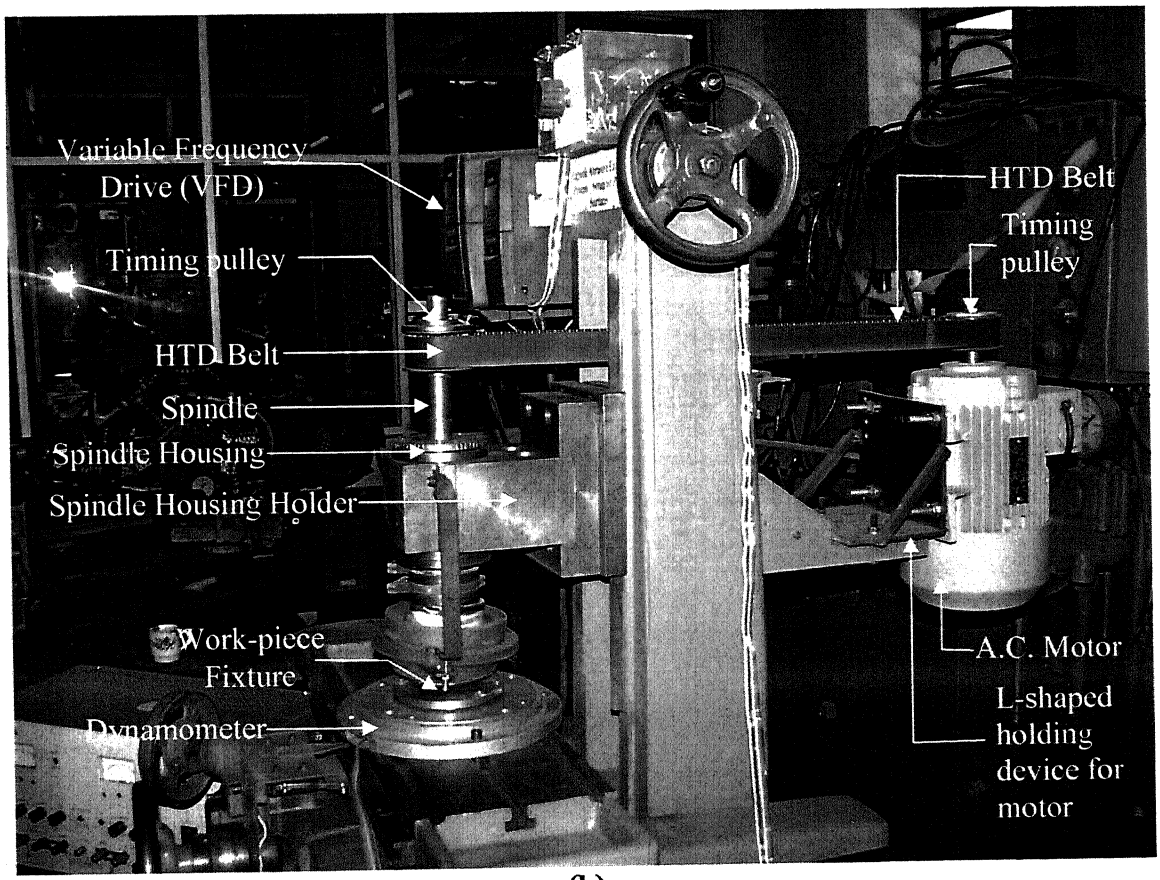

(b)

Figure 2.1 Photographs of the experimental setup: (a) Front View, (b) Side view

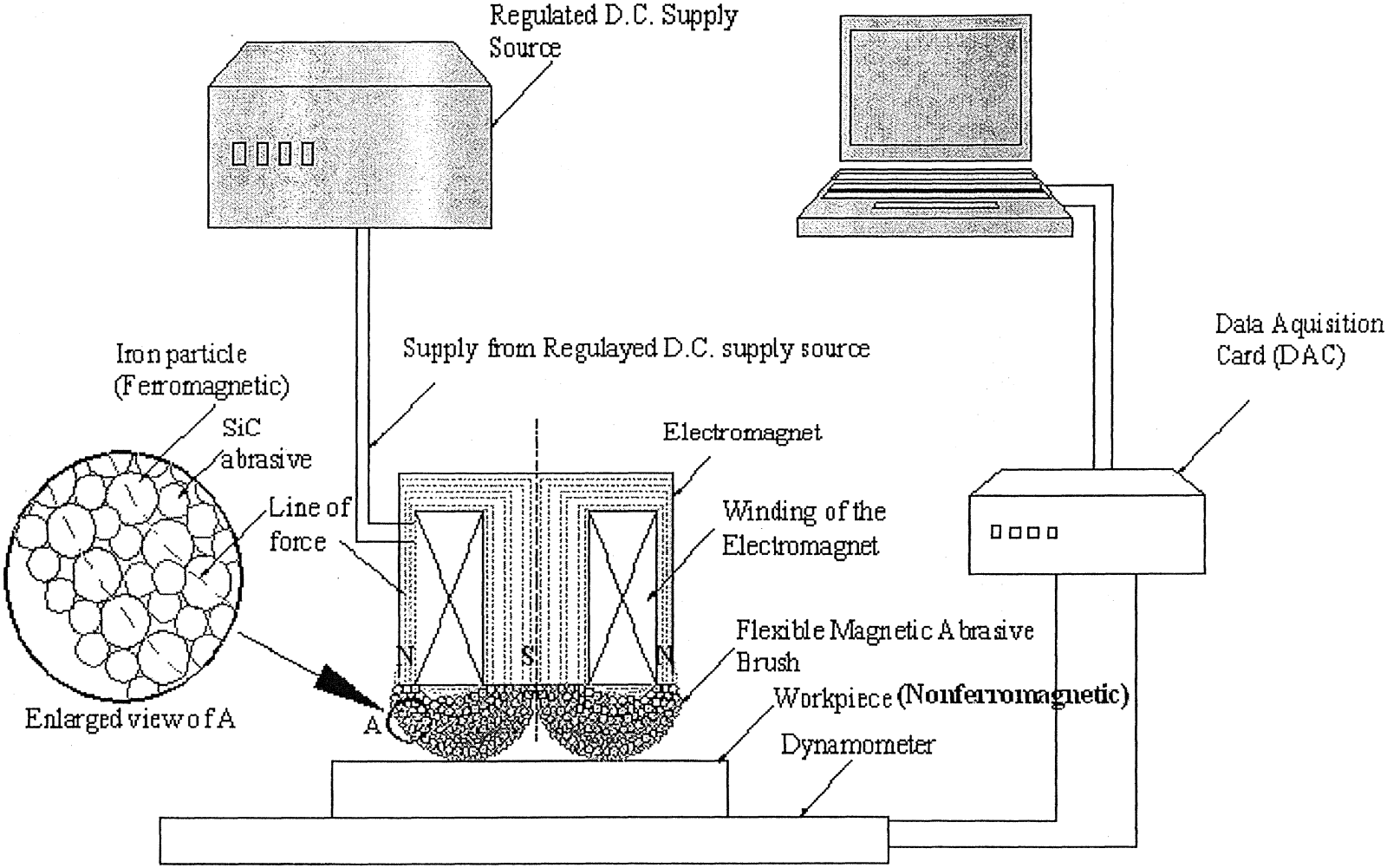

Figure 2.2 Schematic view of the vertical MAF setup used

The arrangements done in the grinder frame to install the MAF set up are as follows:

1. The housing for the spindle of the grinding wheel was a part of a cubical block. The housing and the block were one unit. The cubical portion of this single unit had a vertical lead screw running through it, which was used to give vertical motion to the unit. This unit was removed and a similar cubical block (Fig. 2.3) was fabricated without the grinder spindle housing part. This new part was made by casting and machining.

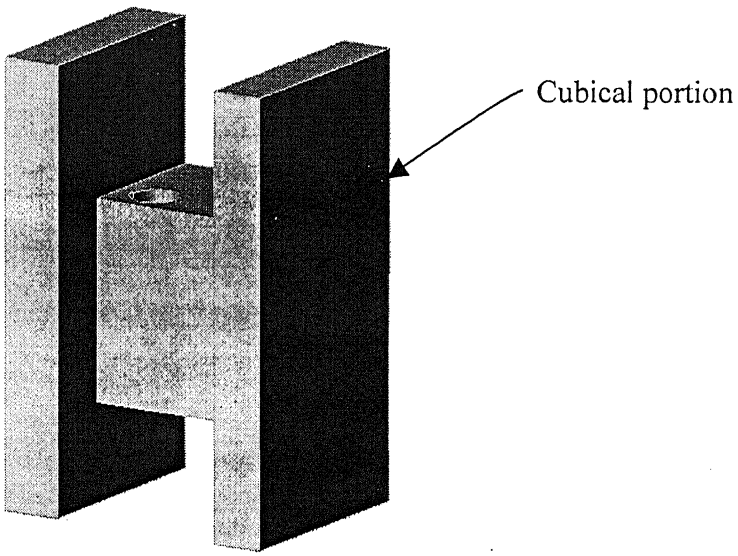

Figure 2.3 Fabricated cubical block (Part A)

2. The motor to give drive to the spindle is mounted on a L-plate (1st L-plate) in vertical position (Fig. 2.4). This L-plate is again mounted on a L-plate (2nd L-plate) situated on the back of Part A.

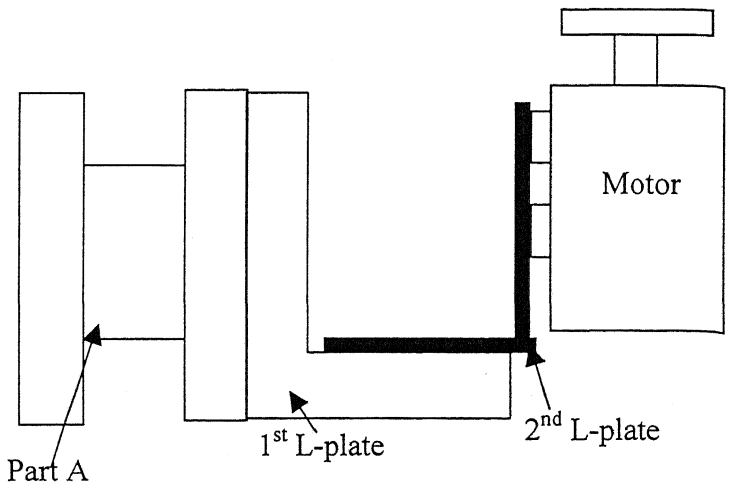

Figure 1.4 Schematic view of motor arrangement

3. The hand wheel to give horizontal (X) movement to the machine table was removed so that a pulley can be attached in its place. This was done to give X-feed to the table through a motor instead of doing manually. The control of table movement in X direction is required to give feed. The hand wheels meant for Y and Z motion were left as such. Both are done manually.

2.3 Cylindrical electromagnet:

The electromagnet used in the present set up is round and flat faced in shape. Diameter D_m =76 mm and height H_m =50 mm.

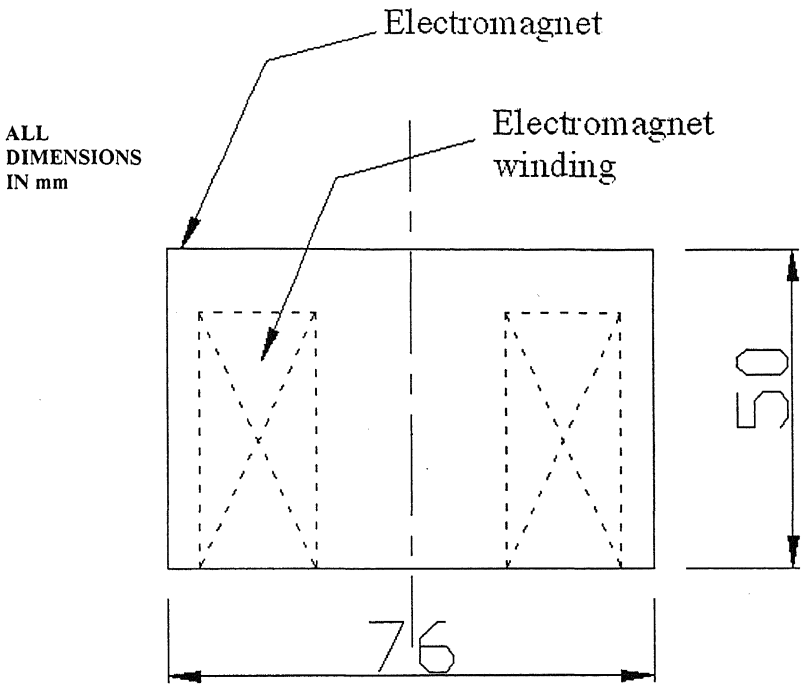

Figure 2.5 Round flat faced electromagnet

2.4 Spindle, spindle housing and housing caps:

2.4.1 *Spindle*

The spindle is the component that carries the electromagnet, and it is supported in a stepped cylindrical housing which is covered from the top and bottom by two housing caps. The spindle is made of stainless steel and the housing is made from cast iron. The spindle and the housing assembly are shown in Fig. 2.6 and 2.7.

The design was started from scratch, so it was not possible to conceive the motor specifications from the beginning itself and design rest of the components according to it. Hence the other approach for design was followed. First the dimensions of the parts were

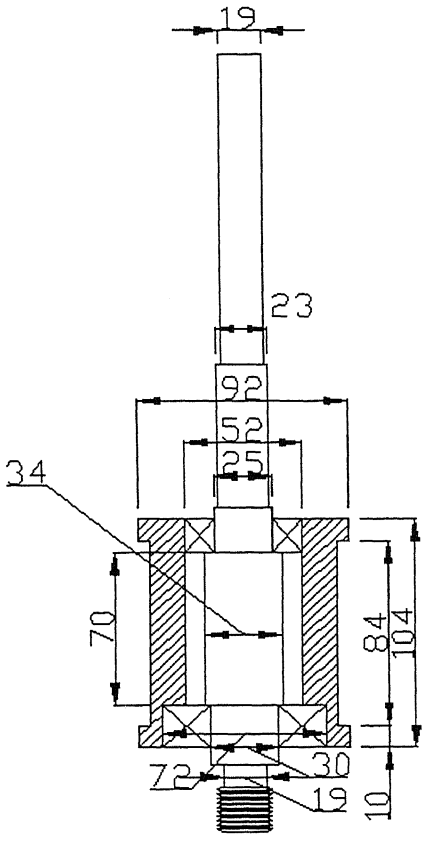

Figure 2.6 Schematic sectioned view of spindle and housing assembly

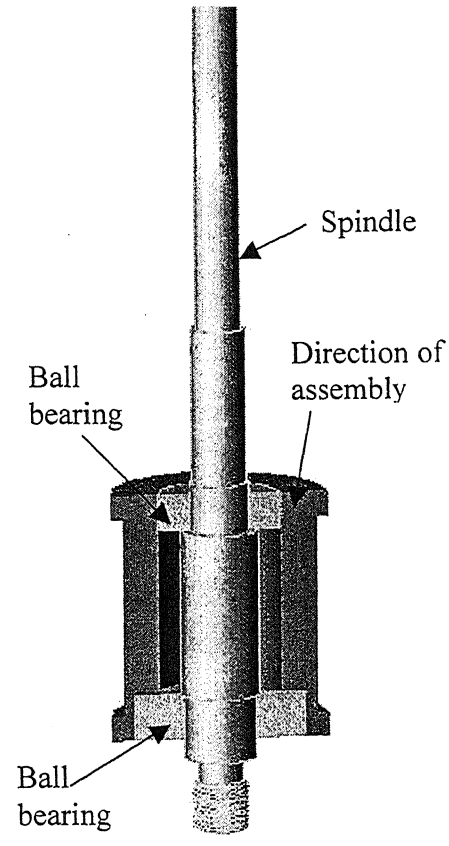

Figure 2.7 3D picture of the schematic view of spindle and housing assembly [housing and bearings sliced for clarity]

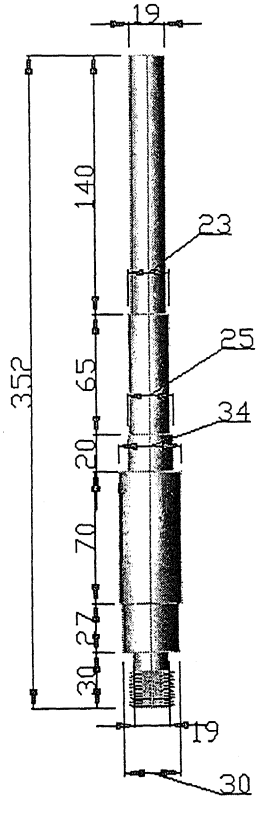

Figure 2.8 Spindle

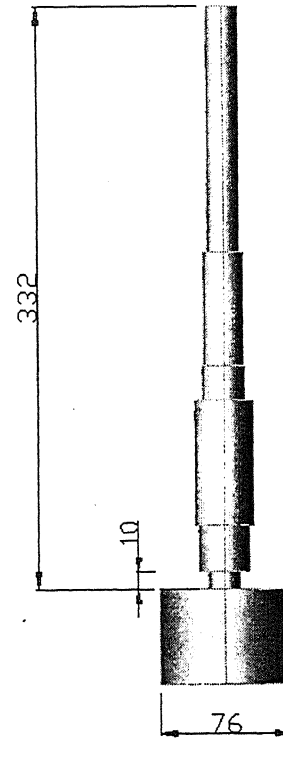

Figure 2.9 Spindle and electromagnet

decided and then a motor of required power was calculated out of them. Wherever any improvement or, reducing of dimensions, without creating any problem for the structure strength could be done, was implemented. Hence the spindle may not be safe under all generated loads at this stage. It can only be done after the motor power directly connected to it is used to calculate its dimensions. The housing can be however designed using the shape of the spindle. The spindle volume from Fig. 2.8 is

$$V_s = \frac{\pi}{4}\begin{bmatrix}(19^2\times140)+(23^2\times65)+(25^2\times20)\\+(34^2\times70)+(30^2\times27)+(19^2\times10)\\+(20^2\times20)\end{bmatrix} mm^3$$

$$= 234975.423 mm^3$$

$$= 234975.423\times10^{-9} m^3$$

Density of stainless steel, $\rho_s = 7800 kg/m^3$ [18].

Hence, weight of the spindle,

$$W_1 = V_s \times \rho_s \times g = 17.962N$$

Weight of the bearings used, $W_2 = 6.8N$ [23].

Weight of the electromagnet and the accessories on the spindle to give current supply to the electromagnet, $W_3 \approx 1.1kg = 10.780N$. Total weight of the spindle, electromagnet and accessories is, $W_4 = W_1 + W_2 + W_3 = 35.55N$.

The finishing force acting on the work-piece is the net resultant force required in the cutting direction of abrasives after overcoming all other forces, including the friction between the abrasives and the work-piece surface. This force will be more for a ferromagnetic material because in a ferromagnetic material the magnetic abrasives indentation will be deeper in their case due to attraction of ferromagnetic material. According to studies done by D.K. Singh [16], under the present conditions, the maximum value of this force for a ferromagnetic alloy steel EN8 is 61 N. So the force acting on magnet work-piece interface is

$$F = 61N.$$

So the torque required to rotate the magnet and cause finishing

$$T_1 = F \times R_m = 2.318 Nm$$

where, R_m=Radius of electromagnet=$\frac{D_m}{2}$ and D_m = Electromagnet diameter=76 mm.

The maximum RPM to be used for finishing, N_1=300 RPM [16].

Taking a factor of safety of 4 in case of torque and increasing the design speed to 1.5 times the minimum required value, it is got,

overall design torque, $T_2 = 4T_1 = 9.272N$,

and overall design RPM, $N_2 = 1.5N_1 = 500RPM$.

Hence design power, $P_1 = T_2 \times \omega_2 = T_2 \times \frac{2\pi N_2}{60} = 485.431$ W

A factor of safety of 4 has been taken in case of torque and 1.5 in case of speed. This is so because our requirement during finishing is both torque and constant speed, but the main requirement is torque. So by the design, it has been taken care that the motor should be able to generate the required torque first and speed will be maintained without slip.

So, P_1=485.431 W is the minimum power required to run the spindle during finishing.

2.4.2 *Housing*

The housing is designed on the basis of bearing and shearing stresses acting on it. A 3D schematic view and a orthographic view of the housing are shown in Fig. 2.10 and 2.11, respectively.

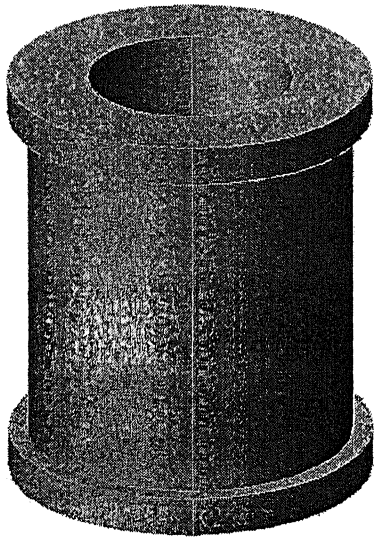

Figure 2.10 3D schematic view of spindle housing

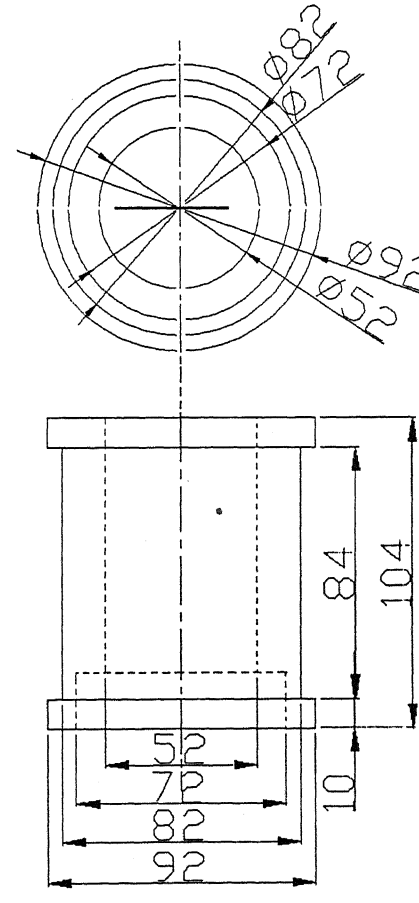

Figure 2.11 Orthographic view of spindle housing

The volume of the housing is

$$V_h = \frac{\pi}{4}\left[92^2 \times 104 - (92^2 - 82^2) \times 84 - 52^2 \times 104 - 72^2 \times 19\right] = 278332.5427 mm^3$$

The housing is made of cast iron and density of cast iron is $\rho_{CI} = 7200 kg/m^3$ [18].

Housing weight, $W_S = V_h \times \rho_{CI} \times g = 20N$.

The housing is supported at the upper stepped portion. It is supported in only one half of the stepped portion. So the load on this portion when the setup is fully assembled is = (self weight of the housing) + (weight of spindle and magnet) + (weight of metal caps)

2.4.3 *Caps or coverings for the housing*

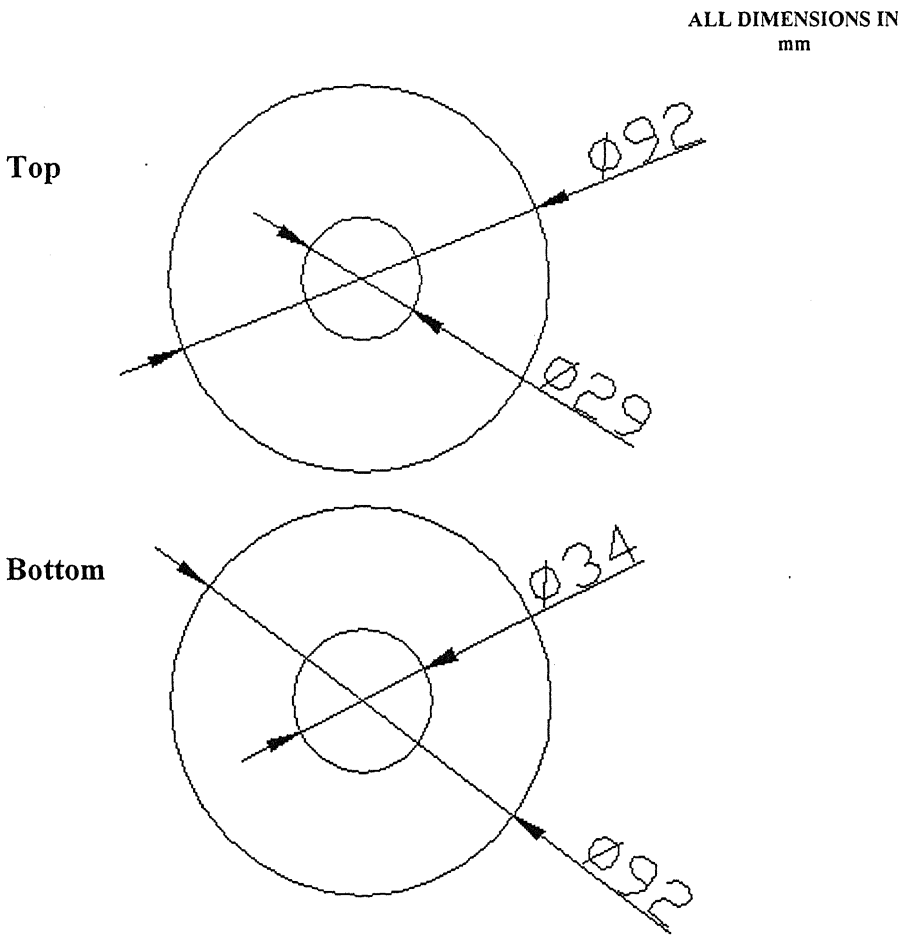

Figure 2.12 Spindle housing caps

The caps or coverings attached to the housing are for protection of the spindle and the bearings from the abrasive powder dust that flies off from the finishing zone and deposits on the things nearby. This abrasive dust can wear the bearing balls. So the coverings are provided.

The caps are two stainless steel disks of 6 mm thickness and 92 mm diameter each. Each carries a through hole at the center. The top cap has a hole of 29 mm diameter and the bottom cap which is adjacent to the electromagnet, has a hole of 34 mm diameter.

The weights of the two caps are

Top cap weight, $W_6 = \left\{\frac{\pi}{4}\times(92^2-29^2)\times 6\times \rho_S \times g\times 1\times 10^{-9}\right\} = 2.75N$ and

Bottom cap weight, $W_7 = \left\{\frac{\pi}{4}\times(92^2-34^2)\times 6\times \rho_S \times g\times 1\times 10^{-9}\right\} = 2.64N$.

2.4.4 *Design of the spindle housing*

Only one half of the stepped portion of the housing supports on the housing holder. The housing is held by the housing holder where one half of the housing is in touch with the major portion of the holder and the other half is with the smaller portion of the holder, the cap of the housing holder (Fig. 2.16). The housing holder is built such that the cap of the holder is a little bit smaller in height than the main part. So when the spindle housing is kept in the holder during assembly, the entire load of the housing is taken by the main part of the holder and the covering is just to grip the housing to keep it in place.

So load on the bearing area of the housing is

W_8 = (Self weight) + (weight of the electromagnet and its accessories) + (weight of the housing caps)

$= W_4+W_5+W_6+W_7$

=(20+35.55+2.75+2.64)N

=60.94N

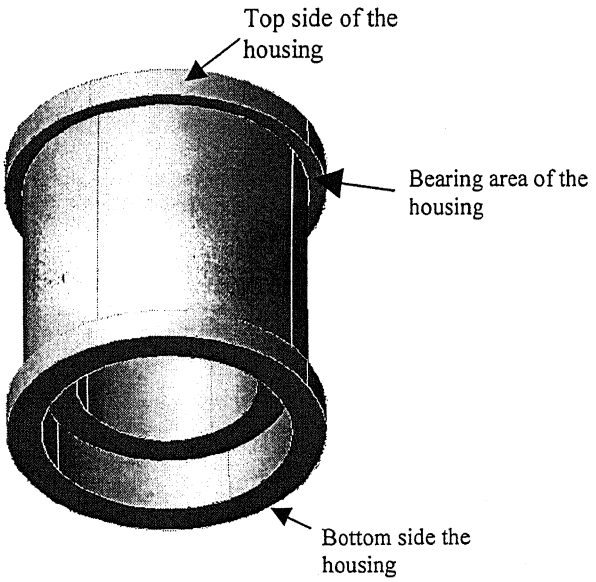

Figure 2.13 Bearing area of the housing

The bearing area is as shown in Fig. 2.13. The bearing stress acting on the bearing area is

$$f_{bh} = \frac{W_8}{\text{Bearing area}} = \frac{60.94}{\left\{0.5 \times \frac{\pi}{4} \times (92^2 - 82^2) \times 10^{-6}\right\}} = 8409.457 Nm^{-2}.$$

The ultimate compressive strength of cast iron is 750 MNm^{-2} [18]. So the housing is safe under the bearing load W_8. W_8 is acting on the shearing area of the housing. The area of the housing under shearing load is shown in Fig. 2.14.

The shearing stress induced in the shearing area of the housing is

$$f_{sh} = \frac{W_8}{\text{Shearing area}} = \frac{60.94}{\pi \times 92 \times 10 \times 10^{-6}} = 21084.568 Nm^{-2}.$$

The ultimate strength of cast iron in tension is 150 MNm^{-2} [18] and so its ultimate strength in shear would be

$$= 1.3 \times 150 MNm^{-2} = 195 MNm^{-2}.$$

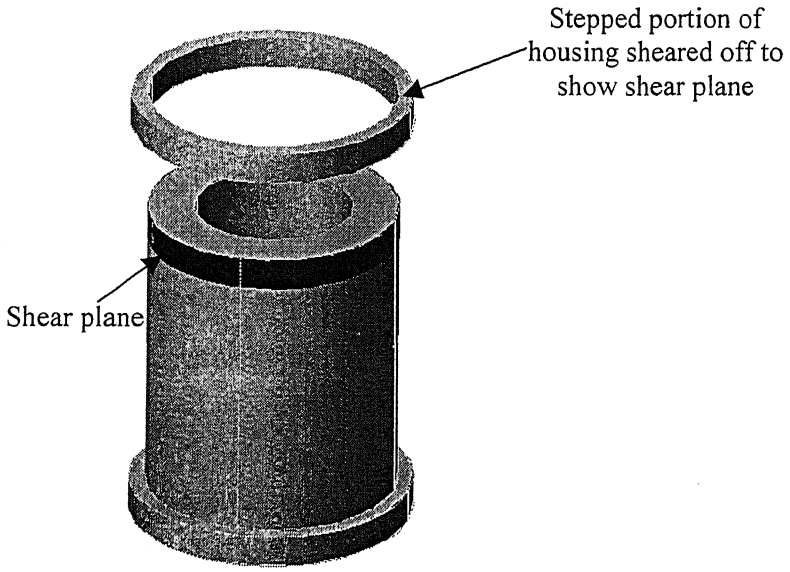

Figure 2.14 Shear plane in the housing

So the housing is safe under the shear load acting on it.

The tensile stress acting on the housing is

$$f_{th} = \frac{W_8}{\text{Area under tension}} = \frac{60.94}{\pi \times (82^2 - 52^2) \times 10^{-6}} = 4825.324 Nm^{-2}.$$

So the housing is safe under the action of tensile load also.

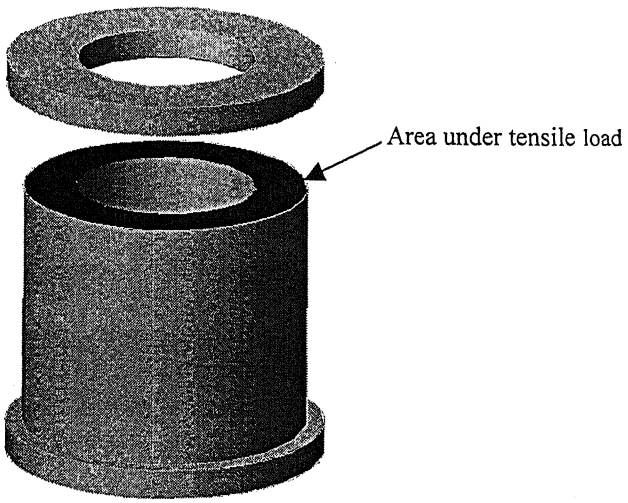

Figure 2.15 Area in the housing under tension

2.5 Spindle housing holder and holding device for housing holder:

The spindle housing holder is the device that holds the spindle housing and keeps it in rigid upright position so that MAF operation can be done. The housing holder is again held by another device to keep it straight and this holding device connects the spindle, its housing and the housing holder with the structure of the machine. The arrangement of the two holding devices is shown below.

2.5.1 *Design of spindle housing holder*

W_8, acting at the tip of the housing holder, tries to bend the spindle housing holder. So the spindle housing holder is designed like a cantilever beam. The shear stresses induced in various sections of the housing holder are calculated and the corresponding bending moment is found out. Then the bending stress in the critical section is checked to see if the housing holder is safe under the acting stress at that particular section.

Self weight of the housing holder

$$= \left\{128\times84\times118-\frac{\pi}{4}\times82^2\times84\right\}\times10^{-9}\times\rho_{CI}\times g = 58.281N.$$

Hence, weight per unit length of the housing holder,

$$s_w = \frac{\text{Self weight of the housing holder}}{\text{length}} = \frac{58.281}{118} = 0.494Nmm^{-1}$$

The pattern of load acting on the housing holder is shown in Fig. 2.18.

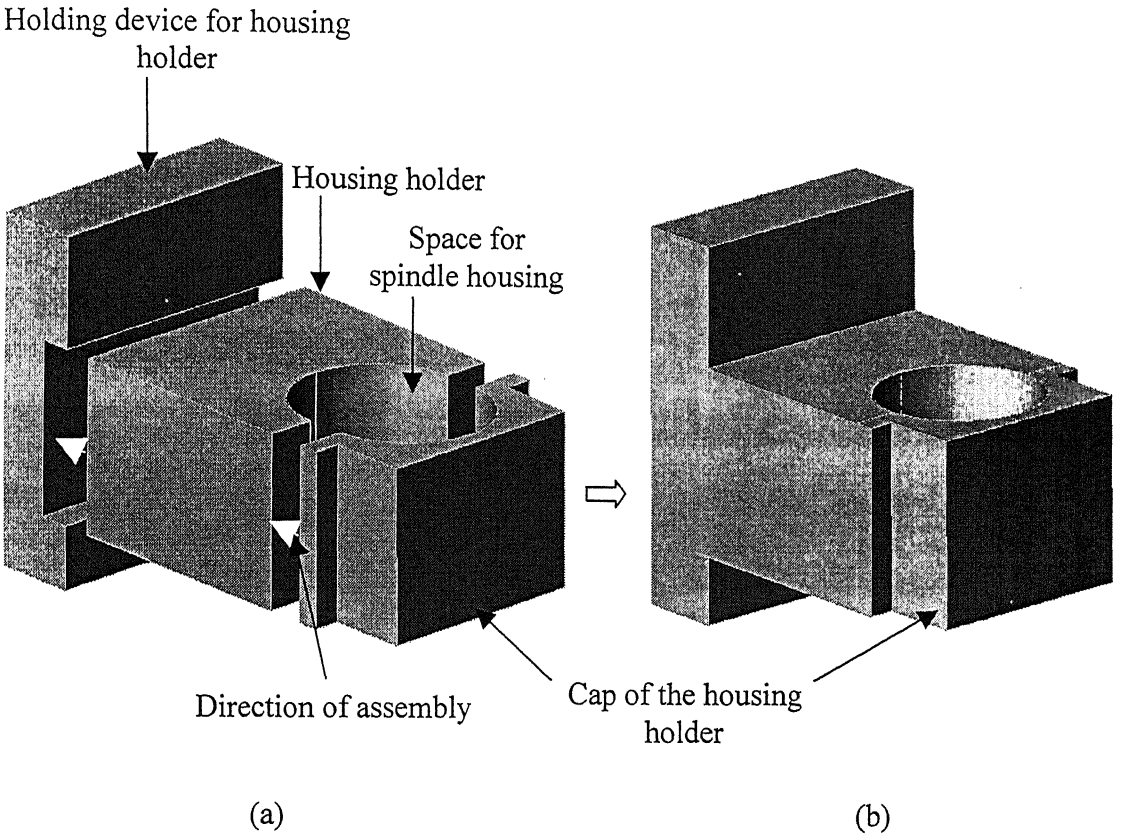

Figure 2.16 (a) Spindle housing holder and the holding device for the housing holder, before assembly (b) The three components assembled

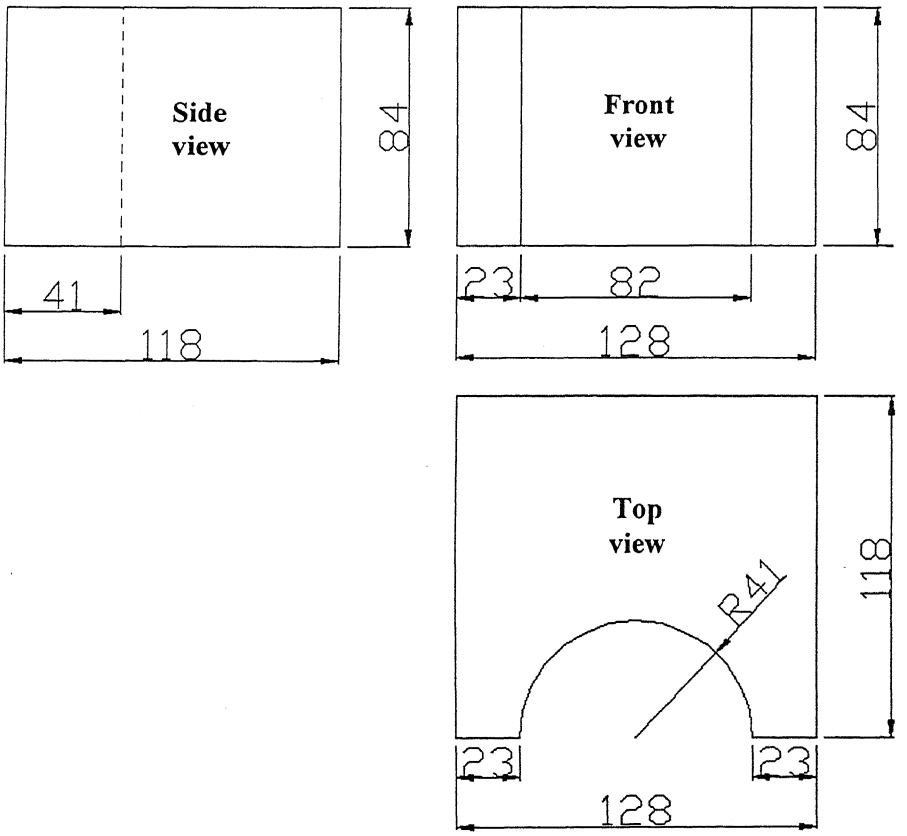

Figure 2.17 Orthographic view of the housing holder

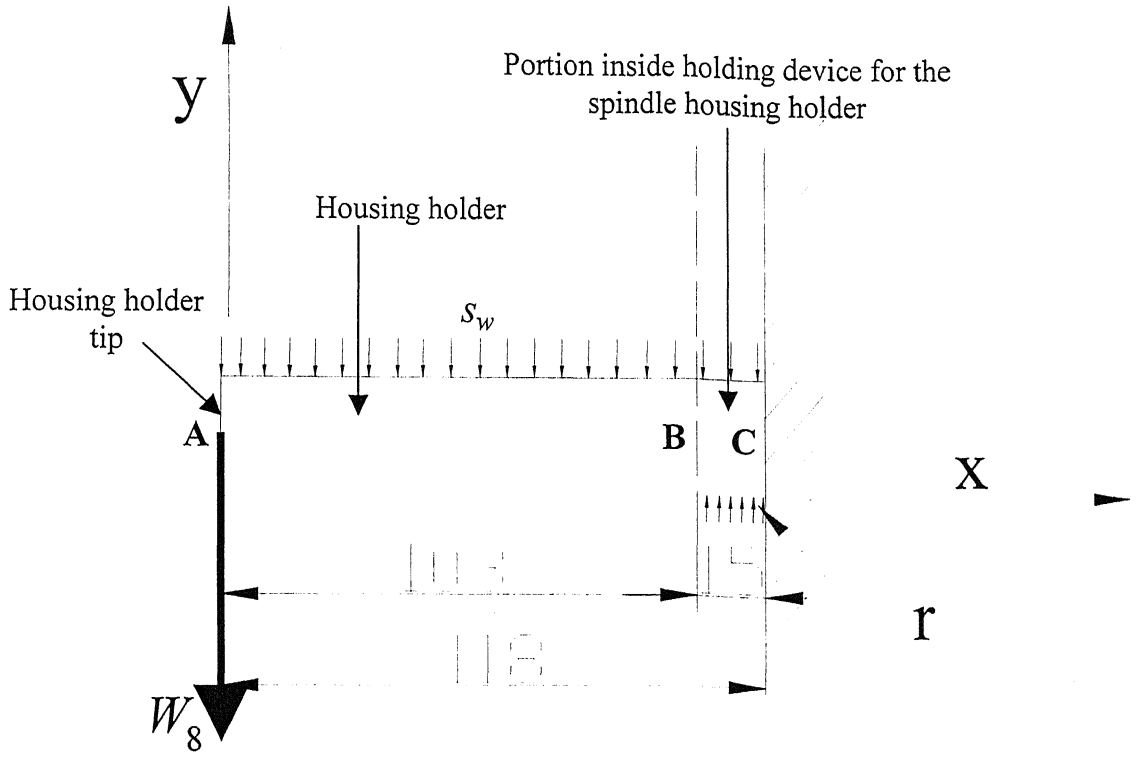

Figure 2.18 Schematic view of the loads acting on the spindle housing holder

As shown in the diagram above,

s_w = weight per unit length of the spindle housing holder = $0.494 Nmm^{-1}$

and r = bearing resistance to the spindle housing holder per unit length (acting on that portion of the holder which lies inside the holding device for the housing holder).

At any section between points A and B,

the shear force is $F_x = -W_8 - s_w x$

and the Bending moment, $M_x = -W_8 x - \frac{s_w x^2}{2}$.

At any section between point B and C, the shear force is $F_x = r(x-103) - W_8 - s_w x$ and the bending moment is $M_x = \frac{r(x-103)^2}{2} - W_8 x - \frac{s_w x^2}{2}$.

Taking moment about point 'C', we have, $\sum M = 0$, i.e.,

$$\frac{r(118-103)^2}{2} - W_8 \times 118 - \frac{s_w \times 118^2}{2} = 0$$

and from the above equation, we get,

r=94.254 Nmm^{-1}.

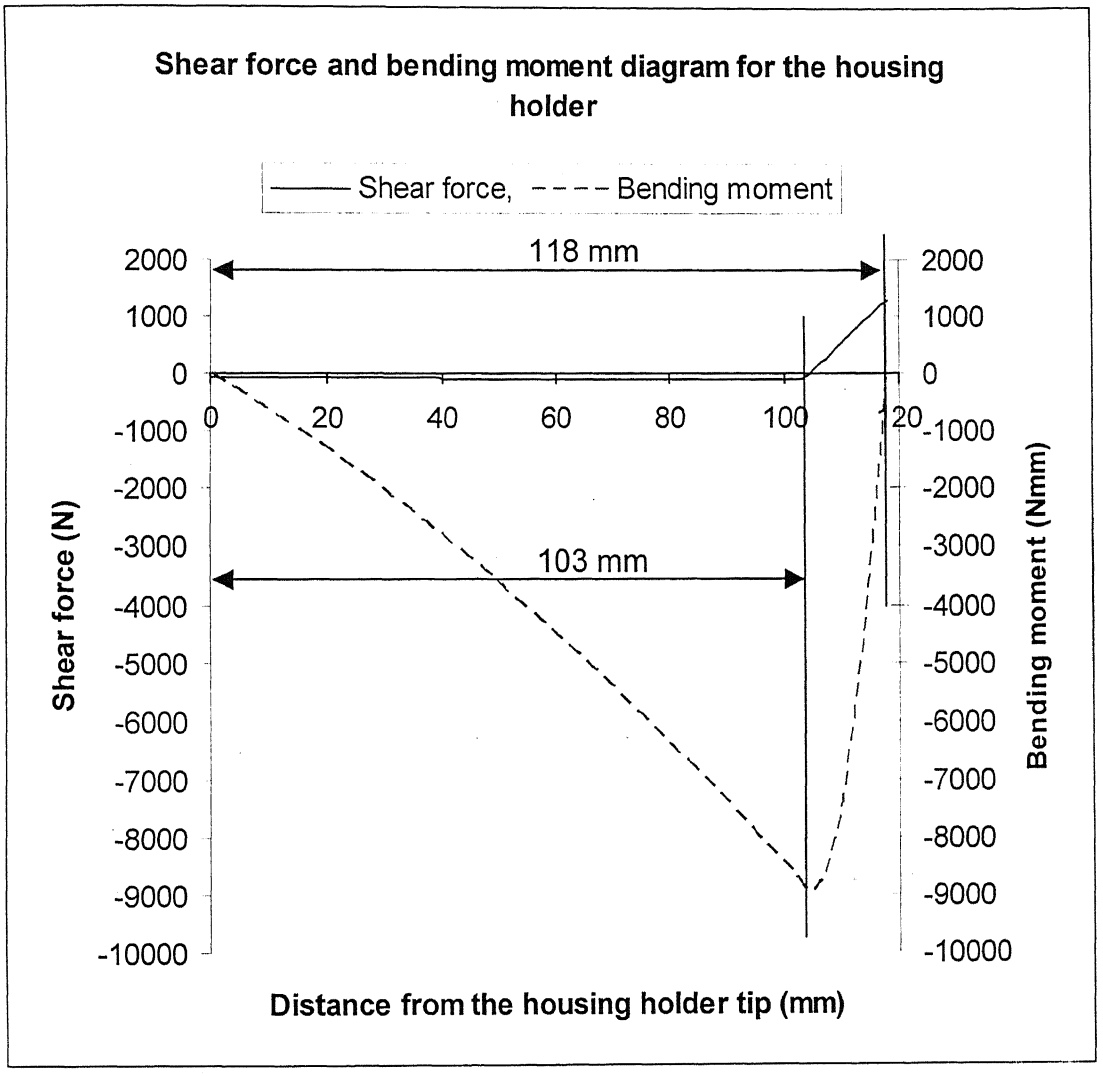

Figure 2.19 Shear force and Bending moment diagram for the housing holder

The maximum shear force and the maximum bending moment calculated are $1294.578N$ and $8.897Nm$ respectively at a distance of 118 mm and 103 mm from the spindle housing holder tip. Hence, the maximum shear stress induced at the section, 118 mm from the tip, is

$$f_{sshh} = \frac{1294.578}{128 \times 84 \times 10^{-6}} = 0.12MNm^{-2},$$

which is quite less than $195MNm^{-2}$, the ultimate strength of cast iron in shear [18]. The maximum bending moment induced is

$$\sigma_{max} = \frac{8.897}{z} = \frac{8.897}{\frac{128 \times 84^3 \times 10^{-9}}{6}} = 0.7MNm^{-2},$$

which is quite less than $150MNm^{-2}$, the value of ultimate strength of cast iron [18].

2.5.2 *Deflection calculations of the spindle housing holder*

There would be deflection in the spindle housing holder due to the acting loads. The equation [27] for bent curvature of a cantilever after application of load is

$$\frac{d^2y}{dx^2} = -\frac{M}{EI}$$

$$\text{or, } EI\frac{d^2y}{dx^2} = -M\,.$$

where, E is the Elastic Limit of the cantilever beam and I is the Moment of inertia of the beam section.

So for a section between the points 'A' and 'B', the equation becomes

$$EI\frac{d^2y}{dx^2} = W_8x + \frac{s_w x^2}{2}$$

$$\Rightarrow EI\frac{dy}{dx} = \frac{W_8x^2}{2} + \frac{s_w x^3}{6} + C_1$$

$$\Rightarrow EIy = \frac{W_8x^3}{6} + \frac{s_w x^4}{24} + C_1x + C_2$$

Putting $\frac{dy}{dx}$=0 for x=103, we get $C_1 = -736480.316 Nmm^2$ and by putting y=0 for x=103, we get $C_2 = 62442336.34 Nmm^3$. So the equation for deflection becomes

$$EIy = \frac{W_8x^3}{6} + \frac{s_w x^4}{24} - 736480.316x + 62442336.34\,.$$

Maximum deflection is at the tip of the housing holder, i.e., when x=0. Hence the maximum deflection got is

$$y = \frac{62442336.34}{EI} = 0.227mm\,.$$

The value of y is small. In the above equation, the value of E for cast iron [18] and the value of I [21] used are

$$E = 43.5MNm^{-2} = 43.5Nmm^{-2}$$

$$\text{and } I = \frac{bh^3}{12} = \frac{128\times 84^3}{12} = 6322176mm^4\,.$$

2.5.3 *Holding device for the spindle housing holder*

The loads acting on the holding device for the housing holder are

- Bearing load due to the weight of the housing holder on the slot base (ABFE)

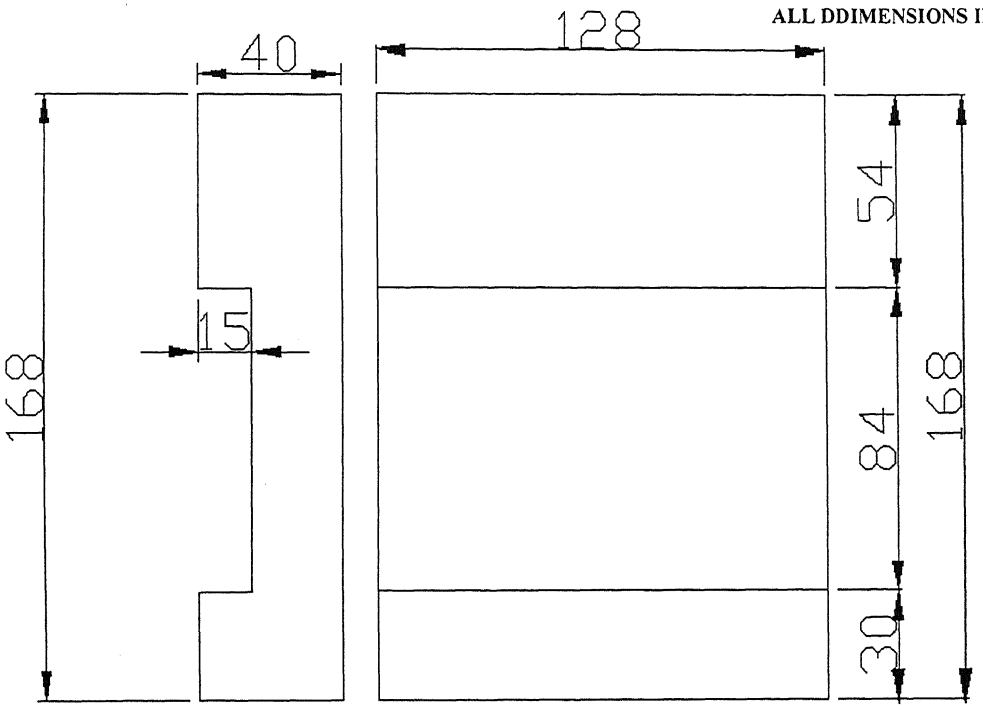

Figure 2.20 Orthographic view of the device for holding the spindle housing holder

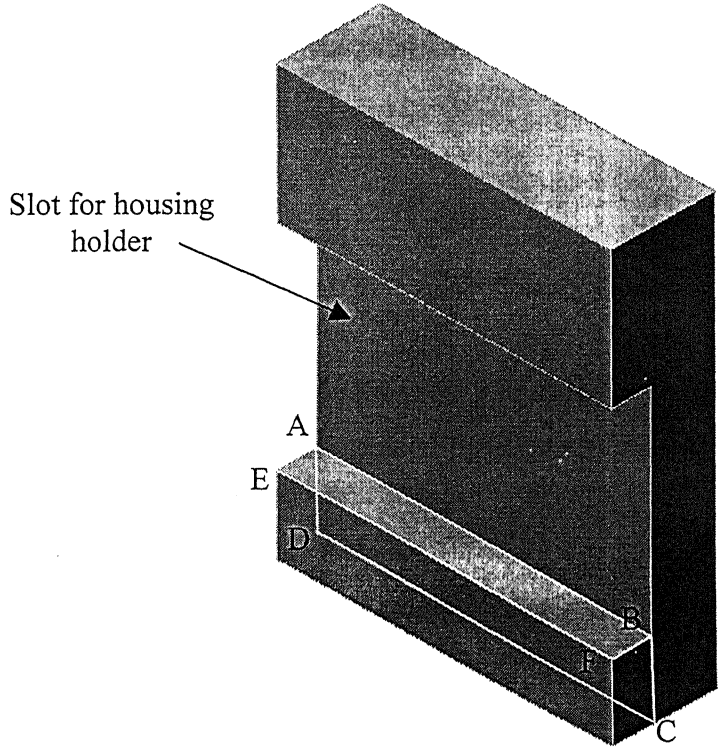

Figure 2.21 Areas stressed in the device for holding the housing holder

- Shearing load due to the housing holder on the area (ABCD)

Bearing load = bearing load per unit length (r) × length of the bearing area

= r×15=1413.810N

$$\text{Bearing stress} = \frac{1413.810}{\text{Bearing area}} = \frac{1413.810}{15\times128} = 0.74 MNm^{-2}.$$

So bearing stress is lesser than $750\,MNm^{-2}$, the ultimate bearing stress of cast iron [18].

$$\text{Shearing stress} = \frac{1413.810}{\text{Shearing area}} = \frac{1413.810}{30\times128} = 0.37 MNm^{-2}$$ which is less than $195\,MNm^{-2}$, the ultimate stress of cast iron in shear [18]. Thus, the holding device for the housing holder is safe.

2.6 Rotation to the spindle through motor:

As stated earlier, the AC motor is chosen on the basis of torque output. Earlier it has been calculated out that the design torque value is $T_2 = 9.272N$. So the motor chosen is a 2 HP motor that gives a rated torque of 10 Nm. The motor is chosen keeping in view the considerations of torque requirement, weight and cost effectiveness.

The specifications of the motor are

Siemens make 3 ∅ squirrel cage induction motor,

Power	1.5 kW (2 HP)
RPM	1420
Power factor	0.81
Rated torque	10 Nm
No of poles	4
Weight	15.6 kg

230 V Δ / 400 V Y 50 Hz or 460 V Y 60 Hz

2.7 L-plate supporting the motor:

The motor, though is a motor meant for horizontal application, has been mounted vertical. It is supported at the back of the setup frame by a L-plate whose 3-D schematic view is given in Fig 2.22 and its orthographic views are given in Fig. 2.23. Two square sectioned steel rod cut pieces are used to give additional support to this supporting L-plate.

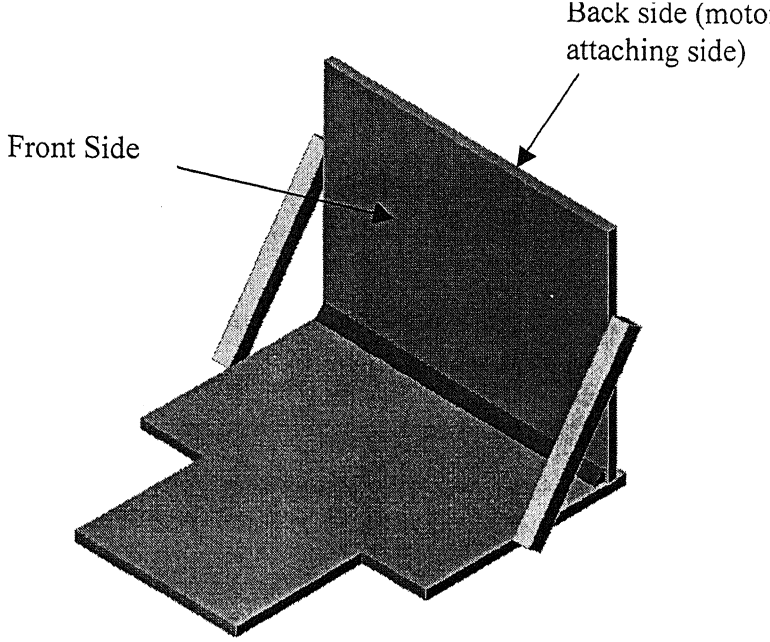

Figure 2.22 3D view of the motor supporting L-plate

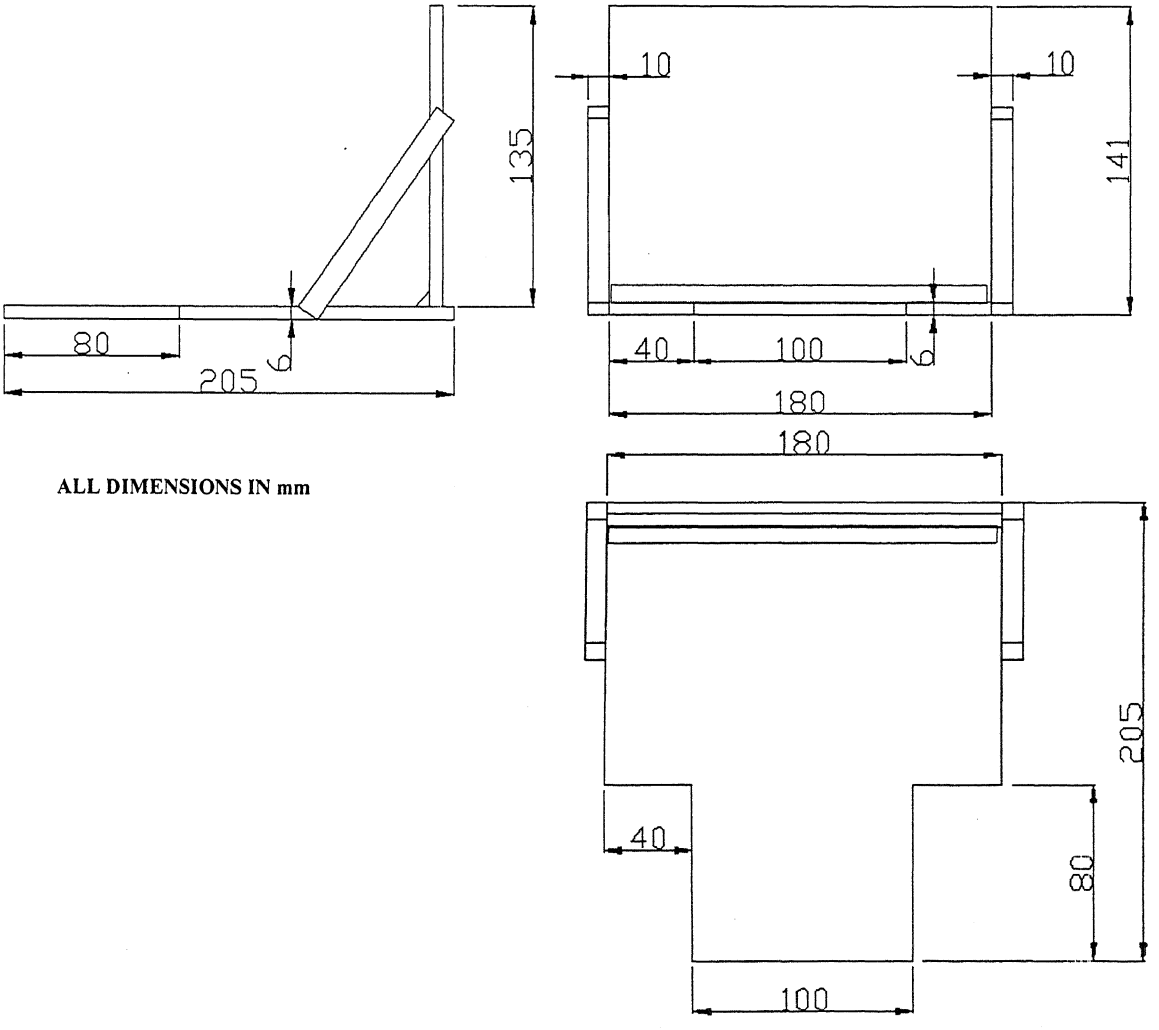

ALL DIMENSIONS IN mm

Figure 2.23 Orthographic view of the L-plate

2.8 Pulley for transferring power from motor to spindle:

Timing belt and pulleys are used to transmit power from the motor to the spindle. Timing belt is a toothed belt having corresponding matching teeth on the pulley so that the valley of one matched with the crest of the other. A timing belt drive system is similar to a gear drive system and offers no slip. Timing belts are used to transfer very high torque and these belts are fabricated to withstand more stress than normal high power V-belts or flat pulley belts. In addition, due to the elimination of slip, timing belt and pulley system is considered very accurate. Thus timing belt drive is also termed as HTD (high tension drive).

The calculated length between the electromagnet spindle axis and the motor spindle axis is $L = 616.8mm$. Taking dimensional requirements in consideration, timing belt and pulleys chosen are:

Pulley

Martin 8M 30 675-599 HTD pulley – 2 in no.

Pitch	8 mm
Belt width	30 mm
Number of teeth	24
Pitch diameter	61.12 mm

Belt

Gates Powergrip HTD belt 1440 8M 30 338-4957

Pitch	8 mm
Belt width	30 mm
Length	1440 mm

For centre distance $L = 616.8mm$ and pulley of diameter 61.12 mm, the length of belt required

$$= (2 \times \pi \times \frac{61.12}{2} + 2 \times 616.8)mm = 1425.614mm.$$

The tension of the belt is taken care by an idler. The idler serves two purposes in the setup.

- The position of the motor spindle and the electromagnet spindle is such that if they be connected directly by a belt, then the belt path will be

obstructed by the lead screw meant for moving the central cubical block (Part A, Fig. 2.3) up and down.

- The idler keeps the belt straight along its path and prevents it from flapping.

Torque being transmitted by the pulley = torque supplied by the motor

= 10 Nm.

If T is the torque supplied by the motor, then $T = F_e \times r_p$

where, F_e is the effective tension in the belt and r_p is the radius of the pulley.

Hence, $F_e = \frac{T}{r_p} = \frac{10}{\left(\frac{61.12}{2\times1000}\right)} = 327N$.

The smallest section of the belt is of thickness 2.6 mm. Hence, the stress induced in the smallest section of the belt due to the effective tension is

$$= \frac{F_e}{area} = \frac{327}{2.6\times30\times10^{-6}} = 4.192MPa$$

which is less than 8.5 MPa, the average ultimate strength for typical rubber belts [18].

Shear stress induced in the pulley due to the torque,

$$\tau_p = \frac{16Td_o}{\pi(d_o^4 - d_i^4)} = \frac{16\times10\times61.12\times10^{-3}}{\pi(61.12^4 - 19^4)} = 0.23MPa$$

which is less than 195 MPa, the ultimate strength of cast iron in shear [18].

'd_o' and 'd_i' are the external and internal radii of the pulley. The internal radius is equal to the diameter of the spindle. The value of the shear stress for both the pulleys is same because both the pulleys are of same dimensions and same bore (since, the spindle for electromagnet and the shaft of the motor are of the same diameter).

2.9 Validation of spindle shaft design:

The shaft has to be shown to be safe under the axial, bending and torsion load acting on it at different sections. A schematic diagram of the spindle and pulley assembly is shown in Fig. 2.24. Smallest section of the spindle is in the section 'AB' and at 'C'. At these points, the spindle is of diameter 19 mm.

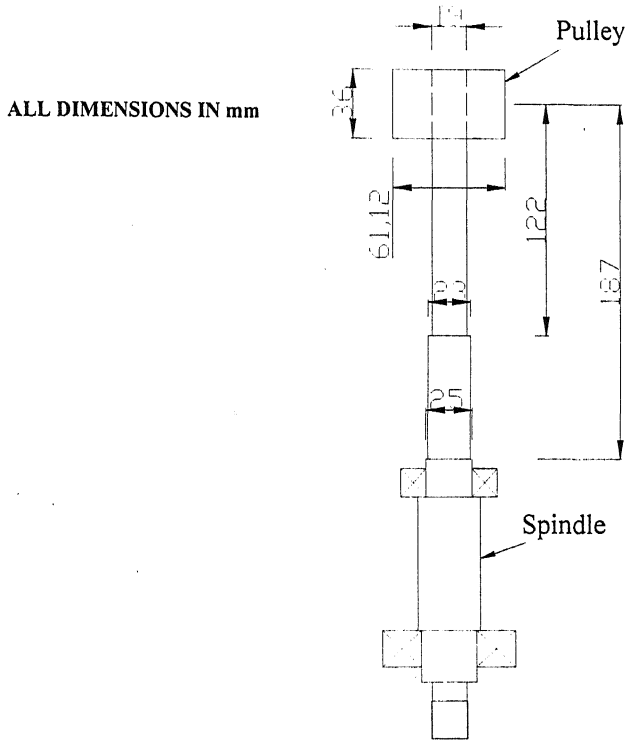

Figure 2.24 Schematic view of spindle and pulley assembly

The overall loads acting on the spindle are

- Torque $T = 10$ Nm transmitted by the pulley to the spindle
- A pulley of weight $W_p = 5N$ (axial load)
- Bending caused by the pull of the belt $F_e = 327$ N

On the top side, the critical section is at point 'B'. So the shear stress induced at this section due to combined effect of torque, axial load and bending

$$(f_s)_{\max} = \left\{ \left[\frac{16T}{\pi d_s^3} \right]^2 + \frac{1}{4} \left[\frac{32M}{\pi d_s^3} + \frac{4F_a}{\pi d_s^2} \right]^2 \right\}^{\frac{1}{2}} \qquad [18]$$

where T = torque = 10 Nm

M = the bending moment = $F_e \times 122 \times 10^{-3}\, Nm$

F_a = axial load = W_p

d_s =spindle diameter=19 mm

The value of shear stress calculated is $(f_s)_{\max} = 30.55$ MPa which is less than 55 MPa, the design shear stress value of a steel shaft [18].

2.10 D.C. voltage supply to the magnet:

The electromagnet uses D.C. current to generate magnetic field. A regulated D.C. power supply source (Make: ELNOVA) is used to supply different voltages and currents.

2.11 Frequency drive:

A frequency drive is used to control the speed of the motor. The specification of the frequency drive is

Siemens make 4th Generation Micro Master Vector Drive

Variable frequency Drive

Series : MM440

Capacity : 2 HP

Input : Single Phase , 200V to 240VAC

Output : 3 phase

2.12 Dynamometer:

The forces developed during MAF process are measured using a ring dynamometer. The dynamometer has been designed, fabricated and calibrated according to standard procedures. It has two Wheatstone full bridge circuits, one for measuring normal thrust force and the other for tangential cutting force. Each of these two circuits uses 8 strain gauges (120 Ω each). The resistances meant for measuring normal force are bonded onto the rim edge to the dynamometer and those for cutting force measurement, are bonded onto the hub. The schematic view of the dynamometer and the calibration curves are shown in Fig. 2.28, 2.29, 2.30.

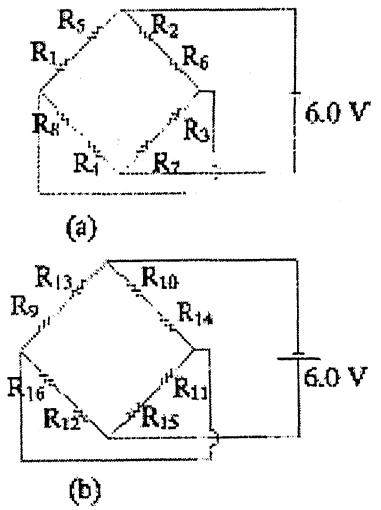

Figure 2.25 Strain gauge configurations in the dynamometer: (a) normal magnetic force, (b) cutting force

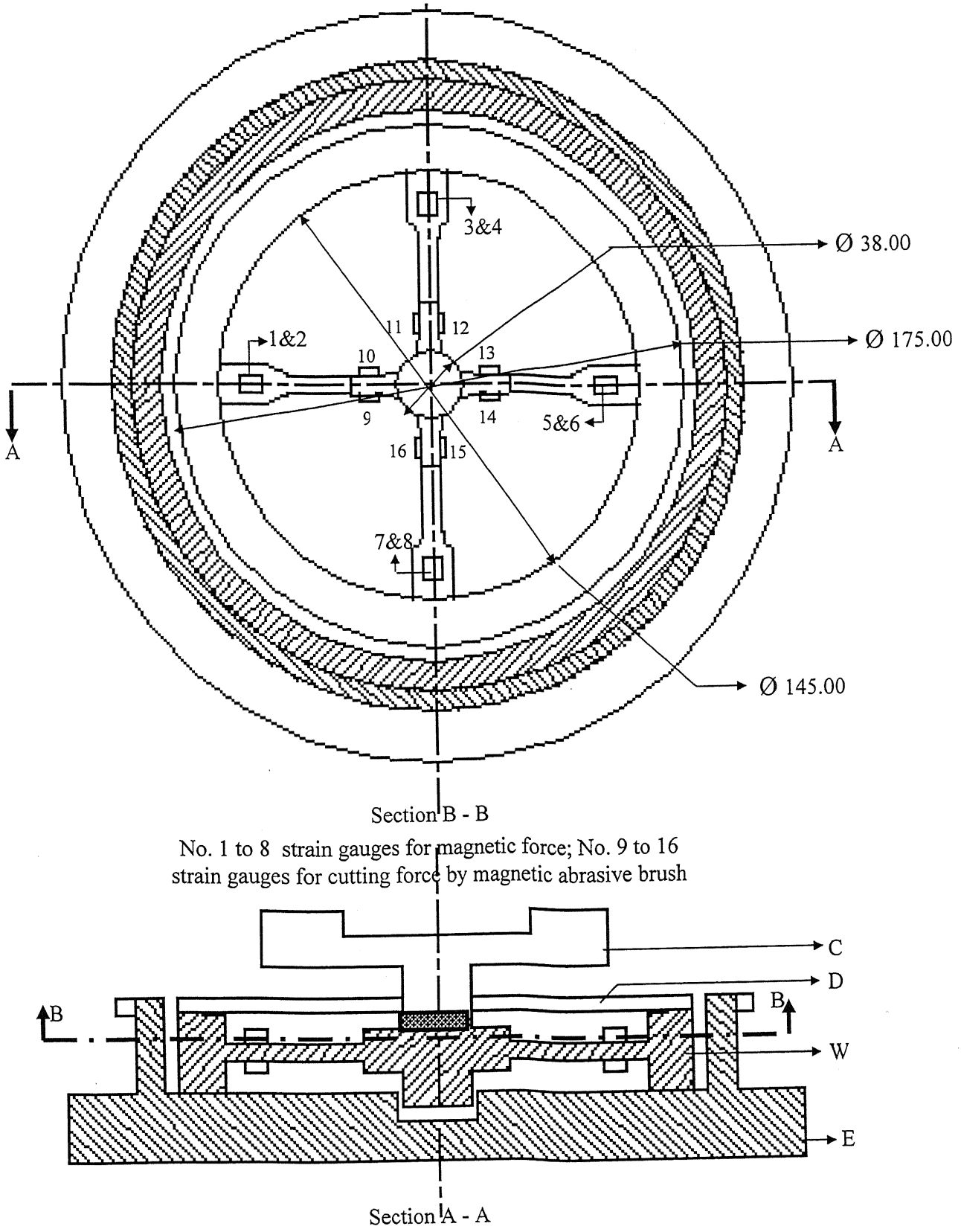

Figure 2.26 Schematic View of Ring Dynamometer (Resistance type force transducer) C: work-piece fixture; D: cover plate; W: dynamometer wheel (Material: M.S.); E: Base Plate (Al)

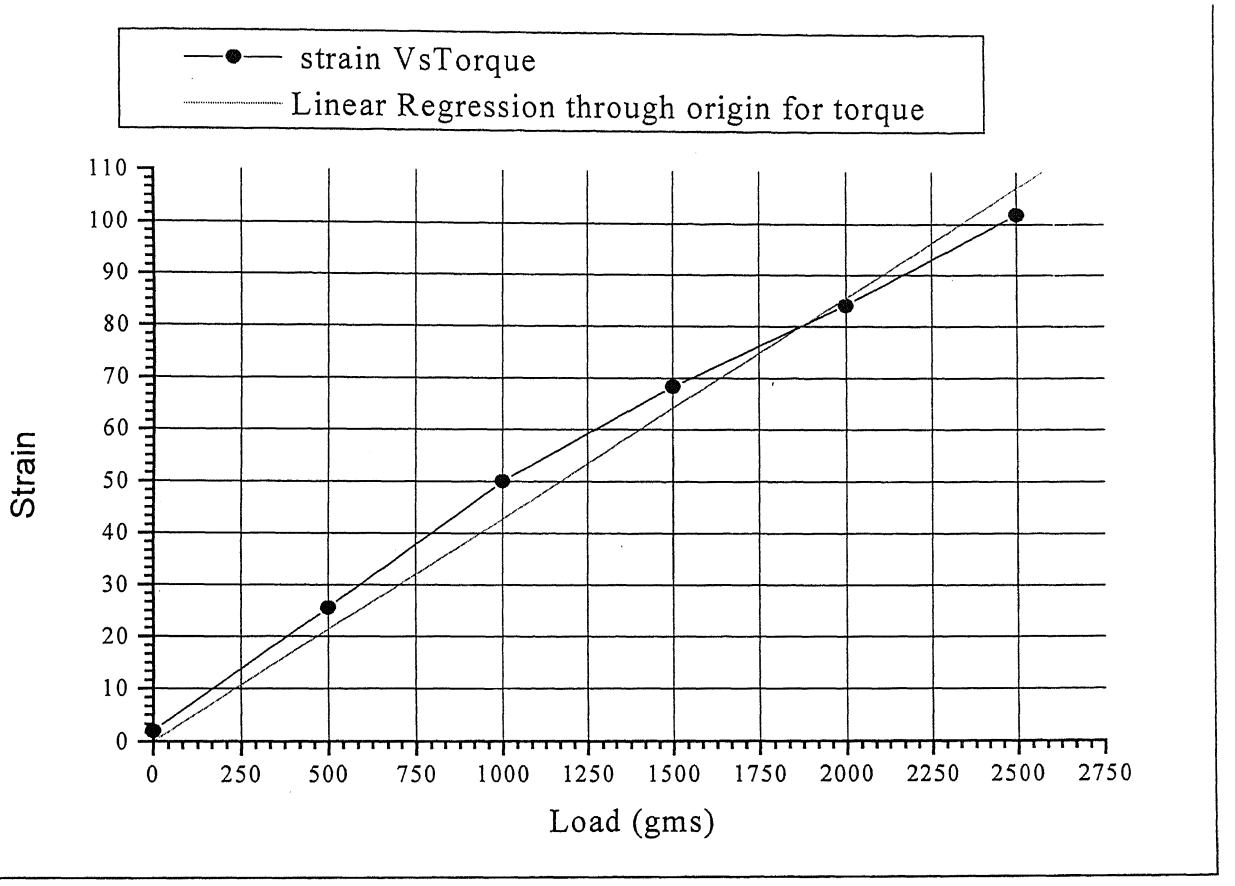

Figure 2.27 Torque calibration curve for dynamometer

Load is applied at a radius of 53 mm from the center.

Linear Regression through origin for Torque:

$Y = B * X$

Parameter	Value	Error
B	0.04277	0.00133

R	SD	N	P
0.99591	4.92408	6	<0.0001

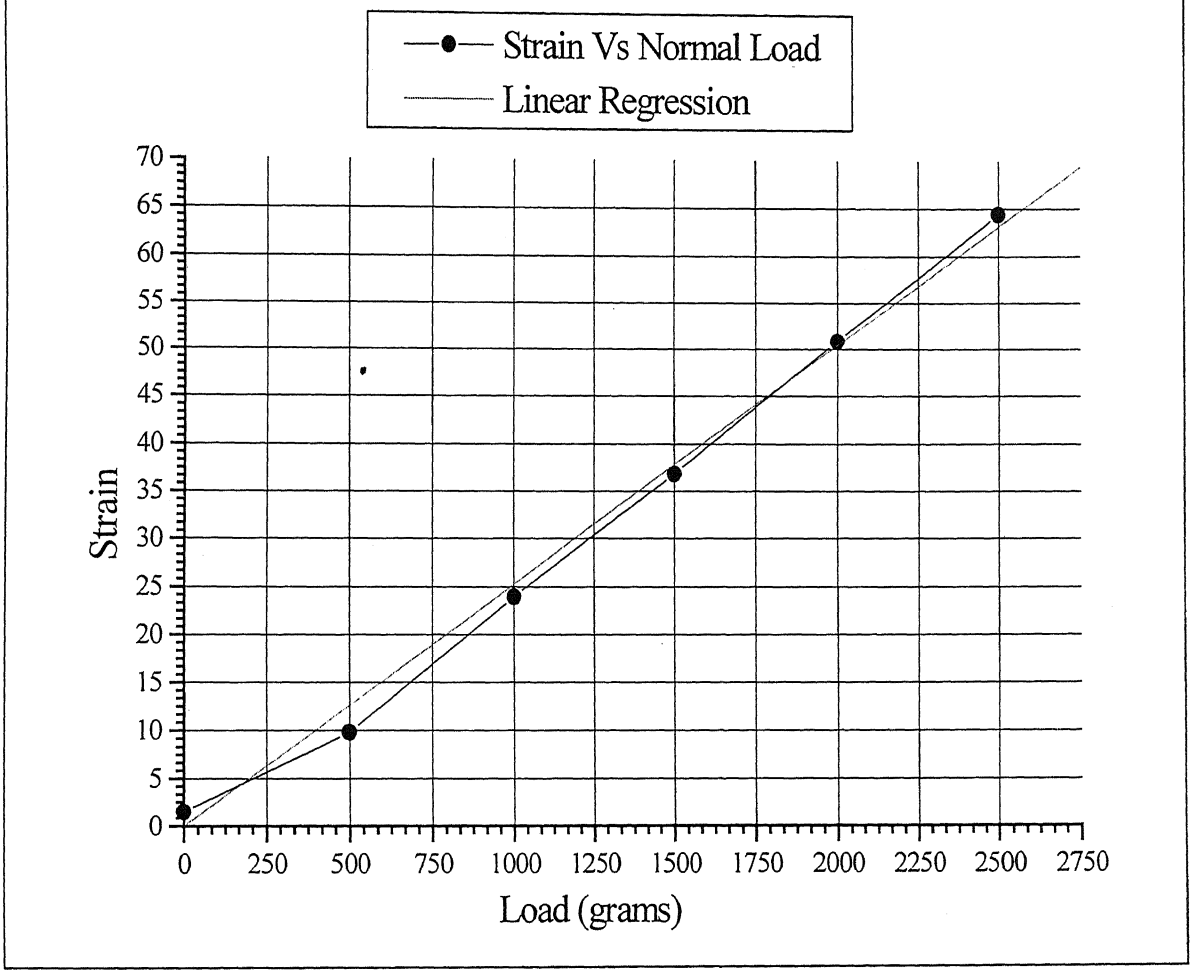

Figure 2.28 Thrust calibration curve for dynamometer

Linear Regression through origin for Thrust force:

$Y = B * X$

Parameter	Value	Error
B	0.02524	4.59172e-4

R	SD	N	P
0.99781	1.70266	6	<0.0001

2.13 Work-piece fixture:

The work-piece and the fixture are made the same material to keep uniformity in the distribution of the magnetic field. The work-piece is of brass. So the fixture is also made of brass.

The fixture is made disk shaped 7 mm in thickness and 112 mm in diameter. The work-piece is shaped like a small rectangular bar of length 100 mm and section 24.5 × 4 mm in cross section. On the top surface of the fixture, a slot of 4 mm depth and 24.5 mm thickness has been cut. The work-piece is placed in the slot and clamped to the fixture by two clips.

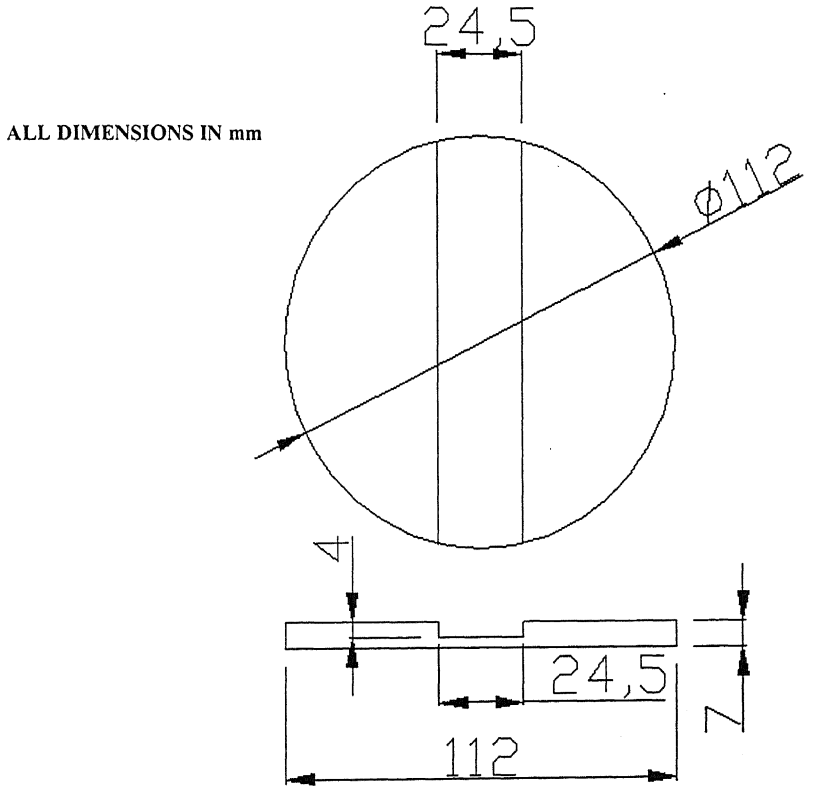

Figure 2.29 Schematic view of the fixture

2.14 Automation of table feed

The X-direction feed of the work-piece has been automated using a 1 HP induction motor and a variable frequency drive to control the speed of the motor. The hand wheel on the shaft meant for X feeding has been removed and pulley and belt system is used to rotate the shaft using the motor. One important feature in table movement during feed is the reciprocation of the table. Reciprocation has been obtained using a control circuit built using two DPDT (Dual pole dual throw) relays, two limit switches and a potentiometer (10 kΩ, 50 turns).

2.15 Parameters affecting MAF and selection of parameters for experimentation:

The aim of the present thesis work is to study the forces generated during MAF of brass which is a non-ferromagnetic material, quantitatively. MAF operation can be affected by many parameters which are discussed below.

2.15.1 Current supplied to the magnet

Flux density in the finishing zone is the factor that determines the amount of energy available at the iron particles for energizing them. The flux density generated by the electromagnet is dependent on the core material of the electromagnet and the coiling, or winding in it. Keeping these two conditions constant for a particular electromagnet, the electromagnet has a particular capacity of generating magnetic flux depending on the amount of current that its winding can handle. The flux density and current supplied to the electromagnet are linearly related to each other. So for a particular electromagnet, the current supplied to it, or the corresponding voltage for the current, may be remarked analogous to the flux density generated by it.

2.15.2 RPM of magnet

The RPM of magnet rotation is an important factor like flux density. The more the RPM of the magnet, more is the energy of the abrasive particles, so more would be the stock removal.

2.15.3 Working gap

The working gap is maintained during the finishing operation. The lesser the gap is more is the flux density, consequently more is the energizing force.

2.15.4 Size or mesh number of iron particles used in the MAP

Bigger sized iron particles hold the abrasives more strongly, for a given amount of excitation magnetic energy.

2.15.5 Type of abrasive particles used in MAP

The hardness of abrasives gives marking difference in the amount of stock removed by MAF.

2.15.6 Size of the abrasives used in MAP

Bigger sized abrasives remove more material from a work-piece, but give poorer surface finish. Size of a particle is expressed in terms of mesh number. Bigger the mesh number, smaller is the diameter of the particle.

2.15.7 Percentage composition of iron particles and abrasive particles in MAP by mass

More amount of iron in MAP makes the brush stiffer because iron improves the strength of magnetic field by its ferromagnetic nature and thereby increases the force of attraction between the iron particles in the MAP. This makes the abrasive brush stiffer. A stiffer brush removes material more efficiently.

2.15.8 Amount of oil added to MAP as a bonding agent

Oil improves bonding among the particles in MAP. But excess amount of oil may cause problems such as, sticking of MAP to the work-piece, sliding of the abrasive on the work-piece surface instead of finishing and so on.

2.15.9 Finishing time

Finishing time has to be carefully chosen. Finishing for more time may cause roughening of the surface, or cause burn marks on the surface and so on. Under finishing won't give the desired finishing effect on the work-piece.

2.16 Selection of parameters for experimentation:

Out of the above specified parameters, all of the above cannot be taken for experimentation due to various practical reasons. So, five of the above parameters are chosen to be variable experimental parameters for the present thesis work, keeping other parameters constant. The parameters chosen are

1. Current supplied to the magnet.
2. Working gap.
3. RPM of electromagnet.
4. Mesh number of abrasive particles.
5. Percentage composition of oil in MAP.

The other parameters are fixed. The values of the variable parameters are specified in Table 2.1.

Table 2.1. Variable parameters and their values

Parameter	Value
Current supplied to electromagnet	0.5 A - 1 A
Working gap	1mm - 2 mm
Speed of electromagnet rotation	100 RPM - 300 RPM
Mesh number of abrasive particles (SiC abrasive)	400 # - 1200 #
Percentage of bonding oil in MAP (by mass)	1% - 5%

The values of the fixed parameters are specified below.

Table 2.2. Fixed parameters and their values

Parameter	Value
Size of iron particles	300 #
Abrasives used in MAP	SiC
Percentage composition of iron in MAP (by mass)	75%
Finishing time	15 min
Work-piece	Flat brass work-pieces

Chapter 3

PLAN OF EXPERIMENTS

3.1 Statistical approach of experimental analysis

Experiments are planned and performed in such a way that the desired conclusions can be drawn by doing minimum number of experiments. To determine this minimum number of experiments, statistical approach of experimental planning is used. According to this approach, the response obtained in the form of experimental data is defined as a function of the levels of quantitative variables [22]. The response or yield of an experiment be designated as 'Y' and the experimental input variables as 'x', and it can be written as,

$$Y_j = \Phi(x_{1j}, x_{2j}, \ldots x_{Nj}) + e_j \quad \ldots\ldots(3.1)$$

where,

$j = 1, 2, \ldots N$ represents the N observations in the experiment,

and x_{ij} = level value of the i^{th} factor in the j^{th} observation.

Φ is the function that gives the relation between 'Y' and 'x' and is called as *Response Surface*. 'e_j' is the error of the j^{th} observation and is termed as *Residual*. The function Φ helps us draw an overall idea of the process which is being experimented on and also gives the scope to predict response for the values of the input parameters which have not been used to test in the experiment.

3.1.1 Quadratic Response Surface:

Usually the mathematical form of Φ is not known and has to be approximated within the range of experimental parameters used, using polynomial functions in 'x'. Basically the functions used are of first or second order and appropriate statistical methods are used for fitting the function to the experimental results obtained.

The general form of the quadratic (second degree) polynomial is illustrated by the equation for N 'x-variables' as

$$Y_j = \beta_0 + \sum_{i=1}^{N} \beta_i x_{ij} + \sum_{i=1}^{N} \beta_{ii} x_{ij}^2 + \sum_{i<j}^{N} \beta_{ij} x_{ij} x_{ij} \quad \ldots\ldots(3.2)$$

The surface contains linear terms (x_{ij}), squared terms (x_{ij}^2) and the cross product terms ($x_{ij}x_{ij}$).

3.1.2 Central Composite Rotatable Design:

Design of experiments, or more generally stated as plan of experiments, helps us to obtain our desired response in minimum number of experiments. Central Composite Rotatable design is a modification of a method of experimental design known as 2^k factorial design of experiments. In this type of design, a factor is assigned two values known as levels, one higher and one lower, coded as -1 and +1 respectively. So the design is called 2^k design and the plan in this design consists of experiments done with the combination of the parameters at these two levels. By adding some more parameter combinations to the plan from 2^k design, a composite design is obtained. For that, some more levels are added to the previously existing level of the input parameters. This is done to fit second order response surfaces.

Out of the parameter combinations added into the 2^k plan of experiments, some are the combinations where all the parameters have 0-level values. This point where all parameters have 0-level value is called as Central point. From the results of any experiment, we can compute the standard error of Y_j at any point on the fitted surface. This standard error will be a function of the coordinates x_{ij} of the point. In a rotatable design, this standard error is same for all points that are at the same distance ρ from the center of the design, i.e., for all points for which

$$x_{1j}^2 + x_{2j}^2 + \ldots + x_{Nj}^2 = \rho^2 = \text{constant.} \quad \ldots\ldots\ldots\ldots\ldots\ldots\ldots\ldots\ldots\ldots(3.3)$$

The plan for experimentation involving five parameters (X_1, X_2, X_3, X_4 and X_5) will be as shown in table 3.1 [22]. The columns headed X1 to X5 specify the actual combinations to be used and constitute the plan of the experiment. Subsequent steps of doing the calculations are as follows.

1. All the columns headed X_i^2 and $X_i.X_j$, where i=1 to 5 and j=1 to 5 are completed. This two way array with 21 columns and 32 rows comprises the '**X – matrix**' of the X-variables. The corresponding values of 'Y' are placed on the right-most column.

Table 3.1 Central Composite Rotatable Design for N=5

X_0	X_1	X_2	X_3	X4	X5	X_1^2	X_2^2	X_3^2	X_4^2	X_5^2	$X_1.X_2$	$X_1.X_3$	$X_1.X4$	$X_1.X_5$	$X_2.X_3$	$X_2.X4$	$X_2.X5$	$X_3.X4$	$X_3.X5$	X4.X5	Y
1	-1	-1	-1	-1	1	1	1	1	1	1	1	1	1	-1	1	1	-1	1	-1	-1	
1	1	-1	-1	-1	-1	1	1	1	1	1	-1	-1	-1	-1	1	1	1	1	1	1	
1	-1	1	-1	-1	-1	1	1	1	1	1	-1	1	1	1	-1	-1	-1	1	1	1	
1	1	1	-1	-1	1	1	1	1	1	1	1	-1	-1	1	-1	-1	1	1	-1	-1	
1	-1	-1	1	-1	-1	1	1	1	1	1	1	-1	1	1	-1	1	1	-1	-1	1	
1	1	-1	1	-1	1	1	1	1	1	1	-1	1	-1	1	-1	1	-1	-1	1	-1	
1	-1	1	1	-1	1	1	1	1	1	1	-1	-1	1	-1	1	-1	1	-1	1	-1	
1	1	1	1	-1	-1	1	1	1	1	1	1	1	-1	-1	1	-1	-1	-1	-1	1	
1	-1	-1	-1	1	-1	1	1	1	1	1	1	1	-1	1	1	-1	1	-1	1	-1	
1	1	-1	-1	1	1	1	1	1	1	1	-1	-1	1	1	1	-1	-1	-1	-1	1	
1	-1	1	-1	1	1	1	1	1	1	1	-1	1	-1	-1	-1	1	1	-1	-1	1	
1	1	1	-1	1	-1	1	1	1	1	1	1	-1	1	-1	-1	1	-1	-1	1	-1	
1	-1	-1	1	1	1	1	1	1	1	1	1	-1	-1	-1	-1	-1	-1	1	1	1	
1	1	-1	1	1	-1	1	1	1	1	1	-1	1	1	-1	-1	-1	1	1	-1	-1	
1	-1	1	1	1	-1	1	1	1	1	1	-1	-1	-1	1	1	1	-1	1	-1	-1	
1	1	1	1	1	1	1	1	1	1	1	1	1	1	1	1	1	1	1	1	1	
1	-2	0	0	0	0	4	0	0	0	0	0	0	0	0	0	0	0	0	0	0	
1	2	0	0	0	0	4	0	0	0	0	0	0	0	0	0	0	0	0	0	0	
1	0	-2	0	0	0	0	4	0	0	0	0	0	0	0	0	0	0	0	0	0	
1	0	2	0	0	0	0	4	0	0	0	0	0	0	0	0	0	0	0	0	0	
1	0	0	-2	0	0	0	0	4	0	0	0	0	0	0	0	0	0	0	0	0	
1	0	0	2	0	0	0	0	4	0	0	0	0	0	0	0	0	0	0	0	0	
1	0	0	0	-2	0	0	0	0	4	0	0	0	0	0	0	0	0	0	0	0	
1	0	0	0	2	0	0	0	0	4	0	0	0	0	0	0	0	0	0	0	0	
1	0	0	0	0	-2	0	0	0	0	4	0	0	0	0	0	0	0	0	0	0	
1	0	0	0	0	2	0	0	0	0	4	0	0	0	0	0	0	0	0	0	0	
1	0	0	0	0	0	0	0	0	0	0	0	0	0	0	0	0	0	0	0	0	
1	0	0	0	0	0	0	0	0	0	0	0	0	0	0	0	0	0	0	0	0	
1	0	0	0	0	0	0	0	0	0	0	0	0	0	0	0	0	0	0	0	0	
1	0	0	0	0	0	0	0	0	0	0	0	0	0	0	0	0	0	0	0	0	
1	0	0	0	0	0	0	0	0	0	0	0	0	0	0	0	0	0	0	0	0	
1	0	0	0	0	0	0	0	0	0	0	0	0	0	0	0	0	0	0	0	0	

2. The sum of products of each column in the X matrix with the column of Y values is formed. These sums of products are denoted as (0Y), (1Y), (2Y) and so on where $(ij) = (ji) = \sum_{u=1}^{K} X_{iu} X_{ju}$ =sum of products of *ith* and *jth* columns in X, K being the total number of experiments.
3. From the values of (ij) s, the regression coefficients are directly computed using the equations given below.

$$\left.\begin{aligned} \beta_0 &= 0.1428579(0Y) - 0.035714(iiY) \\ \beta_i &= 0.041667(iY) \\ \beta_{ii} &= 0.031250(iiY) + 0.003720\sum(iiY) - 0.035714(0Y) \\ \beta_{ij} &= 0.0625(ijY) \end{aligned}\right\} \quad \text{.....(3.4)}$$

Though the above method is used on pen and paper to calculate the regression coefficients manually, there are softwares which can directly give the values of these regression coefficients upon feeding the experimental data directly. One such software is Minitab, which has been used to analyze the experimental data in this thesis work.

3.2 Plan of Experiments

In the present experimental work, the effect of five parameters on the generation of forces during the MAF operation of brass has been studied. As stated before, the parameters are

1. Current supplied to the electromagnet (X_1)
2. Working gap (X_2)
3. Speed of rotation of electromagnet (X_3)
4. Mesh number of SiC abrasive (X_4)
5. Percentage of oil (X_5)

First the relations between the coded X-scales and the original scales in which the levels are recorded are set-up. In central composite design scale, the lowest and the highest values of coded levels are -2 and +2 respectively. So we assign these coded values to the extreme values of the parameters. The assigning of extreme range values is done as per shown in the Table 3.2 below.

Table 3.2 Highest and Lowest value of parameters

Parameter	-2	+2
Current supplied to electromagnet (X_1)	0.5 Amp	1 Amp
Working gap (X_2)	1 mm	2 mm
Speed of rotation of electromagnet (X_3)	100 RPM	300 RPM
Mesh number of SiC abrasives (X_4)	400 #	1200 #
Percentage of oil (X_5)	1%	5%

Then,

$$X = a + b*(\text{variable})$$

where, 'a' and 'b' are chosen to satisfy the desired condition of linearity in the range of the scale.

1. Excitation current supplied to magnet (X_1)

   $X_1 = a + b*(\text{current})$

   When X_1 = -2, current = 0.5 A

   X_1 = +2, current = 1 A

   Solving for 'a' and 'b', we get X_1 = -6 + 8*(current).

2. Working gap (X_2)

   $X_2 = a + b*(\text{gap})$

   When X_2 = -2, gap = 1 mm

   X_2 = +2, gap = 2 mm

   Solving for 'a' and 'b', we get X_2 = -6 + 4*(gap)

3. Speed of rotation of electromagnet (X_3)

   $X_3 = a + b*(\text{RPM})$

   When X_3 = -2, RPM = 100

   X_3 = +2, RPM = 300

   Solving for 'a' and 'b', we get X_3 = -4 + 0.02*(RPM)

4. Mesh number of SiC abrasive (X_4)

   $X_4 = a + b*(\text{mesh \#})$

   When X_4 = -2, mesh # = 400

   X_4 = +2, mesh # = 1200

   Solving for 'a' and 'b', we get X_4 = -4 + 0.005*(mesh #)

5. Percentage of oil (X_5)

$X_5 = a + b*(\text{oil \%})$

When X_5 = -2, oil % = 1 %

X_5 = +2, oil % = 5 %

Solving for 'a' and 'b', we get X_2 = -3 + (oil %)

From the above equations, the values of the parameters at the intermediate levels can be determined by putting the coded values of the parameter levels. By doing so, the values of the parameters obtained are as shown below in the conversion Table 3.3.

Table 3.3 Conversion Table

Parameter	-2	-1	0	+1	+2
Current supplied to electromagnet (X1)	0.5 A	0.625 A	0.75 A	0.875 A	1 A
Working gap (X2)	1 mm	1.25 mm	1.5 mm	1.75 mm	2 mm
Speed of rotation of electromagnet (X3)	100 RPM	150 RPM	200 RPM	250 RPM	300 RPM
Mesh number of SiC abrasives (X4)	400 #	600 #	800 #	1000 #	1200 #
Percentage of oil (X5)	1%	2%	3%	4%	5%

With the above conversion table, the experiments are performed according to the plan in Table [3.4].

Table 3.4 Plan of experiments

Exp. No.	Current, A (X_1)	Gap, mm (X_2)	RPM (X_3)	SiC # (X_4)	Oil% (X_5)
1	0.625	1.25	150	600	4
2	0.875	1.25	150	600	2
3	0.625	1.75	150	600	2
4	0.875	1.75	150	600	4
5	0.625	1.25	250	600	2
6	0.875	1.25	250	600	4
7	0.625	1.75	250	600	4
8	0.875	1.75	250	600	2
9	0.625	1.25	150	1000	2
10	0.875	1.25	150	1000	4
11	0.625	1.75	150	1000	4
12	0.875	1.75	150	1000	2
13	0.625	1.25	250	1000	4
14	0.875	1.25	250	1000	2
15	0.625	1.75	250	1000	2
16	0.875	1.75	250	1000	4
17	0.5	1.5	200	800	3
18	1	1.5	200	800	3
19	0.75	1	200	800	3
20	0.75	2	200	800	3
21	0.75	1.5	100	800	3
22	0.75	1.5	300	800	3
23	0.75	1.5	200	400	3
24	0.75	1.5	200	1200	3
25	0.75	1.5	200	800	1
26	0.75	1.5	200	800	5
27	0.75	1.5	200	800	3
28	0.75	1.5	200	800	3
29	0.75	1.5	200	800	3
30	0.75	1.5	200	800	3
31	0.75	1.5	200	800	3
32	0.75	1.5	200	800	3

Chapter 4

EXPERIMENTATION, RESULTS AND DISCUSSIONS

4.1 Experimentation

Experiments are done taking the parameters as specified in section 2.16. The forces generated in the process are measured in terms of strain using the dynamometer. The strain is measured and converted into digital data using a DAC (Data Acquisition Card). The measured strain is seen online on a computer monitor. Virtual Instrumentation (VI) is developed to acquire data online. In the present set of experiments, the VI has been configured to take 600 readings per minute and also provision is made to record the data in ASCII form.

The dynamometer has been pre-calibrated [16] using standard procedure and a conversion factor has been determined to calculate the imparted force from the strain value measured.

4.2 Experimental results:

The experiments are conducted as per the design or plan of experiments stated in chapter 3. The data read using the software is in the form of strain. The forces are calculated from the recorded strain values through a conversion factor.

4.2.1 Conversion factor

The conversion factors have been determined [16] using standard procedure of calibration of a ring dynamometer. The factors are determined from the calibration curves shown in Fig. 2.27 and 2.28. Known load (in g) is applied on the dynamometer and the corresponding strain is noted. The values of strain are plotted against the applied load and a linear regression line passing through the origin is plotted for the strain values. The slope of this regression line (B in Fig. 2.27 and 2.28) is used to calculate the conversion factor. As for instance in Fig. 2.28, the value of the slope is 0.02524 (≈0.025). So we have,

strain=B× Load (Load is in g)

$$\text{or, Load} = \frac{\left(\frac{\text{strain}}{\text{B}}\right)}{1000} \times g = \frac{g}{\text{B}\times 1000} \times \text{strain} \quad \text{(Load in N)}.$$

So the conversion factor of strain to load is $[g/(\text{B}\times 1000)]$ which is equal to

$$\frac{9.81}{0.025\times 1000} = \frac{9.81}{25}.$$

The conversion factor for the torque load is found in a similar fashion.

The values of the conversion factors are

1. For force generating torque in the dynamometer

For the force generating torque in the dynamometer, the conversion factor to be multiplied to strain is

$$C_T = \frac{9.81}{43}.$$

So for a strain value of 's', the corresponding torque generating force that induces the strain is

$$F_T = C_T \times s.$$

In the present experimental setup, the force generating this torque is the tangential cutting force for polishing.

2. For force imparting thrust on the dynamometer

The force imparting thrust on the dynamometer is the normal force of the abrasive brush on the work-piece. The calibration factor for the strain developed by this force is

$$C_F = \frac{9.8}{25}.$$

For a value of strain 's', the corresponding value of the normal thrust force is

$$F_N = C_F \times s.$$

4.2.2 Steps of force determination

The values of the forces from the corresponding strain values have been obtained in the following way

1. First the data of strains obtained is multiplied by the corresponding conversion factor to obtain the value of normal and tangential force. Considering a case as instance, the variation of strain for Exp. No. 1, done under the conditions as shown in Table 4.1, is shown in Fig. 4.1

Table 4.1 Experimental conditions for experiment no 1

Current supplied to the electromagnet	0.625 Amp
Working gap	1.25 mm
RPM of electromagnet	150
Mesh No of SiC abrasive	600 #
Percentage of oil in the MAP	4%

Each value of strain is multiplied by the corresponding conversion factor to obtain a force plot as shown in Fig. 4.2.

2. This process is done for all the data obtained. The plots for distribution of calculated normal and tangential force with time have been made using MS Excel.
3. The normal and tangential forces are calculated from the recorded strain values after the process is stabilized. For consistency, the time considered for calculation of forces is in between 5000 – 6000 sec for all the experiments.
4. The force values in this zone (5000 – 6000 sec) are averaged to obtain the value of normal force and tangential force for the MAF operation under the specific experimental conditions. The average value of calculated normal force is 30.453 N and tangential force is 3.146 N. Likewise, the value of tangential and normal force has been calculated for rest of all the experimental conditions.

Some plots obtained from the strain data by experimentation are shown in Fig. 4.3 (a)-(c). The forces increase from zero value to a maximum value and then remain stable. But the initial portion of the curves is not a smooth curvature from zero force value to the stable value because initially there are disturbances created due to setting of the working gap. This is attributed to the working procedure as the electromagnet is given rotation first before setting the gap. So as the rotating electromagnet with the MAP below, is brought down onto the work-piece, initial forces created are gradual, but look like impact loads where the load increases suddenly.

The tangential cutting force is represented as 'Fc' and the normal force is represented as 'Fmn' in these plots. The values of the tangential and normal forces calculated and their corresponding experimental conditions are shown in the Table 4.2

4.3 Results and Discussions

The effects of the five parameters namely, current supplied to the electromagnet, working gap, electromagnet RPM, size of SiC (mesh number) and the percentage composition of oil in the MAP by mass, is studied and discussed in this chapter. The data obtained from the experiments are analyzed by statistical surface fitting technique using the software MINITAB and the response curves are drawn using MS EXCEL package.

4.3.1 Response surface analysis

The equation of general quadratic response surface is given in Eq. 3.2. The coefficients are calculated using the software MINITAB and the general equations are obtained.

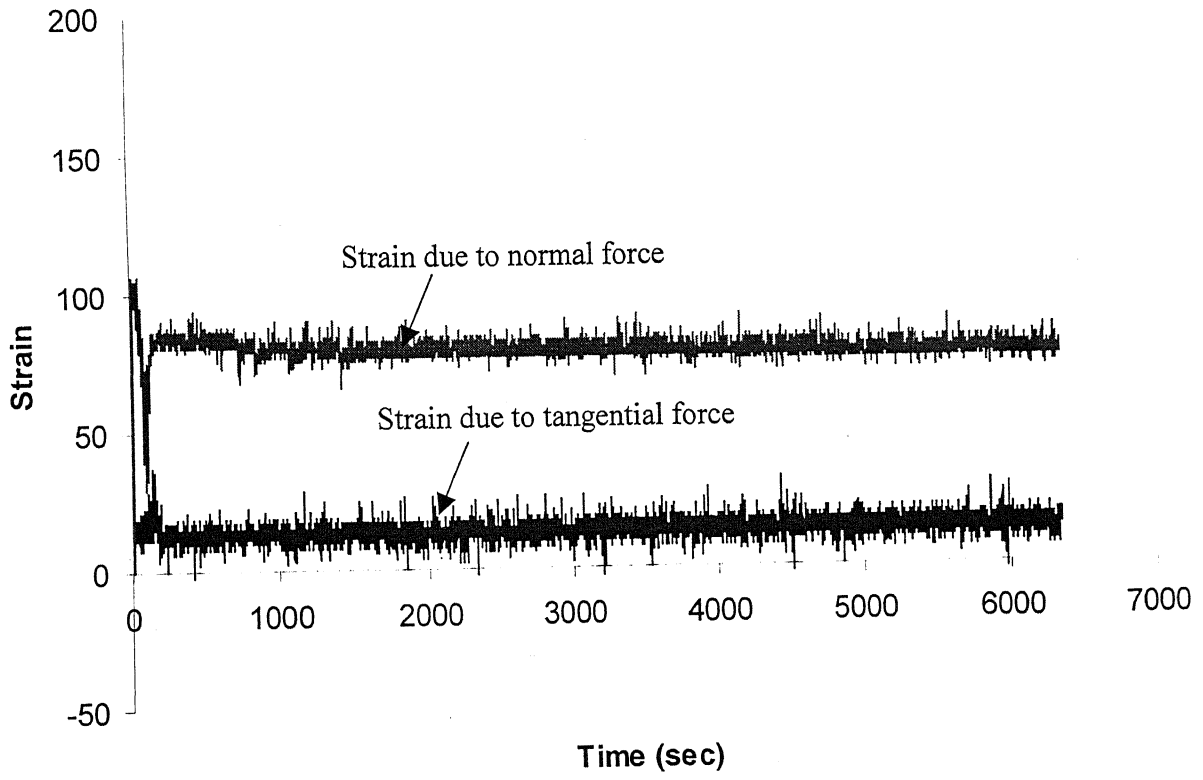

Figure 4.0 Strain - vs - Time plot for experiment no. 1

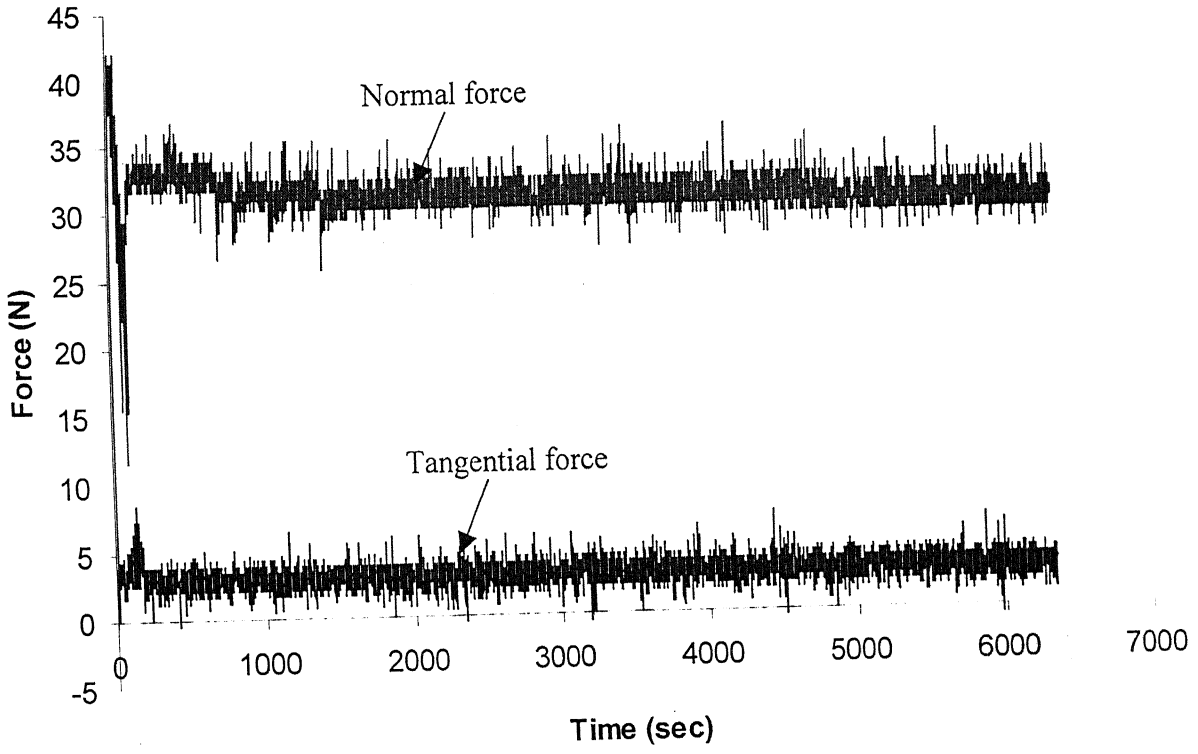

Figure 4.2 Force - vs - Time plot for experiment no. 1

Table 4.2 Experimental results

Exp. No.	Machining Parameters					Responses	
	Current (A)	Gap (mm)	Speed (RPM)	SiC mesh	Oil %	Fc (N)	Fmn (N)
1	0.625	1.25	150	600	4	3.146	30.453
2	0.875	1.25	150	600	2	11.551	124.077
3	0.625	1.75	150	600	2	1.865	12.15
4	0.875	1.75	150	600	4	8.577	102.149
5	0.625	1.25	250	600	2	3.662	36.094
6	0.875	1.25	250	600	4	13.816	138.056
7	0.625	1.75	250	600	4	3.04	21.174
8	0.875	1.75	250	600	2	9.125	113.35
9	0.625	1.25	150	1000	2	3.093	21.545
10	0.875	1.25	150	1000	4	10.466	121.523
11	0.625	1.75	150	1000	4	1.854	11.586
12	0.875	1.75	150	1000	2	8.422	96.443
13	0.625	1.25	250	1000	4	3.441	32.821
14	0.875	1.25	250	1000	2	12.525	124.733
15	0.625	1.75	250	1000	2	2.608	14.362
16	0.875	1.75	250	1000	4	9.055	107.044
17	0.5	1.5	200	800	3	1.701	8.028
18	1	1.5	200	800	3	14.791	139.414
19	0.75	1	200	800	3	8.322	94.28
20	0.75	2	200	800	3	3.688	47.175
21	0.75	1.5	100	800	3	3.792	47.954
22	0.75	1.5	300	800	3	8.149	86.362
23	0.75	1.5	200	400	3	7.947	83.234
24	0.75	1.5	200	1200	3	3.957	49.219
25	0.75	1.5	200	800	1	4.132	60.452
26	0.75	1.5	200	800	5	4.117	54.519
27	0.75	1.5	200	800	3	6.295	76.504
28	0.75	1.5	200	800	3	6.288	75.056
29	0.75	1.5	200	800	3	6.003	73.743
30	0.75	1.5	200	800	3	6.892	67.683
31	0.75	1.5	200	800	3	6.326	65.76
32	0.75	1.5	200	800	3	6.61	63.912

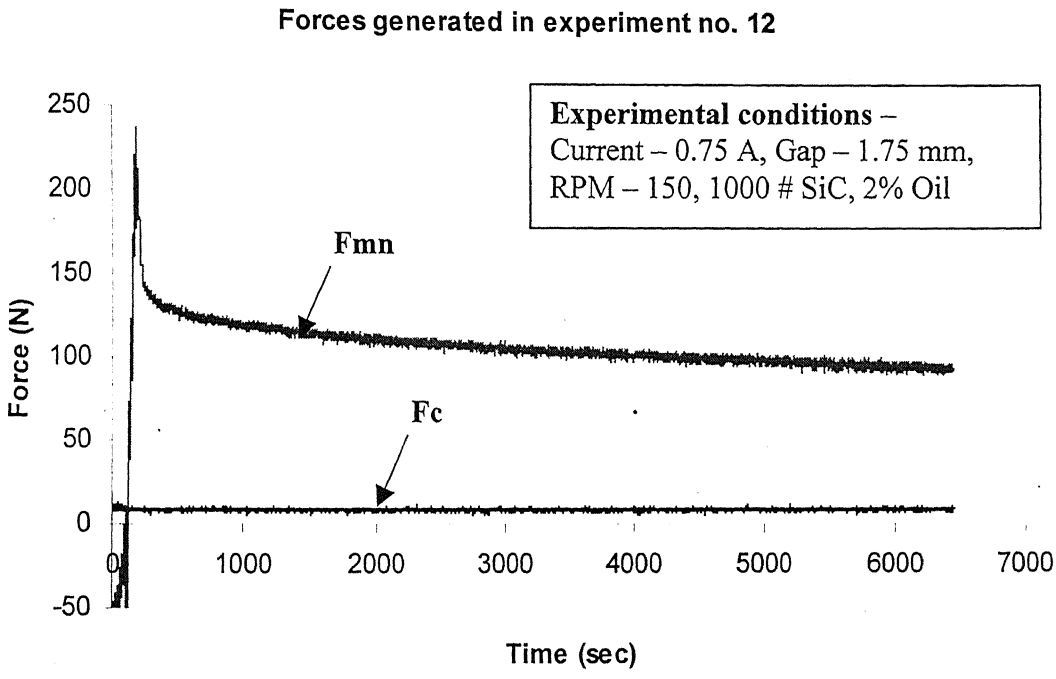

(a)

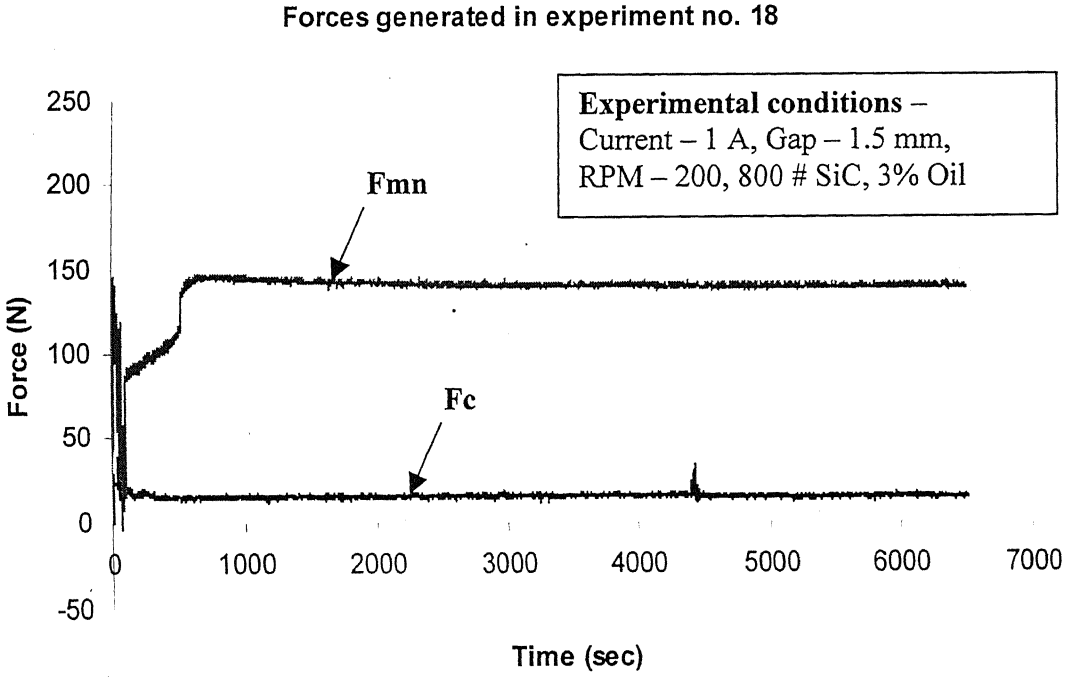

(b)

Figure 4.3 Force - vs - Time plots (a)-(b)

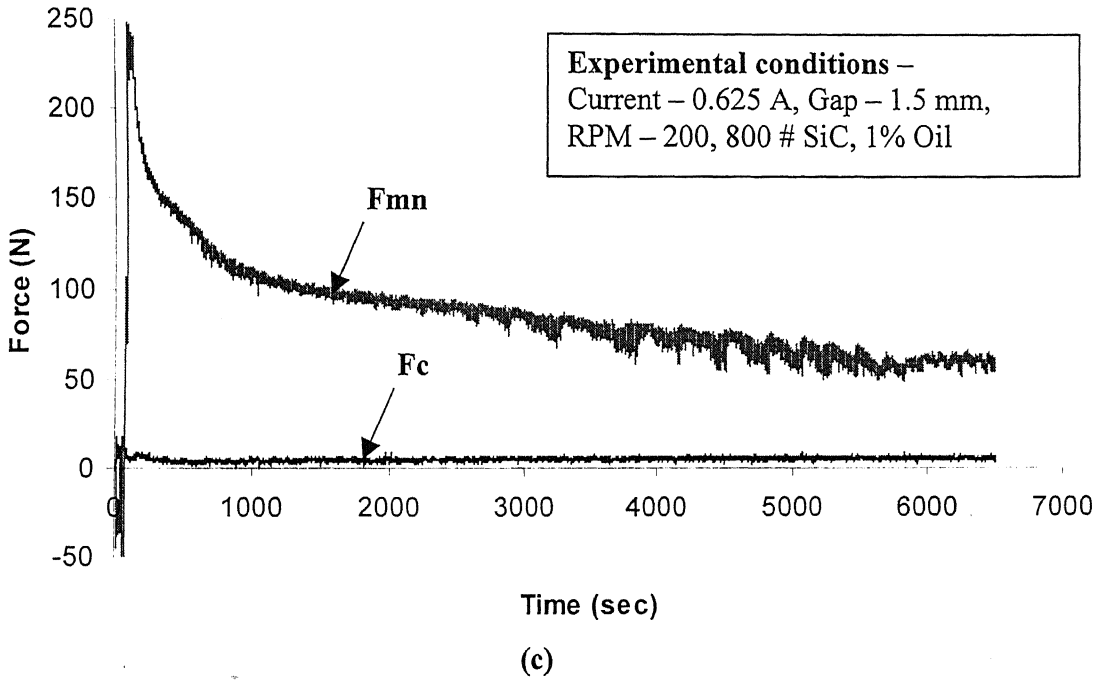

(c)

Figure 4.3 Force - vs - Time plots (c)

4.3.2 Regression equation for tangential cutting force (Fc):

The quadratic response equation obtained for the tangential cutting force is

$$Fc = 6.28 + 3.63X_1 - 1.10X_2 + 0.709X_3 - 0.471X_4 + 0.021X_5 + 0.582X_1^2 + 0.022X_2^2 + 0.013X_3^2 + 0.009X_4^2 - 0.448X_5^2 - 0.575X_1X_2 + 0.170X_1X_3 - 0.118X_1X_4 + 0.002X_1X_5 - 0.130X_2X_3 + 0.124X_2X_4 + 0.029X_2X_5 - 0.044X_3X_4 + 0.145X_3X_5 - 0.263X_4X_5 \quad \text{.....(4.1)}$$

where X_1 represents current supplied to the electromagnet,

X_2 represents working gap,

X_3 represents of RPM of the electromagnet,

X_4 represents SiC abrasive mesh number,

X_5 represents oil percentage in MAP,

X_iX_j represents combination of the X_i and the X_j parameter in the experiment.

For determining the value of Fc generated due to a particular combination of the parameters, the coded values of the parameters' are substituted instead of their actual values.

4.3.3 Regression equation for normal thrust force (Fmn):

The quadratic response equation obtained for the normal thrust force is

$$\begin{aligned} Fmn = {} & 69.9 + 42.1X_1 - 10.2X_2 + 6.02X_3 - 4.81X_4 + 0.42X_5 \\ & + 1.37X_1^2 + 0.62X_2^2 - 0.28X_3^2 - 0.51X_4^2 - 2.69X_5^2 \\ & - 1.74\,X_1X_2 + 0.64X_1X_3 - 0.52\,X_1X_4 - 0.11\,X_1X_5 \\ & - 0.03X_2X_3 + 0.54\,X_2X_4 - 0.67X_2X_5 \\ & - 0.75\,X_3X_4 - 0.06\,X_3X_5 \\ & + 0.61\,X_5X_1 \end{aligned} \quad \text{.....(4.2)}$$

The values of $X_1, X_2 \ldots X_5$ are substituted as stated earlier, with their respective coded values to obtain the value of Normal thrust force.

4.3.4 Model for tangential cutting and normal thrust force

The equations 4.1 and 4.2 are tested using MINITAB to find the validity of the model and the significance level of the each term in the response equation. Using P-value approach for 95% confidence interval (i.e., terms with P-value less than 0.05), it is found for tangential force Fc that the significant terms are

1. X_1, Current supplied to the electromagnet (Amp),
2. X_2, Working gap (mm),
3. X_3, RPM of electromagnet (min^{-1}),
4. X_4, SiC mesh number,
5. X_1^2,
6. X_5^2,
7. X_1X_2.

The P-values for the parameters are calculated using MINITAB. Likewise, for normal force Fmn, the significant terms found are

1. X_1, Current supplied to the magnet (Amp),
2. X_2, Working gap (mm),
3. X_3, RPM of electromagnet (min^{-1}).

So, the approximate response equations for both the forces are

$$\left.\begin{aligned} Fmn &= 69.9 + 42.1X_1 - 10.2X_2 + 6.02X_3 \\ Fc &= 6.28 + 3.63X_1 - 1.10X_2 + 0.709X_3 - 0.471X_4 + 0.582X_1^2 - 0.448X_5^2 - 0.575X_1X_2 \end{aligned}\right\} \quad \text{.....(4.3)}$$

The above equations are experimentally determined empirical models for the tangential cutting force and the normal force.

The P-value for all the terms in both the quadratic response terms is given in Table 4.3.

Table 4.3 Significance level (P-value) of the terms in quadratic response equations

Fmn - Normal force

Predictor	Coefficient	P
Constant	69.897	**0**
X_1 (Current)	42.082	**0**
X_2 (Gap)	-10.219	**0.002**
X_3 (RPM)	6.022	**0.032**
X_4 (SiC)	-4.812	0.076
X_5 (Oil)	0.425	0.866
X_1^2	1.366	0.551
X_2^2	0.617	0.786
X_3^2	-0.275	0.904
X_4^2	-0.508	0.823
X_5^2	-2.693	0.251
X_1X_2	-1.735	0.576
X_1X_3	0.642	0.835
X_1X_4	-0.521	0.866
X_1X_5	-0.107	0.972
X_2X_3	-0.032	0.992
X_2X_4	0.542	0.86
X_2X_5	-0.672	0.827
X_3X_4	-0.749	0.808
X_3X_5	-0.059	0.985
X_4X_5	0.608	0.844

Fc - Tangential force

Predictor	Coefficient	P
Constant	6.2811	**0**
X_1 (Current)	3.6254	**0**
X_2 (Gap)	-1.1009	**0**
X_3 (RPM)	0.7088	**0.003**
X_4 (SiC)	-0.4707	**0.027**
X_5 (Oil)	0.0214	0.91
X_1^2	0.5821	**0.005**
X_2^2	0.0219	0.898
X_3^2	0.0132	0.938
X_4^2	0.0086	0.96
X_5^2	-0.4483	**0.021**
X_1X_2	-0.5754	**0.027**
X_1X_3	0.1696	0.469
X_1X_4	-0.1177	0.613
X_1X_5	0.0024	0.992
X_2X_3	-0.1299	0.578
X_2X_4	0.1239	0.595
X_2X_5	0.0292	0.9
X_3X_4	-0.0444	0.848
X_3X_5	0.145	0.535
X_4X_5	-0.2629	0.27

4.3.5 Parametric analysis of normal force

Abrasives have sharp cutting edges which remove stock from a work-piece. These edges indent on to the work-piece. The normal force is generated due to the indentation of abrasives.

4.3.5.1 *Current supplied to the electromagnet*

From Fig. 4.4, it is seen that the normal force increases when we increase the current supplied to the magnet from 0.5 Amp to 1 Amp. Electromagnet speed, mesh number of SiC abrasive grains and the percentage of oil in MAP are constant at 200 RPM, 800 # and 3%, respectively.

The current supplied to the electromagnet induces magnetic field in the electromagnet. Magnetic lines of force emit from the electromagnet. They start from the north pole of the magnet and continue in air up to the south pole, closing the magnetic circuit running for rest of the distance through the material of the electromagnet. When any other body comes into the space (outside the magnet) through which the magnetic lines of force pass to reach the south pole, the lines of force interact with the material of the body. They rearrange their path depending on the magnetic properties of the body. If the body is a ferromagnetic material then the lines of force will deviate to go through the ferromagnetic body instead of air because the magnetic permeability of a ferromagnetic body is more than air. When the body is a non-ferromagnetic body like brass, very less of the lines of force pass through it.

For the lines of force passing through the work-piece in case of MAF, magnetic stress is created in the work-piece surface and FMAB interface. The magnetic stress prompts the magnetized iron particles to press the work-piece surface either directly or through the abrasive particles. So this stress is the cause of indentation of the abrasives on the work-piece surface.

When higher current supplied to the electromagnet, more number of magnetic lines of force emit from the electromagnet, i.e. the magnetic flux density increases leading to the deeper indent action into the work-piece.

The effects of working gap are explained in the next section.

4.3. 5.2 *Working gap*

From Fig. 4.5, it is seen that as the working gap increases from 1 mm to 2 mm, for various speeds, the normal force shows a decreasing trend.

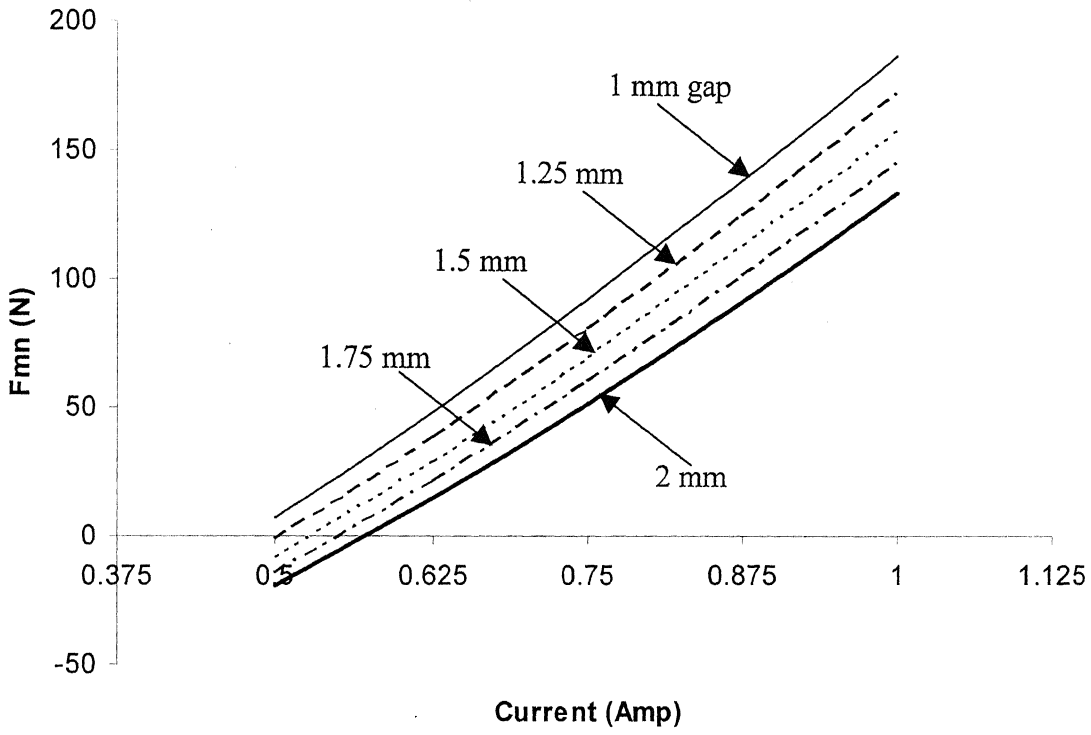

Figure 4.4 Variation of normal force with respect to current supplied to electromagnet at different working gaps, Speed = 200 RPM; 800# SiC mesh no; 3% oil

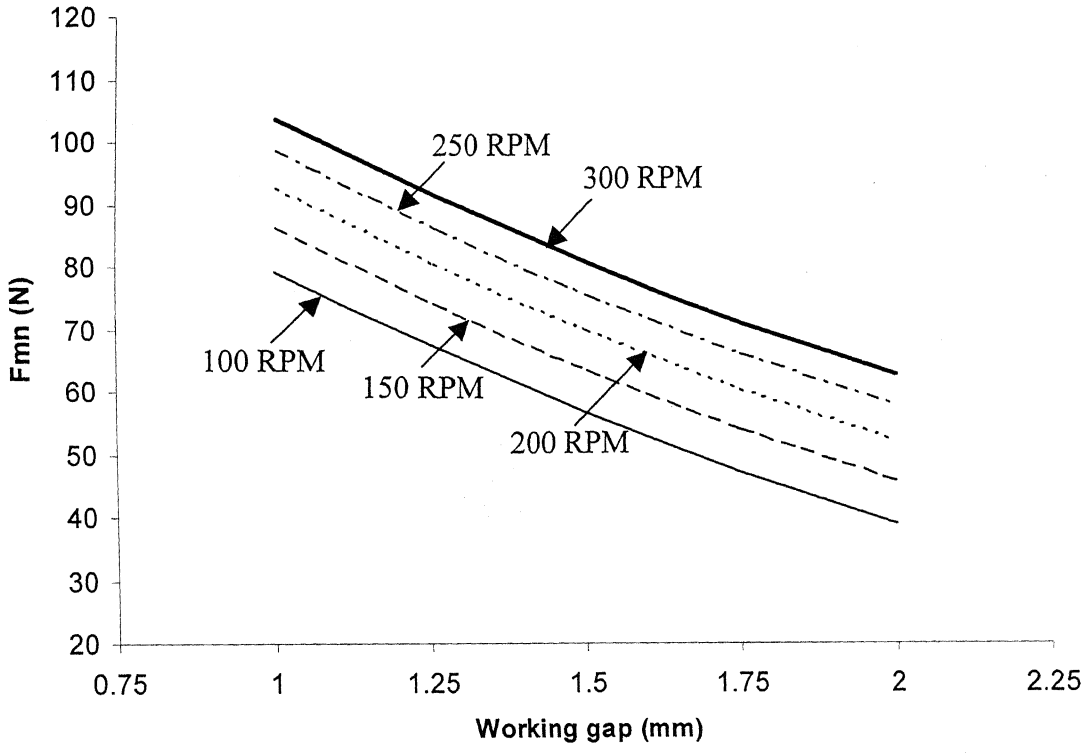

Figure 4.5 Variation of normal force with working gap at different speeds, current = 0.75 A; 800# SiC mesh no; 3% oil

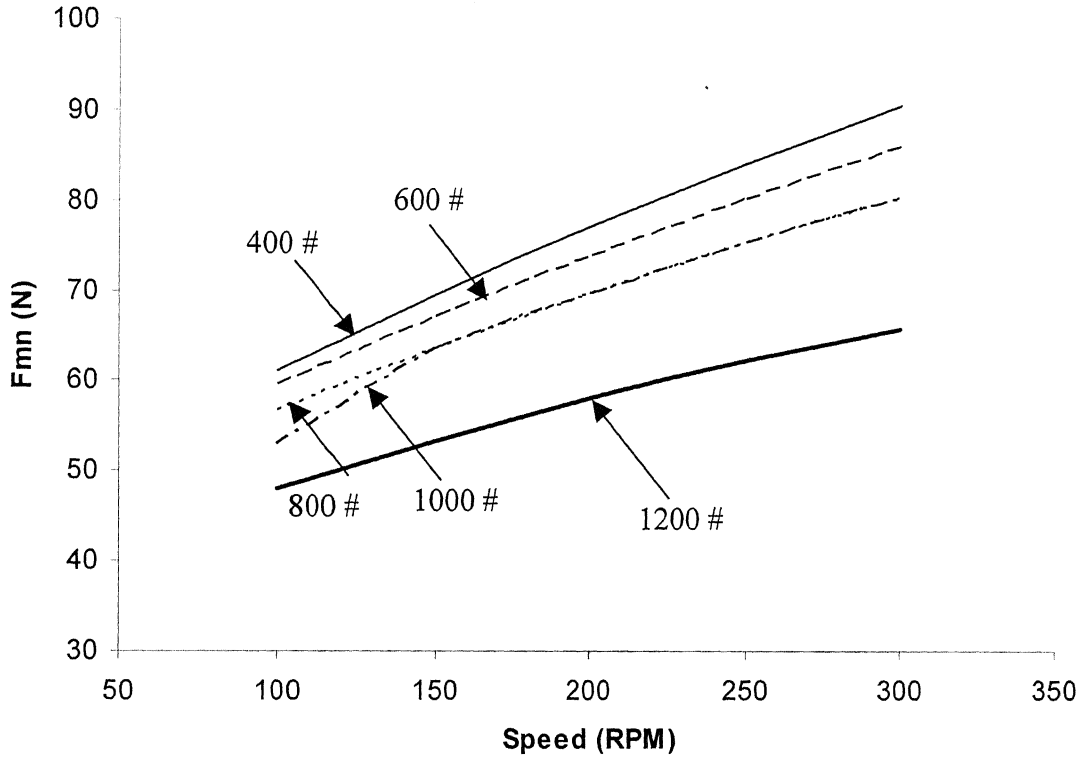

Figure 4.6 Variation of normal force with speed at different abrasive mesh no, current = 0.75 A; gap = 1.5 mm; 3% oil

The lines of force generated from a magnet, travel in the medium between the two poles of the magnet. The lines of force at larger distance from the poles are of weaker strength and generate weak field. Strength of the magnetic field is responsible for the degree of magnetization of the iron particles. The lines of force traveling through the work-piece placed at greater distance are weak lines. So at greater distances the magnetic stress created is of weaker form and a magnetized iron particle is weakly magnetized at such distance. Such an iron particle will impart lesser pressing force on the abrasives at the magnetic stressed region. The stress itself being weak in nature does not help increase the indenting force. So at higher working gap the indentation of the abrasives is less, thus the weak normal force.

The effects of speed (RPM) are explained in the next section.

4.3.5.3 *Spindle speed*

From Fig. 4.6, it is seen that the normal force on a body increases with the increase in the speed of rotation of the electromagnet.

The indentation of the abrasives on the work-piece is shown in Fig. 4.7. The initial indentation of the abrasive is caused by the normal force 'F', generated only due to the magnetic field. After the electromagnet and consequently, the FMAB starts to rotate, the area of contact of

the abrasives is arc shaped. So the total force 'R' imparted on the work-piece will be acting in a direction as shown in Fig. 4.7. This force can be resolved into two components 'F_1' and 'F_2'. F_1 is the cutting force that is imparted on the work-piece and F_2 is the total normal force acting on

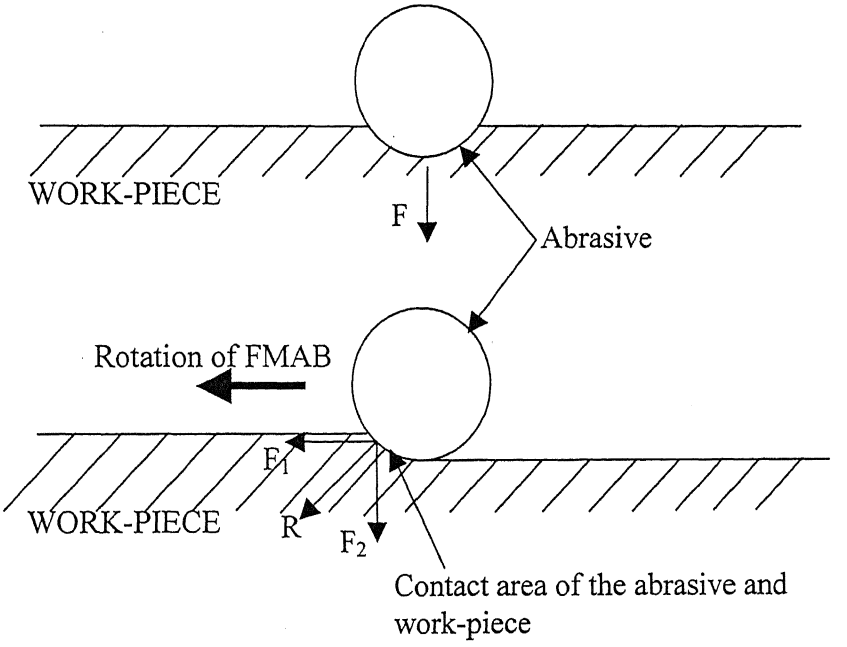

Figure 4.7 Schematic view of abrasive indentation and force pattern when the cutting is taking place

the work-piece.

F_2 = (Pressing force (F) on the abrasive due to magnetic field) + (Force acting normally downwards (F_p) due to rotation and nature of contact of the abrasive with the work-piece surface)

$= F + F_p$

As the speed of rotation of the electromagnet increases, the abrasives get more kinetic energy and so the component F_p increases. This results in overall increase of the normal force acting on the work-piece. It can also be seen that as the magnitude of current supplied to the electromagnet is increased, the measured normal force increases. This is due to the reason discussed in Sec. 4.3.5.1.

4.3.6 Parametric analysis of tangential force

Tangential polishing force is an outcome of the indentation of the abrasives on the work-piece surface. The tangential force will be more, when the indentation of the abrasive is more.

4.3.6.1 *Current supplied to the electromagnet*

From the model equation (Eq. 4.3), Fc is plotted (Fig. 4.8) against current supplied at different working gaps. The other parameters are kept constant at their respective zero level, i.e., speed is 200 RPM, SiC abrasive grain mesh is 800# and percentage of oil is 3%. It is seen that,

for any gap, as the current supplied to the electromagnet is increased, the magnitude of the tangential cutting force imparted on the work-piece increases.

An iron particle at any point in the domain of a magnet is magnetized to a magnitude determined by the strength of the field at that point. More is the strength of the field, magnetization will be higher. After magnetization, iron particle itself behaves like a small magnet. If there are more than one iron particles in the field, than there would be attraction and magnetic bonding between them. The iron particles would then get aligned along the lines of force and form a chain extending between the two magnetic poles. These chains form the necessary iron matrix and trap some of the SiC grains in between them. The magnetic bonding strength between the iron particles is directly proportional to the strength of the magnetizing field.

The magnetic bonding strength of the iron particles in the MAP determines the compactness and rigidity of the MAP. A more rigid MAP can impart greater normal force and thus, cutting force on a work-piece. Hence, increase in supply current to the magnet increases the cutting force imparted.

4.3.6.2 *Working gap*

From Fig. 4.9, it is seen that as the working gap is increased keeping other parameters constant, the tangential cutting force decreases.

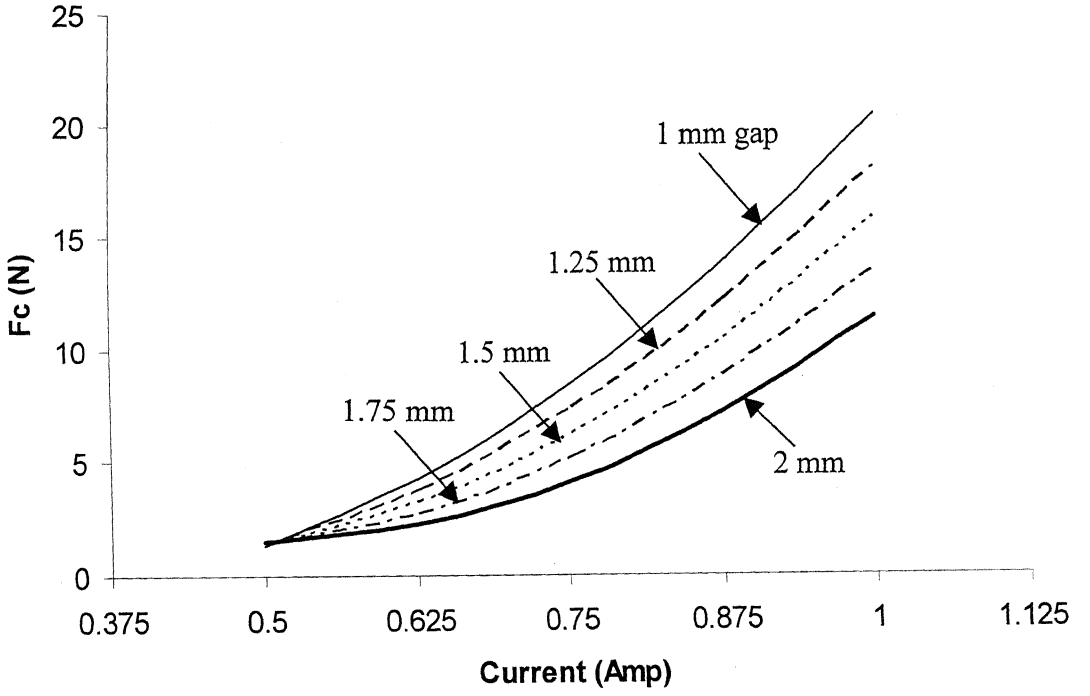

Figure 4.8 Variation of tangential cutting force with current supplied to electromagnet for different working gaps, speed = 200 RPM; 800# SiC mesh no; 3% oil

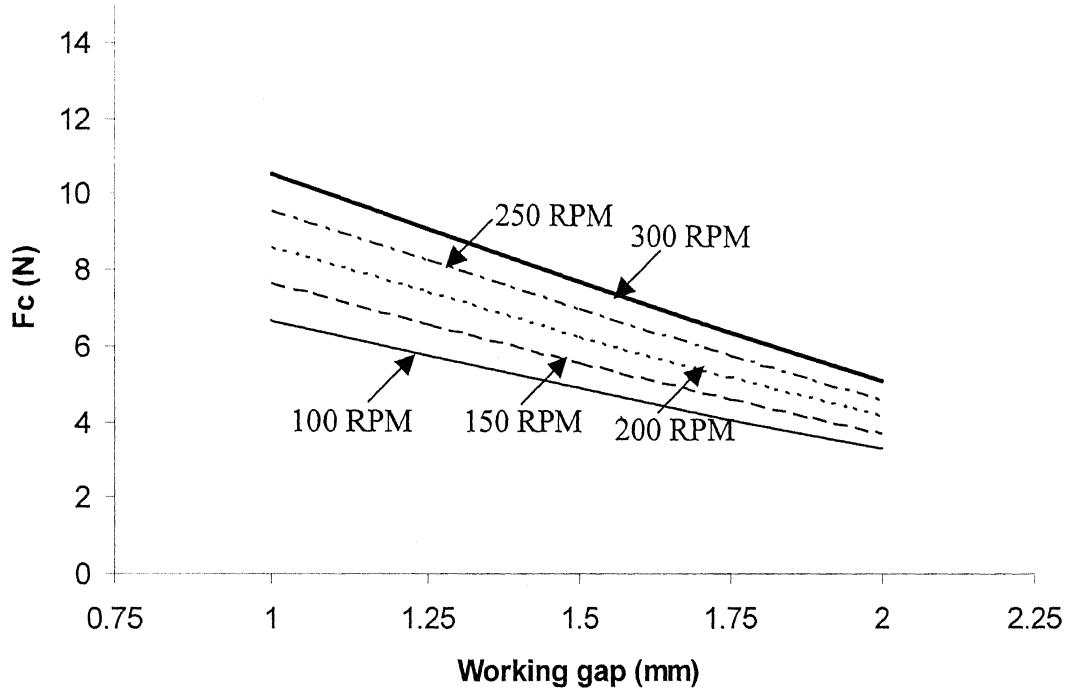

Figure 4.9 Variation of tangential cutting force with working gap for different speed (RPM), current = 0.75 A; 800# SiC mesh no; 3% oil

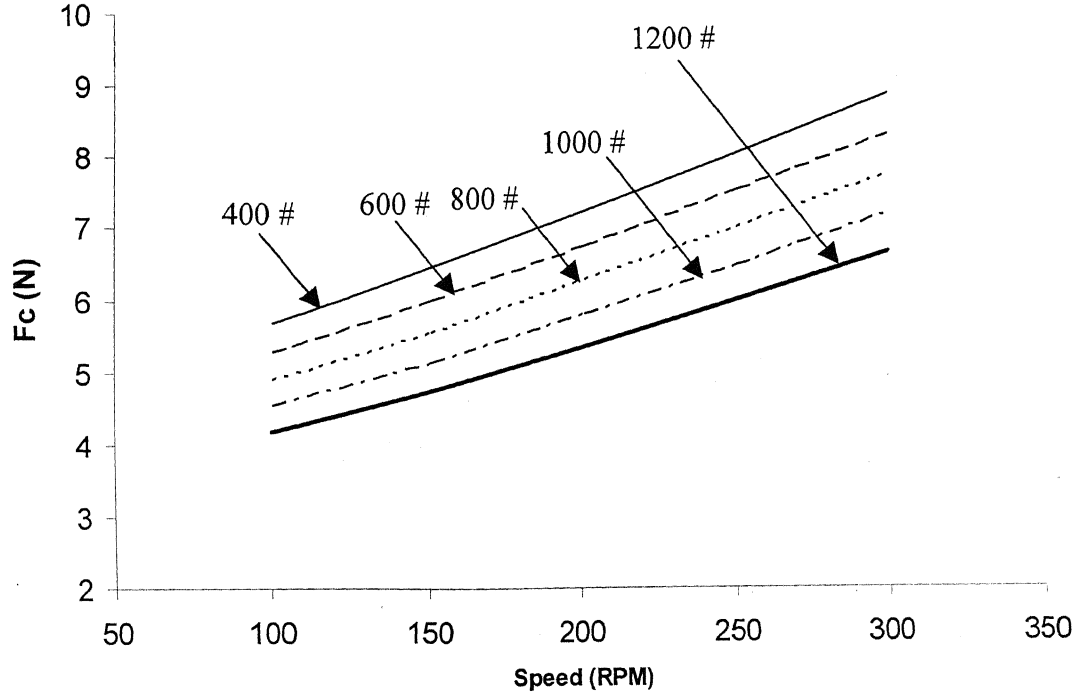

Figure 4.10 Variation of tangential cutting force with speed for different SiC mesh number, current = 0.75 A; gap = 1.5 mm; 3% oil

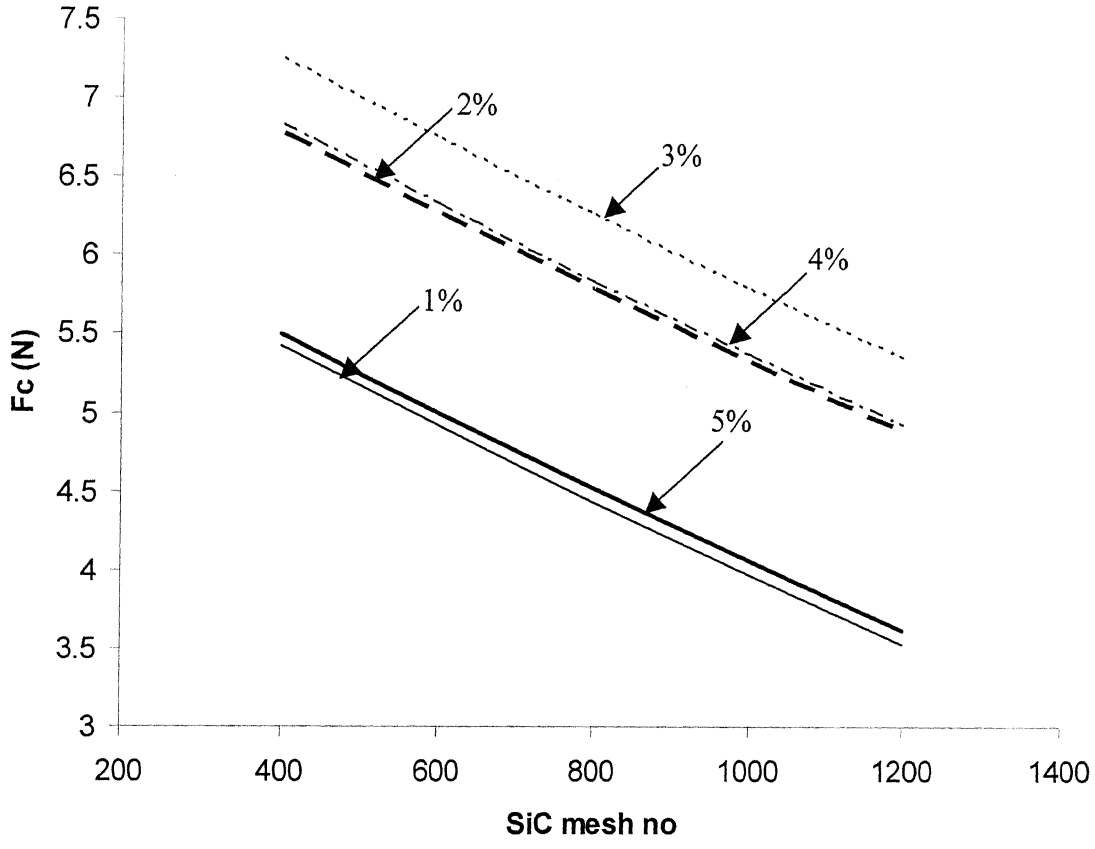

Figure 4.11 Variation of tangential cutting force with SiC mesh number for different percent of oil, current = 0.75 A; gap = 1.5 mm; speed = 200 RPM

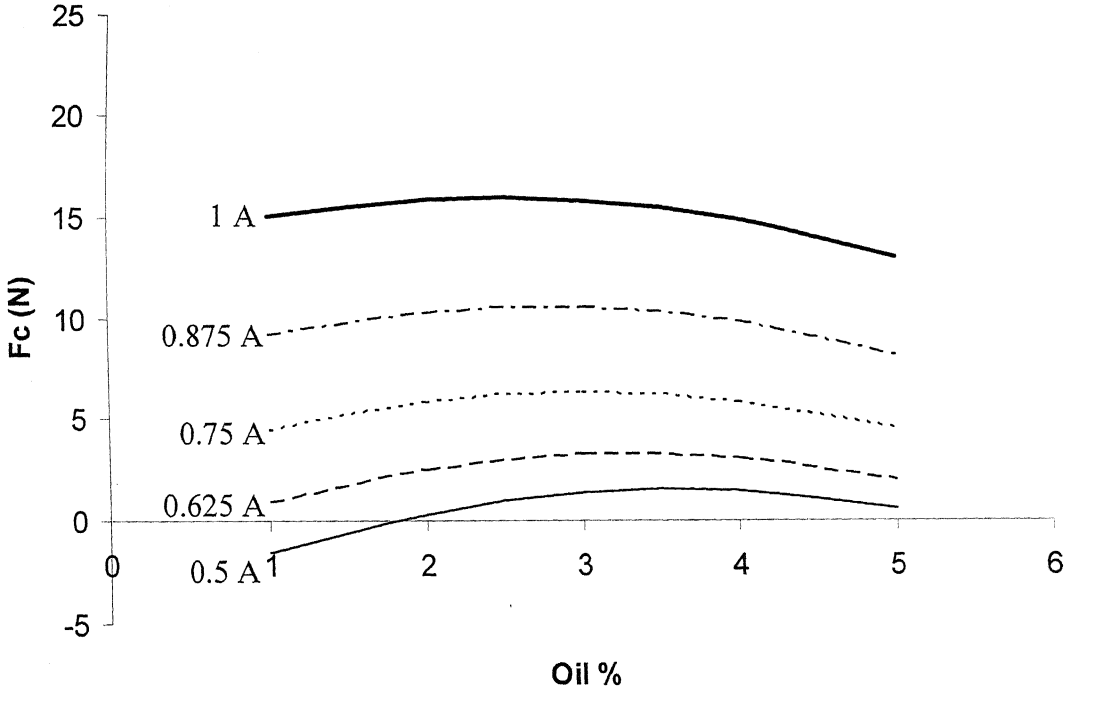

Figure 4.12 Variation of tangential cutting force with oil percentage in MAP for different current to electromagnet, gap = 1.5 mm; speed = 200 RPM; 800# SiC mesh no

Finishing is done only by those abrasive grains in contact with the work-piece surface. These abrasives are held by the iron particles which are aligned along the chain just above these grains. This layer of iron particles is near to the work-piece surface. As stated earlier, the bonding between the iron particles is dependent on the strength of the magnetic field. Field strength is dependent on length of distance from a magnet pole. The higher the distance from the pole, weaker is the field. In this way, the strength of the magnetic bonding between the iron particles is dependent on their distance from the pole nearest to them. As the working gap increases, the distance between the magnet poles and the iron particles nearest to the work-piece surface increases. So the iron particles will press the abrasives on the work-piece with a lower force. Thus, due to the reasons stated in the 4.3.6.1, the abrasives would not be able to impart much force on increase in working gap.

4.3.6.3 ***Speed of the electromagnet (RPM)***

It is seen (Fig. 4.10) that as the RPM of the electromagnet increases, the cutting force increases.

Increase in speed increases the kinetic energy of the abrasives. With increase in rotational speed, the acceleration of the abrasive particles increases. Since,

Fc = (mass of abrasive) × Acceleration,

the cutting force imparted increases. So, abrasives impart more force on the work-piece at higher speed, hence the increase in the imparted cutting force.

4.3.6.4 ***SiC abrasive mesh number***

It is seen (Fig. 4.11) that with increase in mesh number of the SiC grains, the cutting force reduces.

Mesh number is the representation of the size of an abrasive. Greater the mesh number, smaller is the abrasive diameter. For other conditions remaining constant, the volume available in the iron matrix is constant. As the size of the abrasive reduces, the number of abrasive particles present in the finishing zone increases.

The abrasives can impart force on a work-piece because the iron particles are holding them and giving them the necessary physical support to impart the load on the work-piece. This is possible due to the magnetization energy available to the iron particles. This magnetization energy is distributed among the abrasives as holding force and exhibited in the form of imparted cutting force. As the number of abrasives increases, the force per abrasive reduces. So the effective hold of the iron particles on an abrasive particle in its vicinity reduces. Small particles have smaller cutting edges. Due to the above reasons, the cutting force imparted by smaller

abrasives is small in case of MAF. The overall effect of this lessening of force at the particle level is seen to reduce the overall cutting force.

However, since the number of abrasives in the working zone increases due to reduction in the grain size used, the total force may increase also. However in this case, the reduction of force may be accounted to improper mixing of abrasives and iron particles so that the number of particles in the working zone interacting with the work-piece was reduced.

It might so happen that since the number of abrasive grains should increase with reduction in grain size, the overall finishing force remains same.

4.3.6.5 *Percentage of oil*

It is seen (Fig 4.12) that as the amount of oil in the MAP increases, the cutting force shows increasing trend from 1% oil to 3% oil, and then it reduces up till 5% oil.

Oil is added to MAP to improve the bonding strength of the particles in MAP. So oil is added to increase the rigidity of MAP. But more amount of oil induces slip between the abrasives and work-piece as well as iron particles and the abrasives. So the bonding strength is affected and thus the cutting force is affected.

4.4 Comparison of forces generated in ferromagnetic and non-ferromagnetic materials

The obtained model for the normal thrust and tangential cutting force in case of non-ferromagnetic brass is compared with that for the model of forces developed in case of ferromagnetic EN8 medium carbon steel [24]. The model has been developed using the same electromagnet, dynamometer, fixture and work-piece of the same shape and size.

The model for EN8 is

$$\left.\begin{aligned} Fmn_f &= 48.0+12.0X_1-7.22X_2+6.38X_3+3.48X_1^2+2.51X_3^2+4.03X_3X_4 \\ Fc_f &= 35.1+6.27X_1-6.05X_2-2.45X_4-1.04X_4^2 \end{aligned}\right\} \text{.....(4.4)}$$

where, X_1 = current supplied to the electromagnet, X_2 = working gap, X_3 = percentage of oil in the MAP, X_4 = speed in RPM, Fmn_f = normal thrust force generated in case of EN8 work-piece, and Fc_f = tangential cutting force generated.

The above model is compared with the model for brass

$$\left.\begin{aligned} Fmn &= 69.9 + 42.1X_1 - 10.2X_2 + 6.02X_3 \\ Fc &= 6.28 + 3.63X_1 - 1.10X_2 + 0.709X_3 - 0.471X_4 + 0.582X_1^2 - 0.448X_5^2 - 0.575X_1X_2 \end{aligned}\right\} \text{.....from (4.3)}$$

The curves drawn using the above model for ferromagnetic EN8 was superimposed with the curves drawn with the help of the model generated for non-ferromagnetic brass. The two were then compared as follows.

4.4.1 Normal thrust force

In ferromagnetic case, the significant parameters for prediction of normal force are current supplied, working gap, speed and the percentage composition of oil in the MAP. In non-ferromagnetic case, the significant factors are current supplied, working gap and speed. Since, oil percentage does not exist as a significant parameter in non-ferromagnetic model, the effects of oil cannot be compared. Comparison at rest of the parameter levels is done. The normal force seen in case of ferromagnetic material is a tension force for the dynamometer but ultimately compressive on the work-piece surface, whereas it is a compressive force for the dynamometer in case of non-ferromagnetic material. However, still a magnitude based comparison has been done to discuss the reasons for the generation of the so. It is seen from Fig. 4.13 that, all the curves show increasing trend, i.e. the normal force increases with increase in current supplied to the electromagnet. The curves have been drawn keeping rest of the factors at 'zero level'. Though an increasing trend is seen, it is also observed that the maximum value of normal force is higher for non-ferromagnetic and also the minimum limit is lower. This can be attributed to the magnetic property of both the materials. The pattern of distribution of lines of force in the working zone for both non-ferromagnetic and ferromagnetic work-pieces can be seen in Fig. 4.15 and 4.16. It can be seen that very small number of lines of force pass through the non-ferromagnetic work-piece, and the number of lines of force passing through the ferromagnetic work-piece is much more. This is so because of the ferromagnetic nature of the work-piece. Ferromagnetic material is much more permeable than a non-ferromagnetic material. Permeability of EN8 is 2000 times that of air whereas that of brass is a little better than air (still ≈ 1). The ferromagnetic work-piece itself gets magnetized and increases the field strength up to a great extent.

The free body diagram for the forces acting during MAF of brass is shown in Fig. 4.17. During the polishing operation, as the working gap for polishing is set, the abrasive grains in the working gap give a normal indenting force 'Ft' on the work-piece which is the sum of the normal forces given by the abrasive particles and designated as f1, f2.... The work-piece, due to its compressive strength gives a force in the opposite direction which is distributed among the abrasives. The resistance forces on the abrasive particles are designated as s1, s2.... The compressive strength of brass is very low (30 MPa), so the abrasives will indent more in brass work-piece. The force 'Fnet' measured by the dynamometer is Ft, which is normal and compressive for the work-piece and thus the dynamometer.

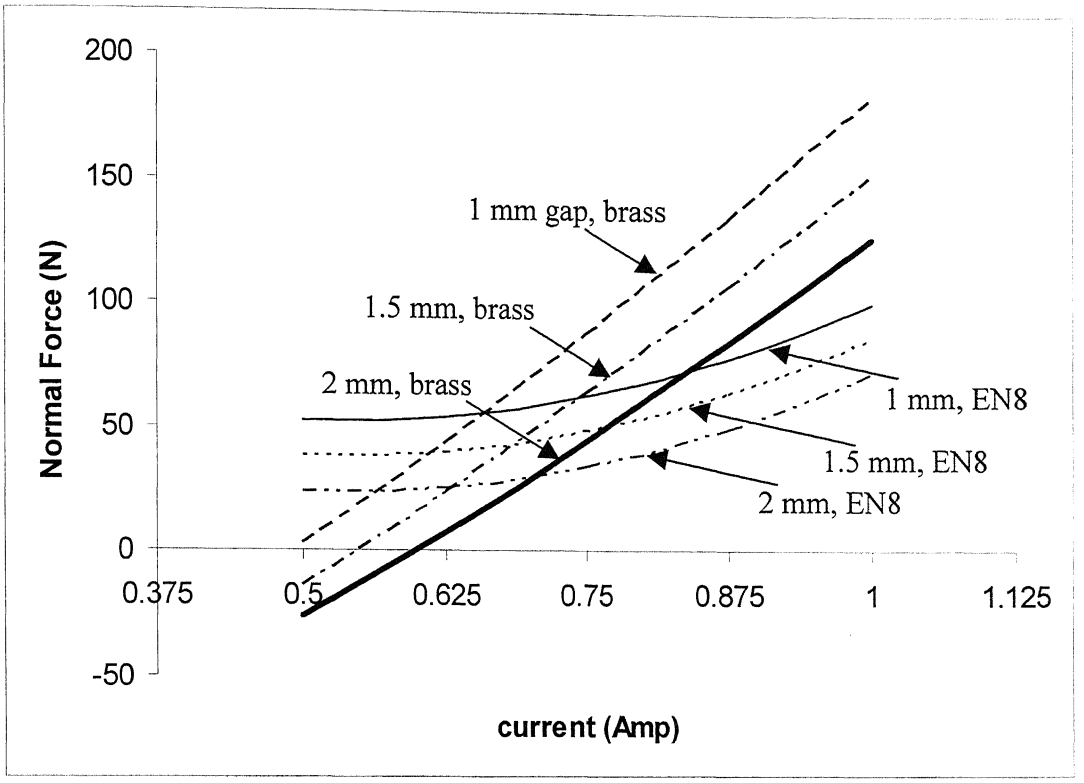

Figure 4.13 Comparison of normal forces of ferromagnetic (EN8) and non-ferromagnetic (brass) material with varying current at different working gaps, speed = 125 RPM; 3% oil; 800# SiC mesh no

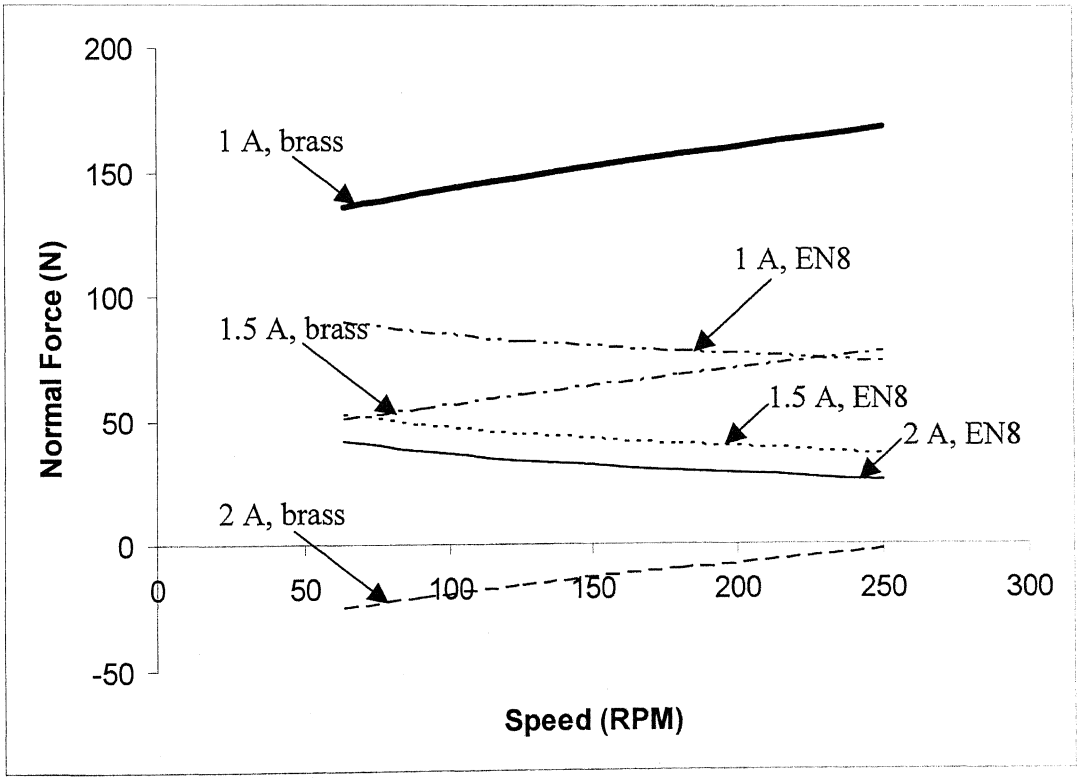

Figure 4.14 Comparison of normal force of ferromagnetic (EN8) and non-ferromagnetic (brass) material with varying speed at different current, current = 0.75 A; 2% oil; 800# SiC mesh no

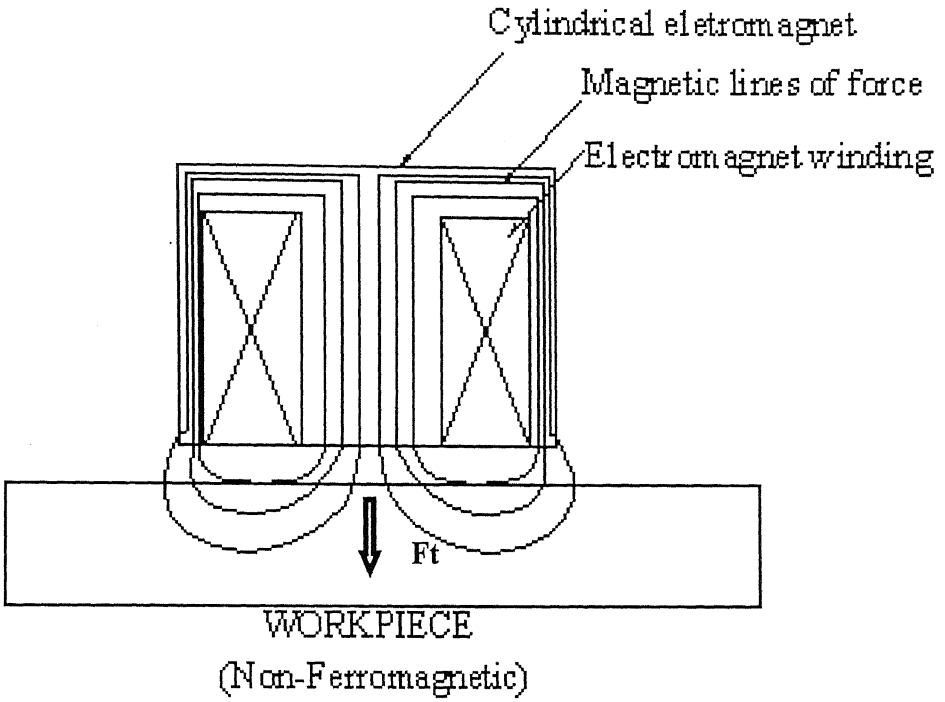

Figure 4.15 Arrangement of lines of force in non-ferromagnetic material

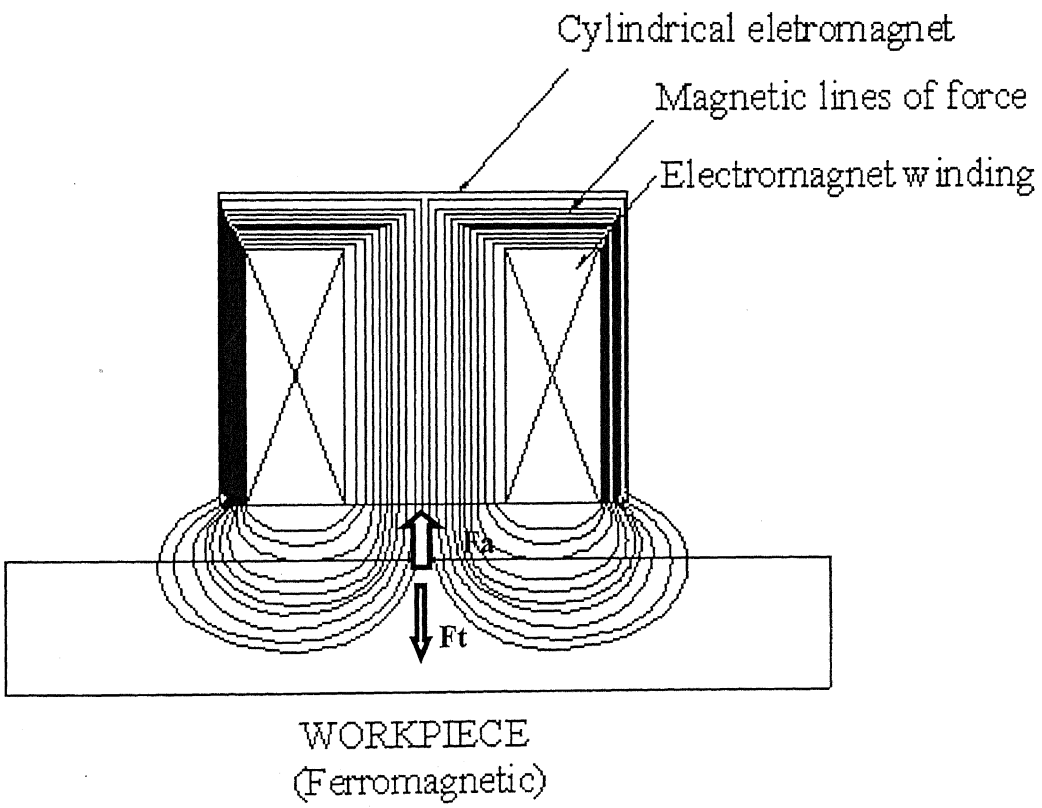

Figure 4.16 Arrangement of lines of force in case of ferromagnetic material

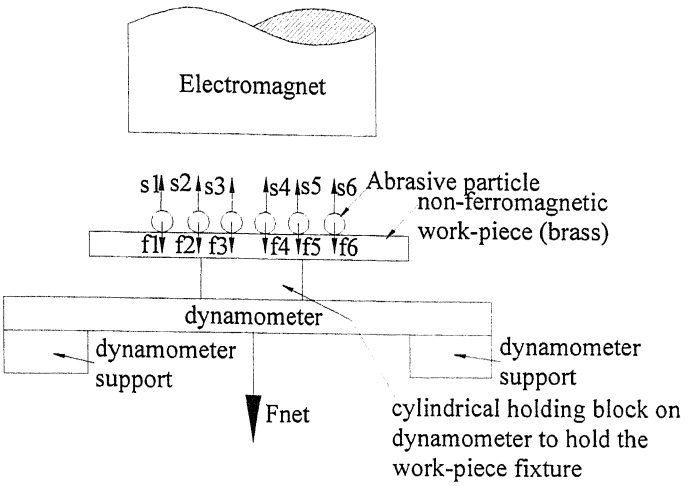

$Ft = f1 + f2 + f3 + f4 + f5 + f6 + ...$
$Fnet = Ft$

Figure 4.17 Free body diagram for forces in MAF of brass

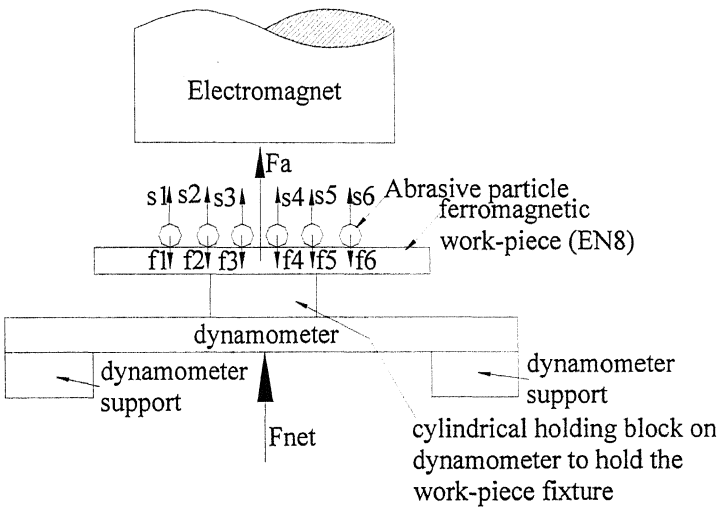

$Ft = f1 + f2 + f3 + f4 + f5 + f6 + ...$
$Fnet = Fa - Ft$

Figure 4.18 Free body diagram for forces in MAF of EN8

As stated earlier, the ferromagnetic work-piece EN8 itself gets magnetized on application of a magnetic field. So an attractive force acts between the electromagnet and EN8 work-piece, designated by 'Fa' in Fig. 4.16 and 4.18, which is a very large force. This creates a tensile force in the dynamometer. The distribution of forces is shown in the free body diagram for MAF of EN8 work-piece in Fig. 4.18. Though the SiC abrasives over the work-piece impart a total normal force 'Ft' on it, but the compressive strength of EN8 being very high (620 MPa), they

will indent lesser in EN8 work-piece as compared to brass. The magnetic attraction force being very high, a net force 'Fnet' (=Fa-Ft) acts upwards, so the force measured is an overall tension force for the dynamometer. But in case of non-ferromagnetic brass, the work-piece and fixture don't get magnetized and so the force acting is purely a thrust force, compressive for the dynamometer. So a net compressive force is measured.

The normal force is seen to be increasing with increase of RPM in case of non-ferromagnetic material and slightly decreasing in case of ferromagnetic material, as seen in Fig. 4.14. This is partly due to the variation in the quantity of powder used. In the experiments for ferromagnetic material, only 1.05 times the calculated volume of powder required was taken. But in case of non-ferromagnetic material, 1.30 times the calculated volume of powder was taken. As the electromagnet is rotated, some powder splashes off, but in non-ferromagnetic case, more powder is retained after splashing because more powder has been taken initially. It will result in higher force.

4.4.2 Tangential cutting force

The force that is measured on a dynamometer is nothing but the net force acting on it. From the Fig. 4.19, it is seen that cutting force increases with increase in current supplied to the electromagnet. This is quite obvious for the reasons already discussed earlier. But the value of cutting force imparted is seen to be more in case of EN8.

EN8 is a medium carbon steel. It is a medium carbon steel and its shear strength value lies in the range 370 MN/m^2 where as that of brass lies in the range 110 MN/m^2 [18]. So the cutting force required to remove material in the form of chips from brass requires lesser cutting force. So in all the curves, the cutting force value for brass is seen to be less than that of EN8.

In Fig. 4.20, the cutting force trend for EN8 is seen to be slightly reducing with increase of speed because of splashing and loss of MAP from working zone. But in the experiments for non-ferromagnetic brass, more amount of MAP had been taken to counteract this problem.

In Fig. 4.21, the cutting force trend for both EN8 and brass are seen to reduce with increase in the working gap. But the value of the cutting forces required for EN8 are more than the value of cutting forces required for brass. This is due to the lesser strength of brass compared to EN8 and the ferromagnetic property of EN8. The contribution of ferromagnetic property of EN8 in increasing the value of cutting force observed has been discussed in Sec. 4.4.1.

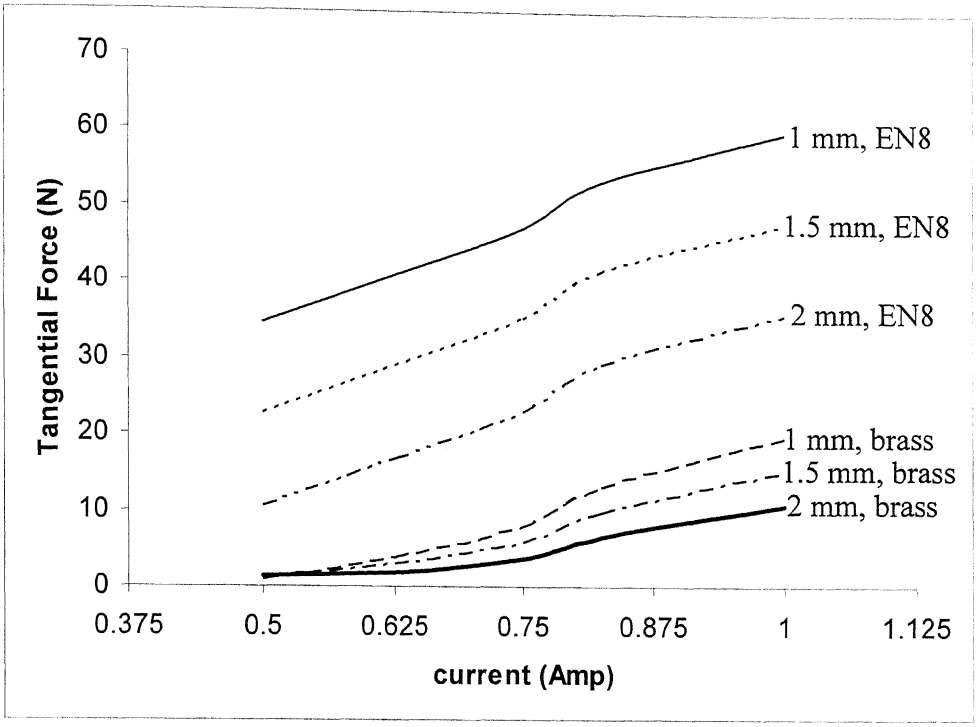

Figure 4.19 Comparison of tangential force of ferromagnetic (EN8) and non-ferromagnetic (brass) material with current supplied to electromagnet at different working gap, speed = 125 RPM; 3% oil; 800# SiC mesh no

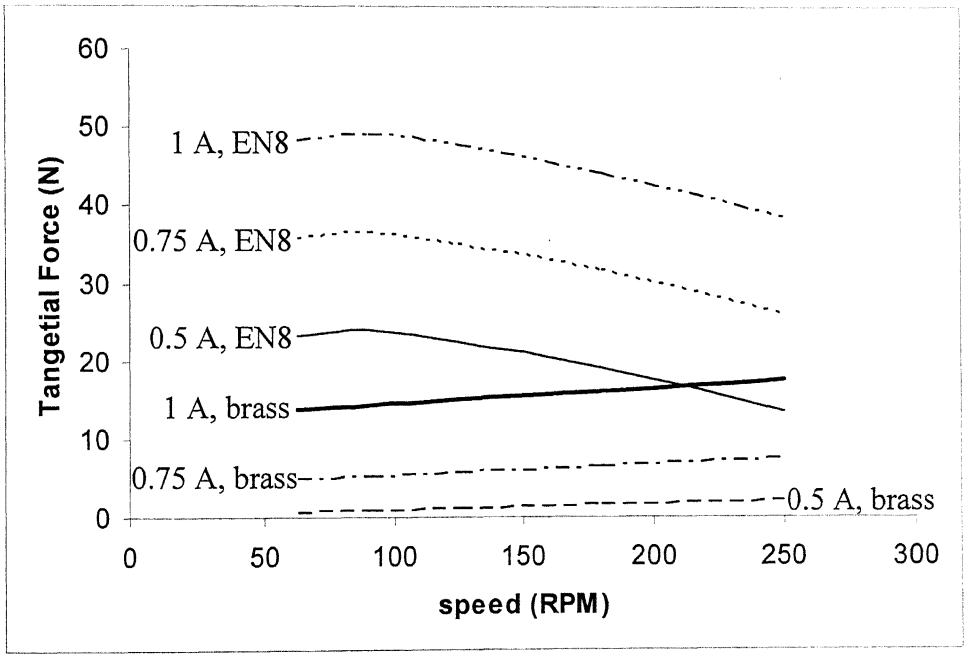

Figure 4.20 Comparison of tangential force for ferromagnetic (EN8) and non-ferromagnetic (brass) material with speed at different current, gap = 1.5 mm; 3% oil; 800# SiC mesh no

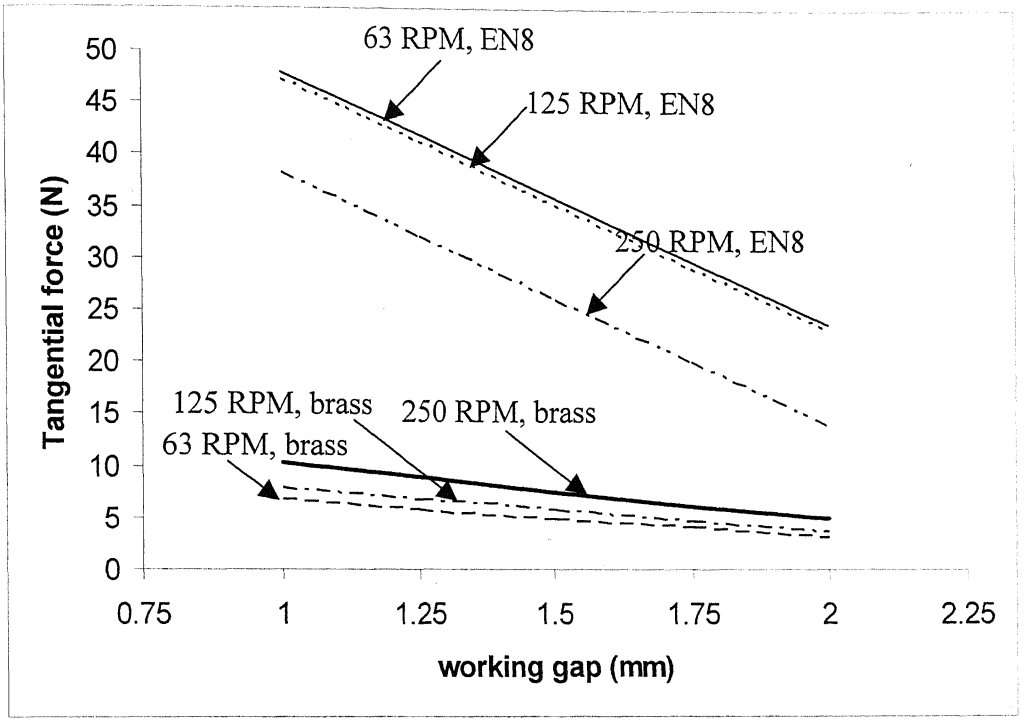

Figure 4.21 Comparison of tangential force for ferromagnetic (EN8) and non-ferromagnetic (brass) material with working gap at different speed, current = 0.75 A; 3% oil; 800# SiC mesh no

Chapter 5

CONCLUSIONS

In this study, Magnetic Abrasive Finishing (MAF) of brass has been carried out to study the forces generated when MAF operation is done on a non-ferromagnetic material. The results of the study have been compared to the results obtained in case of alloy steel EN8, which is a ferromagnetic material. The conclusions derived from the study are

1. The effect of current supplied to the electromagnet and the working gap are the most significant factors in determining the normal force and the tangential force generated during MAF. More current and less working gap increase both the forces.
2. Speed of rotation of the electromagnet is also an important parameter. With increase of speed of rotation, the normal and the tangential force increase.
3. Abrasive mesh size is not found to be a significant factor for influencing force in case of normal force. However it is found to influence tangential force. With increase in the grain mesh number, the tangential force reduces.
4. Percentage composition of oil is a not a significant factor for normal force, but it is seen to affect tangential force. The tangential force increases for about 3% oil percentage in the magnetic abrasive powder, but then starts reducing for 3% to 5% oil percentage.
5. Current and working gap are the significant factors while polishing both ferromagnetic and non-ferromagnetic materials.

Chapter 6

SCOPE FOR FUTURE WORK

Magnetic Abrasive Finishing (MAF) is still going through research stage. In the present thesis, experimentation has been carried out to understand the effect of various working parameters on the forces generated during MAF of brass. The present work can be extended further to study the issues as follows.

1. Though the thesis work has given some idea about the nature of forces generated during MAF of brass, it does not give any idea about other non-ferromagnetic materials. The non-ferromagnetic nature of such materials varies from material to material and so other non-ferromagnetic materials like ceramics should be studied.
2. The effect of forces generated in the MAF of brass to obtain best surface finish is still to be studied. It can be studied by taking surface finish as an output parameter along with the forces.
3. The effect of the magnetic properties of the work-piece on the MAF process is known qualitatively. It can be studied by taking material magnetic properties as parameter as well.
4. Material hardness can be taken as a parameter to study its effect on the forces generated.
5. Optimization of process, both in case of ferromagnetic and non-ferromagnetic materials, has to be done to impart minimum possible force on the surface, thereby obtain best surface finish.

REFERENCES

1. Shinmura Takeo, Takazawa Koya, Hatano Eiju and Aizawa Toshio, "Study on Magnetic Abrasive Process – Finishing characteristics", Bull. Japan Society of Precision Engineering, Vol. 18, No. 4 (December 1984), pp. 347-345.
2. Shinmura T., Takazawa K., Hatano E. and Toshio A., "Study on Magnetic Abrasive process – Process principle and finishing possibility", Bull. Japan Soc. of Prec. Engg., Vol. 19, No. 1 (March 1985), pp. 54-55.
3. Shinmura T., Takazawa K., and Hatano E., "Study on Magnetic Abrasive Process – Application to edge finishing", Bull. Japan Soc. of Prec. Engg., Vol. 19, No. 3 (Sep. 1985), pp. 218-220.
4. Shinmura T., Takazawa K. and Hatano E., "Study on Magnetic Abrasive Process – Application to Plane Finishing", Bull. of Japan Society of Precision Engineering, Vol. 19, No. 4 (Dec. 1985), pp. 289-291.
5. Shinmura T., Takazawa K., and Hatano E., "Study on Magnetic Abrasive Finishing – Effects of various types of magnetic abrasives on finishing characteristics", Bulletin of Japanese Society of Precision Engineering, Vol. 21, No. 2 (June 1987), pp. 139-141.
6. Shinmura T. and Aizawa T., "Study on Internal Finishing of a Non-ferromagnetic tubing by Magnetic Abrasive Machining process", Bull. Japan Soc. of Prec. Engg., Vol. 23, No.1 (March 1989), pp. 37-41.
7. Shinmura T., and Aizawa T., "Study on Magnetic Abrasive Finishing Process", Bulletin of Japan Society of Precision Engineering, Vol. 23, No. 3 (Sept, 1989), pp 236-239.
8. Shinmura T., Wang Feng Hui and Aizawa T., "Study on a New Finishing Process of fine ceramics by Magnetic Abrasive Machining – On the improving effects of finishing efficiency obtained by mixing diamond magnetic abrasives with ferromagnetic particles", Int. J. Japan Soc. Prec. Engg., Vol. 28, No. 2 (June 1994), pp. 99-104.
9. Shinmura T.and Yamaguchi Hitomi, "Study on a new Internal Finishing Process by the application of Magnetic Abrasive Machining (internal finishing of stainless steel tube and clean gas bomb)", Jap. Soc. Mech. Engg. International Journal, Series C, Vol. 38, No.4 (1995), pp. 798-804.

10. Yamaguchi H. and Shinmura T., "Magnetic abrasive finishing of inner surfaces of tubes", Proceedings, International Symposium for Electro-machining, EPFL Lausanne, Switzerland (April 17-21, 1995), pp. 963-976.
11. Yamaguchi H., Shinmura T., "Study of an internal magnetic abrasive finishing using a pole rotation system: Discussion of the characteristic abrasive behavior", Precision Engineering (Journal of the International Societies for Precision Engineering and Nanotechnology), Vol. 24 (2000), pp. 237-244.
12. Jain V.K, Kumar P., Behera P.K., Jayswal S.C., "Effect of working gap and circumferential speed on the performance of magnetic abrasive finishing process", Wear, Vol. 250 (2001), pp. 384-390.
13. Chang Geeng-Wei, Yan Biing-Hwa, Hsu Rong-Tzong, "Study of cylindrical magnetic abrasive finishing using unbonded magnetic abrasives", International Journal of Machine Tools & Manufacture, Vol. 42 (2002), pp. 575-583.
14. Mori T., Hirota K., Kawashima Y., "Clarification of magnetic abrasive finishing mechanism", Journal of Materials Processing Technology, Vol. 143-144, (20 December 2003), pp. 682-686.
15. Yamaguchi H. and Shinmura T., "Internal finishing process for alumina ceramic components by a magnetic field assisted finishing process", Precision Engineering, Vol. 28, Issue 2, April 2004, pp. 135-142.
16. Singh Dhirendra K., Jain V.K. and Raghuram V., "Parametric study of magnetic abrasive finishing process", Journal of Material Processing Technology, Vol. 149 (2004), pp. 22-29.
17. Baron Yuri M., Ko Sung Lim, Repnikova Elena, "Experimental verification of deburring by magnetic abrasive finishing method", 2nd Asia Pacific Forum on Precision surface finishing and deburring technology, Seoul, Korea (22-24 July, 2002), pp. 159-170.
18. Sharma P.C., Aggarwal D.K., "A Textbook of Machine Design", S.K. Kataria and sons publishers, New Delhi, 1999.
19. "Machine Tool Design Handbook", Central Machine Tool Institute, Tumkur Road, Bangalore, 1978.
20. Timoshenko S.P., Young D.H., "Elements of Strength of Materials (Fifth Edition)", Affiliated East-West Press Pvt. Ltd, New Delhi, 1968.
21. Timoshenko S., Young D.H., "Engineering Mechanics (Fourth Edition)", McGraw-Hill Book Company, Singapore, 1956.

22. Cochran William G. and Cox Gertrude M, "Experimental Designs", John Wiley & Sons Inc., New York, 1962.
23. S.K.F bearing catalogue No. 190, "SKF Ball and Roller bearings", Skefko India Bearing Co. Ltd, Mumbai.